SYNCHRONIZATION OF CHAOS THROUGH UNPREDICTABILITY IN DYNAMICAL SYSTEMS

A THESIS SUBMITTED TO
THE GRADUATE SCHOOL OF NATURAL AND APPLIED SCIENCES
OF
MIDDLE EAST TECHNICAL UNIVERSITY

BY

KAĞAN BAŞKAN

IN PARTIAL FULFILLMENT OF THE REQUIREMENTS
FOR
THE DEGREE OF DOCTOR OF PHILOSOPHY
IN
PHYSICS

JANUARY 2024

Approval of the thesis:

SYNCHRONIZATION OF CHAOS THROUGH UNPREDICTABILITY IN DYNAMICAL SYSTEMS

submitted by **KAĞAN BAŞKAN** in partial fulfillment of the requirements for the degree of **Doctor of Philosophy in Physics Department, Middle East Technical University** by,

Prof. Dr. Halil Kalıpçılar
Dean, Graduate School of **Natural and Applied Sciences** _____

Prof. Dr. Seçkin Kürkcüoğlu
Head of Department, **Physics** _____

Prof. Dr. Seçkin Kürkcüoğlu
Supervisor, **Physics, METU** _____

Prof. Dr. Marat Akhmet
Co-supervisor, **Mathematics, METU** _____

Examining Committee Members:

Prof. Dr. İsmet Yurduşen
Mathematics, Hacettepe University _____

Prof. Dr. Seçkin Kürkcüoğlu
Physics, METU _____

Prof. Dr. İsmail Rafatov
Physics, METU _____

Prof. Dr. İsmail Turan
Physics, METU _____

Assist. Prof. Dr. Gönül Ünal Mesta
Biomedical Engineering, Başkent University _____

Date:26.01.2024

I hereby declare that all information in this document has been obtained and presented in accordance with academic rules and ethical conduct. I also declare that, as required by these rules and conduct, I have fully cited and referenced all material and results that are not original to this work.

Name, Surname: Kağan Başkan

Signature :

ABSTRACT

SYNCHRONIZATION OF CHAOS THROUGH UNPREDICTABILITY IN DYNAMICAL SYSTEMS

Başkan, Kağan
Ph.D., Department of Physics
Supervisor: Prof. Dr. Seçkin Kürkcüoğlu
Co-Supervisor: Prof. Dr. Marat Akhmet

January 2024, 118 pages

The investigation of chaos synchronization spans three decades, resulting in the development of several methods such as identical, phase, and generalized synchronization. However, conventional methods often fail to detect synchronized patterns in systems lacking fully unison dynamics. To address this limitation, delta synchronization of Poincaré chaos is introduced, aiming to explain partially synchronized patterns. This novel synchronization type is built upon unpredictability, a concept that reveals chaotic dynamics in systems based on characteristic time sequences—specifically, sequences of convergence and separation. The presence of unpredictability guarantees Poisson stable motion and sensitivity by examining a single trajectory (or single initial condition set) of a system.

Numerically, delta synchronization captures the common characteristic time sequences of unpredictability in both coupled and uncoupled systems. This method is applied to various models in this thesis, encompassing distinctive dynamics defined by ordinary, partial, and delay differential equations. In the case of unidirectionally coupled gas-discharge semiconductor systems, the absence of generalized synchroniza-

tion is noted. For Mackey-Glass delay systems, generalized synchronization occurs only after surpassing a well-known threshold. Importantly, delta synchronization is demonstrated to occur in regions where generalized synchronization is absent for these models. Additionally, the same phenomenon is observed in the uncoupled Hindmarsh-Rose neural network for noise intensity domains where identical synchronization is absent, yet delta synchronization exists. This model is constructed with Markovian noise, and noise-induced synchronization is investigated. In the domains of generalized and identical synchronization, a stronger form of delta synchronization—complete synchronization of unpredictability—is detected.

Keywords: Unpredictability, Delta synchronization, Gas-discharge semiconductor systems, Mackey-Glass systems, Hindmarsh-Rose neural network

ÖZ

DİNAMİK SİSTEMLERDE ÖNGÖRÜLEMEZLİK YOLUYLA KAOS SENKRONİZASYONU

Başkan, Kağan
Doktora, Fizik Bölümü
Tez Yöneticisi: Prof. Dr. Seçkin Kürkcüoğlu
Ortak Tez Yöneticisi: Prof. Dr. Marat Akhmet

Ocak 2024 , 118 sayfa

Kaos senkronizasyonunun araştırılması otuz yıla yayılıyor ve bu da özdeş, fazlı ve genelleştirilmiş senkronizasyon gibi çeşitli yöntemlerin geliştirilmesiyle sonuçlanıyor. Bununla birlikte, geleneksel yöntemler, tamamen uyumlu bir dinamiğin bulunmadığı sistemlerde senkronize kalıpları tespit etmekte sıklıkla başarısız oluyor. Bu sınırlamayı gidermek için, kısmen senkronize edilmiş kalıpları açıklamayı amaçlayan Poincaré kaosunun delta senkronizasyonu tanıtılmıştır. Bu yeni senkronizasyon türü, karakteristik zaman dizilerine, özellikle de yakınsama ve ayrılma dizilerine dayalı olarak, sistemlerdeki kaotik dinamikleri ortaya çıkaran bir kavram olan öngörülemezlik üzerine inşa edilmiştir. Öngörülemezliğin varlığı, bir sistemin tek bir yörüngesini (veya tek bir başlangıç koşul kümesini) inceleyerek Poisson kararlı hareketini ve hassasiyetini garanti eder.

Sayısal olarak, delta senkronizasyon hem bağlı hem de bağlı olmayan sistemlerde öngörülemezliğin ortak karakteristik zaman dizilerini yakalar. Bu yöntem, bu tezdeki adi, kısmi ve gecikmeli diferansiyel denklemlerle tanımlanan farklı dinamikleri

kapsayan çeşitli modellere uygulanmıştır. Tek yönlü olarak bağlı gaz deşarjlı yarı iletken sistemler durumunda, genelleştirilmiş senkronizasyonun bulunmadığı belirlenmiştir. Mackey-Glass gecikme sistemleri için genelleştirilmiş senkronizasyon yalnızca belirli bir eşiğin aşılmasından sonra gerçekleşir. Bu modeller için genelleştirilmiş senkronizasyonun bulunmadığı bölgelerde delta senkronizasyonunun meydana geldiği gösterilmiştir. Ek olarak aynı fenomen, özdeş senkronizasyonun olmadığı ancak delta senkronizasyonunun mevcut olduğu gürültü yoğunluğu alanları için bağlı olmayan Hindmarsh-Rose sinir ağında da gözlemlenir. Bu model Markov gürültüsü ile oluşturulmuş ve gürültü kaynaklı senkronizasyon araştırılmıştır. Genelleştirilmiş ve özdeş senkronizasyonun olduğu alanlarda, delta senkronizasyonunun daha güçlü bir biçimi - öngörülemezliğin tam senkronizasyonu - tespit edilmiştir.

Anahtar Kelimeler: Öngörülemezlik, Delta senkronizasyon, Gaz deşarjlı yarı iletken sistemler, Mackey-Glass sistemleri, Hindmarsh-Rose sinir ağı

To my family...

ACKNOWLEDGMENTS

I would like to express my sincere appreciation to Prof. Dr. Marat Akhmet for his unwavering support, patience, and motivation. His immense knowledge has guided me through my research, providing invaluable insights that have greatly enriched my research.

Special thanks to Prof. Dr. Seçkin Kürkcüoğlu for his support, understanding, and guidance throughout my studies. His immense knowledge and continuous support have encouraged me in my studies.

I am thankful to Dr. Cihan Yeşil for his illuminating discussions, collaboration, and friendship. We endured the challanges of this research and found solutions to various problems together.

Heartfelt gratitude to my parents, whose encouragement and support during my most challenging times have been indispensable. This accomplishment would not have been possible without them. I appreciate my wife's continuous support and understanding. Her perspective and encouragement helped me to overcome the most diffucult times.

This thesis has been supported by the 2247- A National Leading Research Program of TÜBITAK (The Scientific and Technological Research Council of Turkey), Turkey, with the project number 120C138.

TABLE OF CONTENTS

ABSTRACT v

ÖZ vii

ACKNOWLEDGMENTS x

TABLE OF CONTENTS xi

LIST OF TABLES xiv

LIST OF FIGURES xvi

LIST OF ALGORITHMS xviii

LIST OF ABBREVIATIONS xix

CHAPTERS

1 INTRODUCTION 1

1.1 Motivation 1

1.2 Historical perspective 2

1.3 Types of chaos synchronization 3

1.4 Unpredictability 6

1.5 Delta synchronization of Poincaré chaos 9

1.6 Gas-discharge semiconductor model 11

1.7 Mackey-Glass model 14

1.8 Hindmarsh-Rose neural network 16

1.9 Contributions and Novelties 18

1.10 Organization of the thesis 20

2 UNPREDICTABILITY AND SYNCHRONIZATION 23

2.1 Introduction 23

2.2 Unpredictability 24

2.2.1 Theoretical Backgrounds 25

2.2.2 Numerical Implementation 29

2.3 Synchronization through Unpredictability 30

2.4 Identical Synchronization 36

2.5 Generalized synchronization 37

3 DELTA SYNCHRONIZATION OF POINCARÉ CHAOS IN GAS DISCHARGE-SEMICONDUCTOR SYSTEMS 39

3.1 Introduction 39

3.2 Fluid Modeling of Plasma 40

3.2.1 Two-fluid model 43

3.2.2 Drift-Diffusion Approximation 44

3.3 Simple Fluid Model 45

3.4 Description of the Gas-Discharge Semiconductor Model 46

3.5 Periodic and Chaotic Oscillations 48

3.6 Delta synchronization of chaos in the coupled GDSS 50

3.7 Discussion 59

3.8 Further analysis on gas-discharge systems 60

4 REVEALING CHAOS SYNCHRONIZATION BELOW THE THRESHOLD IN COUPLED MACKEY-GLASS SYSTEMS 63

4.1 Introduction 63

4.2 Mackey-Glass System 65

4.3 Transition to chaos 66

4.4 Synchronization of chaos 69

4.4.1 Synchronization of chaos above the threshold 71

4.4.2 Synchronization of chaos below the threshold 75

4.5 Discussion 78

5 MARKOVIAN NOISE-INDUCED DELTA SYNCHRONIZATION APPROACH FOR HINDMARSH-ROSE MODEL 81

5.1 Hindmarsh-Rose Model with Markovian Noise 83

5.1.1 Markovian noise 83

5.1.2 Uncoupled Hindmarsh-Rose neurons with Markovian noise . . 87

5.2 Numerical Results 88

5.3 Discussion 93

6 CONCLUSION 97

REFERENCES 103

CURRICULUM VITAE 117

LIST OF TABLES

TABLES

Table 3.1 Input parameters of the one-dimensional simple fluid model 48

Table 3.2 Sequences of convergence t_n and divergence s_n with δ_n values for the drive system. 54

Table 3.3 Sequences of convergence t_n and divergence s_n with δ_n values for the response system. 56

Table 3.4 Common u_n, v_n and δ_n values of drive and response systems 57

Table 4.1 Sequences of convergence t_n and separation s_n with δ_n values for the drive system. 73

Table 4.2 Sequences of convergence t_n and separation s_n with δ_n values for the response system for $\varepsilon = 0.71$. 74

Table 4.3 Common sequences of convergence u_n and separation v_n with δ_n between drive and response systems $\varepsilon = 0.71$. 75

Table 4.4 Sequences of convergence t_n and divergence s_n with δ_n values for the response system with $\varepsilon = 0.60$. 78

Table 4.5 Common sequences of convergence u_n and divergence v_n with δ_n between drive and response systems $\varepsilon = 0.60$. 79

Table 5.1 Sequences of convergence and separation at $D = 1$ for unpredictability analysis. 91

Table 5.2 Sequences of finite convergence and separation at $D = 1$ in synchronization analysis. 92

Table 5.3 Sequences of convergence and separation for $D = 4.7$ 93

Table 5.4 Common sequences of convergence and separation for $D = 4.7$ . . . 94

LIST OF FIGURES

FIGURES

Figure 1.1 Illustration of unpredictability. 9

Figure 2.1 The types of recurrence 24

Figure 3.1 The schematic illustration of a planar gas discharge coupled with a semiconductor layer. 46

Figure 3.2 Bifurcation diagram separating stable stationary region from unstable region. Points denoted by (a), (b), (c) and (d) indicate regimes with $\boldsymbol{U_t} = 17.04$, 17.68, 18.71 and 20.11 at $\boldsymbol{R_s} = 30709$, respectively. . 49

Figure 3.3 Phase portraits of trajectories in the $\boldsymbol{U}$-$\boldsymbol{J}$ plane, computed for corresponding (a), (b), (c) and (d) points in figure (3.2). 50

Figure 3.4 $\boldsymbol{U} - \boldsymbol{J}$ plot of the drive system at $\boldsymbol{U}_t = 20.11$ and $\boldsymbol{R}_s = 30709$. 53

Figure 3.5 $\boldsymbol{V} - \boldsymbol{J}$ plot of the response system at $\boldsymbol{V}_t = 20.11$ and $\boldsymbol{R}_s = 30709$ 55

Figure 3.6 $\boldsymbol{U}, \boldsymbol{V} - \boldsymbol{J}$ plot of both drive (blue) and response (red) systems . 55

Figure 3.7 $\boldsymbol{W} - \boldsymbol{V}$ plot at $\boldsymbol{W}_t = 20.11$, $\boldsymbol{R}_s = 30709$ 58

Figure 4.1 Time oscillations of variable x at $\tau = 1.40$ and $\tau = 1.565$. Point A at $\tau = 1.40$ evolves into an inflexion point at $\tau = 1.565$. 66

Figure 4.2 Emerging of a new period along the curve $f(x, x_\tau) = 0$. 67

Figure 4.3 The beginning of a new period formation along the curve $f(x, x_\tau) = 0$. Calculations are carried out at $\tau = 1.40, 1.456, 1.49$, and 1.565. . . . 67

Figure 4.4 Time oscillations of x, $\frac{\mathrm{d}x}{\mathrm{d}t}$, $\frac{\mathrm{d}^2x}{\mathrm{d}t^2}$, where the intersection point of $\frac{\mathrm{d}x}{\mathrm{d}t}$ and $\frac{\mathrm{d}^2x}{\mathrm{d}t^2}$ along the y-axis corresponds to the point A on the solution x. 68

Figure 4.5 The onset of the period-doubling bifurcation cascade. The regimes (a), (b), (c), and (d) correspond to those in Fig. (4.6). 69

Figure 4.6 Phase space trajectories of the oscillations in the plane of $\frac{\mathrm{d}x}{\mathrm{d}t}$ and x for various delay values τ defined in Fig. (4.5). 70

Figure 4.7 Projection of response and auxiliary systems on (y, z) plane for $\epsilon = 0.71$ after transient regime. 71

Figure 4.8 Phase portraits of drive and response systems for $\varepsilon = 0.71$. Red marks represent $(x(t_n), \dot{x}(t_n))$ and $(y(t_n), \dot{y}(t_n))$. 72

Figure 4.9 Projection of response and auxiliary systems on (y, z) plane for $\epsilon = 0.60$ after transient regime. 76

Figure 4.10 Phase portrait of response system for $\varepsilon = 0.6$. Red marks represent $(y(t_n), \dot{y}(t_n))$. 77

Figure 5.1 Different bursting patterns of membrane potential x for various external currents I. 84

Figure 5.2 Bifurcation diagram of ISIs vs external current I. 85

Figure 5.3 Time evolution of $\rho(t)$. 85

Figure 5.4 Time evolution of $\sigma(t)$. 86

Figure 5.5 Time evolution of the noise. 87

Figure 5.6 Average errors for different noise intensities. 88

Figure 5.7 Degrees of numerical unpredictability for different noise intensities. 89

Figure 5.8 Degrees of numerical synchronization for different noise intensities. 90

LIST OF ALGORITHMS

ALGORITHMS

Algorithm 1 Algorithm for Unpredictability 31

Algorithm 2 Algorithm for Delta Synchronization of Chaos 35

LIST OF ABBREVIATIONS

ABBREVIATIONS

DSC	Delta synchronization of chaos
GDSS	Gas-discharge semiconductor system
LFA	Local field approximation
LMEA	Local mean energy approximation
CVC	Current-voltage characteristic
NDR	Negative differential resistivity
ISI	Interspike interval
Ref.	Reference
Def.	Definition
Fig.	Figure

CHAPTER 1

INTRODUCTION

1.1 Motivation

The analysis of synchronization in chaotic systems spans three decades [1–9]. Existing methods to detect synchronization, such as generalized and identical synchronization [7, 10], primarily focus on fully synchronized trajectories of coupled or uncoupled dynamical systems. However, these conventional methods fails to detect partially synchronized patterns, resulting in undetected synchronization in various systems.

The primary motivation of this thesis is to introduce a method capable of detecting synchronized behavior in chaotic systems, especially in the absence of conventional synchronization types. This novel method, termed delta synchronization of Poincaré chaos, is introduced in Ref. [11]. It is built upon the concept of unpredictability [12], which has been both theoretically and numerically applied to various systems [13–21]. The method utilizes characteristic common time values of unpredictability among coupled or uncoupled systems, forming sequences of convergence and separation, to detect unified chaotic behavior.

The choice of models to which delta synchronization is applied aims to provide a comprehensive view of various dynamical systems, including ordinary, partial, and delay differential equations. Gas-discharge plasma systems, Mackey-Glass delay systems, and the Hindmarsh-Rose neural network are investigated within the framework of delta synchronization. The studies constituting this thesis are published in Refs. [11, 22–24].

1.2 Historical perspective

The Dutch researcher Christiaan Huygens, renowned for his work in optics, telescope, and clock construction, was likely the first scientist to observe and describe the synchronization phenomenon in the seventeenth century [10]. During a sea trial of clocks designed for longitude determination, Huygens noticed that a pair of pendulum clocks hanging from a common support had synchronized. Their oscillations coincided perfectly, with the pendula moving in opposite directions. This discovery had a significant impact on the technological and scientific advancements of the time, greatly enhancing the accuracy of time measurements.

Huygens provided not only a precise description but also a qualitative explanation of the mutual synchronization effect. He correctly grasped that the alignment of the rhythms of two clocks was the result of an imperceptible motion of the beam. In contemporary terms, this implies that the clocks were synchronized in anti-phase due to coupling through the beam [10].

In the mid-nineteenth century, in his renowned treatise "The Theory of Sound," famous physicist William Strutt (Lord Rayleigh) [25] described the intriguing phenomenon of synchronization in acoustical systems [10]. He explained that when two organ pipes of the same pitch stand side by side, complications may arise, occasionally causing issues in practice. In extreme cases, the pipes may almost silence each other. Even with more moderate mutual influence, the pipes may speak in absolute unison, despite small inevitable differences. Rayleigh observed not only mutual synchronization, where two distinct but similar pipes start sounding in unison, but also the quenching effect (oscillation death) when coupling leads to the suppression of oscillations in interacting systems.

A new phase in the exploration of synchronization emerged with the progress of electrical and radio engineering [10]. On February 17, 1920, W. H. Eccles and J. H. Vincent submitted a British patent application confirming their discovery of the synchronization property of a triode generator—an uncomplicated electrical device based on a vacuum tube that produces a periodically alternating electrical current [26]. The frequency of this current oscillation is determined by the parameters of the scheme's

elements, such as capacitance. In their experiments, Eccles and Vincent coupled two generators with slightly different frequencies and demonstrated that the coupling compelled the systems to vibrate with a common frequency.

A few years later, Edward Appleton and Balthasar van der Pol replicated and expanded upon the experiments of Eccles and Vincent, marking the first step in the theoretical exploration of this effect [27, 28]. Examining the simplest case, they demonstrated that the frequency of a generator can be entrained or synchronized by a weak external signal with a slightly different frequency. These studies held significant practical importance as triode generators became fundamental components of radio communication systems. The synchronization phenomenon was employed to stabilize the frequency of a powerful generator with the assistance of a weak but highly precise one [10].

Since the publication by Pecora and Carroll [1] on the synchronization of chaotic systems, this phenomenon has garnered significant attention in the literature on chaotic phenomena for three decades. The authors discovered that it is feasible to achieve synchronization between two identical chaotic systems under appropriate unidirectional coupling schemes. This result is somewhat counterintuitive due to the intrinsic instability of chaotic systems, leading to the exponential divergence of trajectories that are initially close [7].

Various synchronization types have been developed in literature including identical (complete) synchronization [1], phase synchronization [29], generalized synchronization [3,4], anticipated synchronization [30], amplitude envelope synchronization [31], lag synchronization [32] and delta synchronization [11].

1.3 Types of chaos synchronization

The synchronization of chaos can be explored between two or more chaotic systems, whether they are coupled or uncoupled. Unidirectional coupling involves two systems: a drive (master) and a response (slave). In this arrangement, the response is influenced by the data from the drive, but the reverse is not true. These systems can either be identical or differ in nature, and are predominantly investigated in physical

and engineering contexts. Conversely, bidirectional coupling necessitates information transfer between two systems, a phenomenon commonly applicable to physiological systems as well.

Identical synchronization involves two identical chaotic systems within a unidirectional coupling scheme [1]. Following a transient period, the attainment of an identical trajectory for the parameters of interest results in identical synchronization. The asymptotic stability of synchronization can be assessed through conditional Lyapunov exponents or an approach based on Lyapunov functions [7]. This type of synchronization finds applications in diverse scientific fields, including secure communication devices and meteorological models [7].

Drive-response systems composed of systems described by delayed equations can exhibit a type of synchronization where the response state, $x(t)$, synchronizes with a state of the drive that occurs at a time τ in the future, $x(t + \tau)$. This form of synchronization is termed *anticipated synchronization* [30] because the actual value of the state variable of the response is the same as the corresponding drive state variable will have at a time τ in the future [7].

In the examination of identical synchronization under unidirectional coupling, it has been assumed that the response is an identical, or nearly identical, copy of the drive. However, the response can differ from the drive. The synchronization of these types of systems is investigated under *generalized synchronization* [3], wherein the trajectory of the response system can be predicted based on the given trajectory of the drive system.

The first case involves response system parameters that are very different from the corresponding parameters of the drive. This occurs when the drive and the response are systems of the same nature, sharing the same physical structure but with individual differences that might be substantial. For instance, the drive could be an electric circuit with a specific design or arrangement of elements, and the response could be a copy of this circuit with the same design but with one or more specific elements being notably different.

The second case arises when the nature of the two systems is different; that is, the

systems are structurally different. Using the example of an electric circuit, the drive and the response could both be electric circuits but with distinct designs, meaning different elements arranged in different ways. Alternatively, the drive could still be an electric circuit controlling a system of an entirely different nature, such as an optical system or a biological tissue [7].

The existence of generalized synchronization is achieved by the satisfaction of an asymptotic stability condition, which involves the solution of the response system and a functional of the drive system. This condition must be met for a set of initial conditions for both the drive and response systems. Approaches for detecting generalized synchronization can be classified into three categories: the analysis of conditional Lyapunov exponents [4], the auxiliary system approach [5], and the statistical estimations of predictability [3].

Amplitude envelope synchronization is a type of synchronization observed between two mutually coupled chaotic oscillators that are parametrically different [31]. It can manifest on its own or in combination with other forms of synchronization. In its pure form, it emerges at very low coupling strength and is a subtle form of synchronization that does not introduce significant correlations between the amplitudes or phases of the variables of the oscillators. In this case, the only correlated results are the envelopes of equivalent variables of the two oscillators. This implies that the extrema each system variable can reach in a given time interval are correlated [7].

Phase synchronization in periodically driven chaotic systems implies that the chaotic oscillator aligns its evolution with the applied force. This means that the phase of the oscillator is adjusted to match the phase of the external force. Beyond its significance as a fundamental phenomenon, this has implications in various scientific and engineering scenarios. For instance, when dealing with an ensemble of similar but not identical chaotic oscillators, achieving phase synchronization can introduce coherence in their collective behavior, even if they initially exhibit incoherence. This is particularly relevant when a weak external force is applied.

The concept of phase synchronization extends to situations involving non-identical, mutually coupled chaotic oscillators. In such cases, the same principles, definitions of phase, and observation techniques used for a single chaotic oscillator apply to each

of the coupled oscillators. Here, phase synchronization indicates that, due to the coupling, the phase dynamics of each oscillator are adjusted to synchronize with the phase of the other oscillator, while their amplitudes remain uncorrelated [7, 29].

Beyond phase synchronization, there exists a state known as *lag synchronization* [32]. In the phase-synchronized state, the maxima or minima of the dynamical variables in the system, while uncorrelated in amplitude, do not occur simultaneously. Specifically, the signal from the system with a lower frequency experiences some delay compared to the system with a higher frequency. With a further increase in coupling strength, a correlation between the amplitudes of the system variables may emerge, although a time lag between them is still present, resulting in a shifted relationship between the systems [7].

Delta synchronization examines the characteristic time values of unpredictability to reveal the synchronized behavior of systems [11]. The common sequences of convergence and separation, which characterize an unpredictable trajectory, between the drive and response systems indicate unified dynamics. The numerical degree of synchronization serves as a metric demonstrating the presence and strength of the synchronization.

In this thesis, delta synchronization is employed across various models to show synchronization in models where conventional methods fail to detect the phenomenon. For comparison, identical and generalized synchronization with auxiliary system approach are also employed. The advantages of our method are presented in detail with numerical features of the method. It is important to note that this study considers the numerical detection and applications of delta synchronization with a robust theoretical foundation in unpredictability.

1.4 Unpredictability

There are various types of chaos, each characterized by specific features. The first type is homoclinic chaos [33], originating from Poincaré's famous manuscript [34]. Another type is Devaney chaos [35], defined by transitivity, Lorenz sensitivity [36], and the presence of infinitely many unstable periodic motions that are dense in the

chaotic attractor. The third type is Li-Yorke chaos [37], identified by the presence of a scrambled set in which any pair of distinct points are proximal and frequently separated.

It's important to note that the key distinction of homoclinic chaos from the others lies in its sensitivity and frequent separation features. Homoclinic chaos assumes the presence of a homoclinic structure and, crucially, instability. Lorenz [36] was the first to certify the divergence of nearby motions as sensitivity, a specific form of instability. Li and Yorke [37] later employed frequent separation and proximality for the same purpose. The absence of a quantitative description of instability in homoclinic chaos sets it apart from more recent definitions, causing some inconvenience. This is because sensitivity is considered one of the essential ingredients of chaos in its modern understanding. While Poincaré himself was aware of the divergence of initially nearby trajectories, he did not provide precise instructions on how it should be quantified.

In Ref. [12], the concept of a Poisson stable point is developed, extending the idea to the concept of an unpredictable point, which is characterized by convergence to the initial state and separation from this state as time evolves, by using unpredictability as individual sensitivity for a motion. Therefore, starting from a single point on a trajectory, it leads to a phenomenon referred to as Poincaré chaos in Ref. [12]. This phenomenon brings various types of chaos closer together, providing an alternative description of motions in dynamics with a homoclinic structure. Additionally, it incorporates ingredients similar to more recent chaos types, including transitivity, sensitivity, frequent separation, and proximality. The presence of infinitely many periodic motions in later definitions can be substituted by a continuum of Poisson stable orbits.

The concept of unpredictable motion examines time sequences at the moments of convergence to the initial point and separation from the initial trajectory [12–14]. These are termed the sequence of convergence and the sequence of separation, respectively. The coexistence of these sequences indicates the presence of Poincaré chaos in the system [12–14]. Chaos was initially introduced in the Poincaré recurrence theorem [38], which states that certain dynamical systems in continuous time

will, after a sufficiently long but finite time, return to a state arbitrarily close to their initial state. Individual motions of the dynamics are Poisson stable. The final version of the theorem was proved using methods of measure theory in [39].

The motions of Poincaré chaotic dynamics [12–14] are Poisson stable and additionally equipped with an unpredictability property. In literature, sensitivity is defined by the change of motion due to the change of initial conditions. By focusing on a single trajectory, unpredictability defines sensitivity by the separation of motions starting with a small difference which converges to zero. It is demonstrated in Ref. [12] that the dynamics are sensitive, and consequently, all ingredients of chaos are present. Reconsidering the recurrence theorem under the condition of unpredictability is of strong interest to maximize its connection with chaotic dynamics.

Numerically, the sequence of convergence captures the moments in time when a single trajectory passes close to its initial state within a distance δ, a value that diminishes with each recurrence. Let's denote these time values in the sequence as t_n. If the same single trajectory start from times t_n and initial state (or the state at $t = 0$) separate from each other with a distance greater than Δ, which is a relatively large number, then the time values are recorded at the sequence of separation. The existence of both sequences demonstrates the sensitivity and inherently chaotic dynamics of a system. Consequently, if one mistakenly considers nearby points instead of the initial position of an orbit, an error larger than a specific number is guaranteed in subsequent observations of the dynamics, even though the initial mistake can be arbitrarily small. This motion is illustrated in Fig. (1.1).

The numerical degree of unpredictability arises from an algorithm designed to detect unpredictable motions within a dynamical system. It is defined as $min(\delta)/\Delta$, signifying how much the trajectory numerically converges to its initial point while maintaining a constant separation distance. The presence and intensity of unpredictability can be inferred from this numerical characteristic, with smaller values indicating stronger unpredictable trajectories [11].

The topology of uniform convergence on any compact subset of the real axis is employed to introduce unpredictable functions, utilizing the same dynamics that introduced Poisson functions in Ref. [15]. This study integrates chaos investigation into

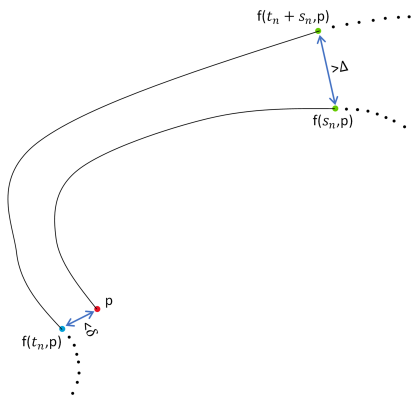

Figure 1.1: Illustration of unpredictability.

the theory of differential equations, as initiated in Refs. [16–19]. The detailed construction of an unpredictable function and its application to differential equations is presented in Ref. [15]. To outline the procedure, the construction begins with unpredictable sequences as motions of symbolic dynamics and the logistic map. Subsequently, an unpredictable function is determined through an improper convolution integral with a relay function.

The theoretical relationship between unpredictable motions and generalized synchronization is explored in a recent study [20]. This paper establishes that if the drive system has an unpredictable solution and generalized synchronization exists in the coupled system, then the response system must also have an unpredictable solution. The papers [11, 22–24] provide numerical support for this argument. Another noteworthy exploration of unpredictability is presented in the paper [21], which broadens the scope of unpredictable motions. The approach is highlighted as applicable to chaos synchronization research.

1.5 Delta synchronization of Poincaré chaos

Delta synchronization of Poincaré chaos is introduced in Ref. [11], rooted in the theory of unpredictability. Diverging from other synchronization methods, it does not emphasize a full synchronization of systems, or identical trajectories. Instead, it an-

alyzes the characteristic time values of unpredictability to demonstrate a unified dynamical behavior. Nevertheless, the specific conditions of delta synchronization lead to complete synchronization of unpredictability, implying fully synchronized motion. This coexists with other types of chaos synchronization [23, 24].

Let us consider two systems. The sequence of finite convergence captures the time values, u_n, for both systems, during which they simultaneously approach their initial state with a distance smaller than δ. If, starting from the initial time and u_n, the trajectories of both systems diverge concurrently, the time values of this separation constitute the common sequence of separation. These specific times characterize unpredictability, and it is established that they are sufficient to demonstrate the sensitivity of a system.

Numerically, 'finite' convergence implies that the distance between the trajectories at the recurrence, δ, does not approach zero sufficiently even over an extended simulation time. The case of numerically sufficient convergence represents a distinctive feature, termed as complete synchronization of unpredictability [11, 22–24]. While this special case still centers on the characteristic times of the trajectory, the coexistence of full synchronization and complete synchronization of unpredictability is demonstrated in Refs. [23, 24]. The theoretical analysis for delta synchronization is not yet developed except within the theory of unpredictability.

The primary advantage of the delta synchronization lies in its ability to detect both weak and strong synchronization patterns. Unlike other methods in the literature that rely on complete unison patterns, delta synchronization is capable of identifying partially synchronized dynamics between two systems. This is achieved by leveraging characteristic features of Poincaré chaos, enabling the detection of both subtle and robust synchronization patterns.

Synchronization strength refers to the dominance of synchronized patterns over the corresponding motions. The numerical degree of synchronization has been developed to detect the existence and strength of synchronization in systems. This feature also enables a comparison of synchronization strength across different parameter regimes of the systems. The effectiveness of the method requires a sufficiently long simulation time to reveal synchronized patterns. In this thesis, the corresponding time sequences

are presented in tables along with their numerical degrees of synchronization.

Delta synchronization is systematically compared to generalized and identical synchronization in the models presented in this thesis. The chosen models span different dynamical systems, including ordinary, partial, and delay differential equations. Notably, the delta synchronization method is versatile and applicable to various dynamical systems, irrespective of whether they are coupled or uncoupled.

The method has demonstrated its advantages over other synchronization methods in a range of models, including gas discharge semiconductor models with a simple fluid approach [11], extended fluid models of gas discharge systems [22], the Mackey-Glass model [23], and the Hindmarsh-Rose neural network [24].

1.6 Gas-discharge semiconductor model

Gas discharge plasmas play a crucial role in various industrial technologies and scientific applications [40–43]. Advancing our understanding of the fundamental physics underlying plasma processes is essential for progress in these fields. While experiments and numerical modeling serve as key points for enhancing this understanding, experimental investigations can be impractical in certain scenarios due to their cost and labor-intensive nature. Consequently, numerical modeling approaches become preferable in such situations [44].

Modeling gas discharge, however, presents challenges due to the large number of particles involved and the complexity of their interactions. The sheer scale makes it impractical to follow each particle individually. Instead, statistical descriptions are employed, involving the definition of probability distribution functions for each species of particles within the discharge medium. The time evolution of these functions is then described by the Boltzmann equation. Analytical solutions for the Boltzmann equation are feasible only for idealized models and within a limited range of conditions [44]. To address a broader range of scenarios, numerical modeling approaches have been developed and categorized into fluid models, kinetic (particle) models, and hybrid models. These numerical methods offer a more versatile means of tackling the complexities involved in gas discharge modeling across various conditions and

systems.

Fluid models are constructed from moments of the Boltzmann equation, which are obtained by multiplying the Boltzmann equation by powers of velocity and integrating over velocity space. The first three moments of the Boltzmann equation correspond to particle, momentum, and energy conservation, respectively. To simplify this reduced set of equations, a drift-diffusion approximation for fluxes is introduced in this study.

Fluid models can be categorized into two main approaches: the "simple fluid approach" and the "extended fluid approach." [44] The simple fluid approach relies solely on the first two moments of the Boltzmann equation. In this approach, transport and rate coefficients are dependent on the local value of the reduced electric field. This assumption is referred to as the local field approximation (LFA). To enhance the accuracy of the simple fluid model, the extended fluid model is introduced, incorporating the electron energy balance equation. This allows the definition of transport and rate coefficients as functions of the local mean energy, known as the local mean energy approximation (LMEA).

Fluid models offer the advantage of computational efficiency, making them suitable for conducting analyses and calculations involving geometrically complex, higher-dimensional scenarios, and intricate chemistry. However, their main disadvantage lies in their inability to provide high accuracy, as they do not treat particles at the kinetic level. For instance, fluid models cannot accurately capture nonlocal transport of electrons comprehensively [45]. As a result, they are more suitable for high-pressure discharges where nonlocal effects are not as crucial, as opposed to scenarios where such effects play a significant role [45].

In addition to the structures mentioned earlier, gas-discharge semiconductor systems (GDSSs) can exhibit a diverse range of temporal behaviors, including homogeneous stationary and oscillating modes, as well as chaotic behavior [46, 47]. Experimental investigations have identified the presence of homogeneous oscillations in a GDSS containing nitrogen gas [48]. These varied behaviors underscore the complex and dynamic nature that can emerge in GDSSs.

A well-established occurrence in gas discharge systems involves the onset of insta-

bility within the uniform steady state of an electric current-carrying medium. This phenomenon arises when the differential resistivity, denoted by the relationship between the applied voltage and discharge current, turns negative [49, 50]. Specifically, it occurs when an increase in current coincides with a decrease in voltage across the discharge. Consequently, the current-voltage characteristic (CVC) displays a segment with a negative slope, signifying the existence of negative differential resistivity (NDR) in the system. This scenario corresponds to the sub-normal glow regime situated between the Townsend discharge and the normal glow discharge phases within the classical glow discharge context. The NDR in this regime plays a crucial role in the emergence of instabilities and oscillations, frequently observed in gas discharges [51,52]. These instabilities have the potential to give rise to various structural patterns within the gas discharge, underscoring the intricate and dynamic nature of plasma behavior in this specific regime.

A one-dimensional simple fluid model is considered for synchronization investigation in this thesis, specifically examining temporal oscillations of plasma variables in the direction perpendicular to both the gas discharge and semiconductor layers, resulting in a transition between Townsend discharge and the normal glow discharge (referred to as the subnormal regime). Along the transverse dimension, the system demonstrates spatial homogeneity. Previous research, including works by Refs. [53–57], has delved into the transition of GDSSs from regular periodic behavior to fully chaotic states during subnormal oscillations. The unpredictable dynamics of the model is further explored in Ref. [11].

The primary focus of our investigation is on the regime characterized by chaotic oscillations. We establish unidirectional coupling between GDSSs to explore chaos synchronization. The unperturbed system is denoted as the drive system, with the discharge potential serving as a perturbation for the response system. Despite the coupled system, consisting of the drive and response systems, not exhibiting generalized synchronization as outlined by Ref. [53], our goal is to identify a more comprehensive form of synchronization. We have demonstrated that both the drive and response systems display delta synchronization of chaos (DSC). Utilizing the DSC method in the coupled system, we illustrate that the two models behave in harmony, characterized by a shared sequence of finite convergence and a sequence of separation

determined through numerical analysis [11].

To enhance the analysis of the semiconductor gas discharge system concerning chaos synchronization, a more realistic and advanced one-dimensional fluid model was developed, as outlined in [22]. This model, based on the extended fluid model or local mean energy approximation [58], was applied to the same system and the chaos synchronization is investigated in a manner similar to the simple fluid model. Although the specific details of this study are not covered in the current thesis, the results are briefly acknowledged due to their significance in the context of the delta synchronization method's development. This approach offers a more comprehensive understanding of the system's dynamics, and its findings can contribute to the refinement of delta synchronization techniques, as elaborated in the reference [22].

1.7 Mackey-Glass model

Several chronic and acute diseases manifest altered periodicity in observable symptoms. Examples include irregular breathing patterns observed in adults with Cheyne-Stokes respiration and fluctuations in peripheral white blood cell counts in chronic granulocytic leukemia. Prior to famous Mackey-Glass paper [59], theoretical studies on the control of respiration [60] and hematopoiesis [61] have linked disease processes to oscillatory instabilities within mathematically complex models. In Ref [59], the initiation of disease is linked to bifurcations in the dynamics of the first-order differential-delay equations, which model physiological systems. The study reveals that simple mathematical models of physiological systems anticipate the existence of periodic and aperiodic dynamic regimes, mirroring those observed in human disease. Referred to as the Mackey-Glass model, this model extends the work of Li and Yorke [37], May [62], May and Oster [63].

The model is also investigated in electronics. An analog electronic circuit is developed and examined in Ref. [64]. This circuit serves as a high-dimensional chaos generator and provides a tool for investigating chaos in infinite dimensional delay systems. Electronic circuit applications of Mackey-Glass model are also utilized in chaos synchronization research as in Refs. [65, 66].

Chaos synchronization is of utmost importance in the field of secure communication. The concept has been explored in the context of delay differential equations in the literature [67–69]. Additionally, the Mackey-Glass system offers a straightforward yet powerful tool for applications in secure communication [70, 71].

The Mackey-Glass model, a delay differential equation, exhibits chaotic behavior across various parameter regimes [59, 72]. Adjusting the delay time induces transitions from periodic to chaotic oscillations. This thesis comprehensively investigates this transition, showing the emergence of new periods and the dynamics behind it. The chaos analysis is substantiated by a bifurcation diagram. The unpredictable behavior of specific parameter regimes is demonstrated through sequences of convergence and separation, as well as the numerical degree of unpredictability [23].

Investigations into the synchronization behavior of unidirectionally coupled Mackey-Glass drive-response systems have been undertaken, with specific synchronization thresholds highlighted in previous studies [65, 73–76]. Notably, according to the findings in Ref. [75], generalized and complete synchronization in coupled systems are only achieved above a particular threshold of coupling parameter.

Furthermore, Ref. [73] delves into synchronization's existence when the coupling parameter surpasses a specific threshold, considering different delay times in the drive and response systems. Analytical and numerical insights into the relationship between synchronization thresholds and delay times are provided by Ref. [74]. Additionally, Ref. [76] conducts a comprehensive analysis of synchronization regimes and stability conditions for two linearly and nonlinearly coupled Mackey-Glass systems.

In the present thesis, we aim to explore the synchronized behavior of Mackey-Glass drive-response systems [23], employing parameters identical to those in Ref. [75] on both sides of the previously defined synchronization threshold. The assessment of synchronization behavior is conducted using the DSC. The primary motivation is to demonstrate the occurrence of synchronous chaotic behavior in drive-response Mackey-Glass systems, particularly within regions lacking generalized synchronization.

Previous research emphasizes the sensitivity of synchronization in these systems to

the coupling constant between the Mackey-Glass systems, leading to a distinct synchronization threshold. Consistent findings in prior studies indicate synchronization's presence on one side of this threshold and its absence on the other [65, 73–76]. Furthermore, evidence suggests the coexistence of both generalized and complete synchronization on the same side of the threshold [73, 75].

Our investigation demonstrated that synchronization can occur and be detected by the DSC method even below the synchronization threshold, where no synchronization was previously identified [23]. Furthermore, in the region where generalized synchronization is known to exist, we have discovered the coexistence of complete synchronization of unpredictability, a specific case of DSC. To substantiate our argument, we have rigorously analyzed the numerical characteristics of our method.

1.8 Hindmarsh-Rose neural network

The Hindmarsh-Rose neural model, introduced in the work by Hindmarsh and Rose [77], originated from the discovery of a unique cell in the brain of the pond snail Lymnaea. This cell, initially silent, exhibited a prolonged burst when depolarized by a short current pulse. A similar response was observed in various molluscan burst neurons that had been hyperpolarized to cease bursting, as reported in Ref. [78]. Continually hyperpolarized cells, when depolarized by a short current pulse, generated an action potential followed by a slow depolarizing after-potential. Burst discharges triggered by depolarizing current pulses have also been documented in crustaceans [79] and vertebrates [80].

To explain these phenomena, Hindmarsh and Rose introduced a small deformation to the narrow channel in their model, creating two additional equilibrium points. The resulting three equilibrium point model featured both a stable equilibrium point (silent state) and a stable limit cycle (repetitively firing state). The transition between these states could be triggered by a short current pulse. The introduction of a third and slower differential equation representing adaptation was found to terminate the discharge, producing either an isolated burst or a depolarizing after-potential, depending on parameter choices. Application of a steady depolarizing current to this model led

to periodic bursting. In the phase plane, these bursts were observed to be generated by the movement of one of the nullclines between a position with one equilibrium point and a position with three equilibrium points.

In a related work by Plant and Kim [81], a model of bursting, extending the Hodgkin-Huxley model [82], was discussed. The Hindmarsh-Rose model retained the main features of Plant and Kim's model but presented a simpler explanation of bursting using a two-dimensional phase plane. This simplicity facilitated a better understanding of interactions between bursting neurons.

The Hindmarsh-Rose model consists of three differential equations that capture different facets of a single neuron's behavior. These equations pertain to the neuron's membrane potential, the recovery variable responsible for fast ion transport, and the adaptation current [77]. The model has been a subject of extensive research, with investigations delving into various synchronization scenarios [83–88].

The significance of synchronization extends to studies of neural networks, particularly in the context of information exchange among neurons within an ensemble [89–91]. Its relevance becomes pronounced in the investigation of neurodegenerative diseases such as Alzheimer's and Parkinson's, where abnormal synchronization patterns in the brain have been observed [92, 93]. This emphasizes the crucial need to understand and quantify synchronization, presenting potential applications in both scientific inquiry and practical contexts.

Experimental evidence underscores the ability of external currents to induce chaotic behavior in neurons [94, 95]. Nevertheless, deterministic models often face challenges in capturing real-world scenarios due to inherent external perturbations, commonly referred to as noise. Previous studies have demonstrated that this noise can lead to synchronization in neural networks [96–101]. Our research aims to comprehend noise-induced synchronization within individual Hindmarsh-Rose neurons, employing innovative methods to explore this phenomenon more comprehensively.

In the realm of noise-induced synchronization, prior investigations have predominantly utilized Gaussian white noise, as evident in references [99–101]. In contrast, our study adopts a novel approach by examining synchronization within the

Hindmarsh-Rose model in the presence of Markovian noise. Noise terms characterized by Markov properties have diverse applications in various research domains [102–104]. In our research, we generate noise using Markov chains, ensuring adherence to the fundamental principles of Markov properties [105–107]. The methods employed for generating these noise terms are elaborated in Ref. [108], which introduces the concept of Markov coefficients in Duffing-type equations. The stochastic noise produced through these methods possesses a notable attribute—unpredictability [109].

The noise-induced synchronization research in this thesis [24] demonstrates the presence of delta synchronization of chaos in the absence of identical synchronization. Furthermore, it reveals complete synchronization of unpredictability beyond a certain threshold of noise intensity. The findings are supported by tables of corresponding sequences and numerical characteristics.

1.9 Contributions and Novelties

This thesis comprises four publications [11,22–24], which focus on the application of delta synchronization to gas-discharge semiconductor models [11, 22], the Mackey-Glass model [23], and the Hindmarsh-Rose neural network [24]. The contributions to the literature and the novelties introduced by these studies can be explained as follows:

Gas-discharge semiconductor systems [11, 22]:

- Conventional methods, such as generalized synchronization, prove inadequate in detecting unison patterns within unidirectionally coupled gas-discharge systems utilizing a simple fluid approach [53]. The effectiveness of generalized synchronization is tested in the model using the auxiliary system approach, and its absence is conclusively demonstrated.

- The numerical proof of unpredictable trajectories in phase space is established through sequences of convergence and separation, as well as the numerical degree of unpredictability.

- Delta synchronization of chaos is observed in the coupled systems, as evidenced by the accompanying tables and the numerical degree of synchronization.
- Similar results are obtained within the same model, utilizing a more realistic approach known as the extended fluid model. The outcomes of this study are mentioned briefly, but the detailed discussion is beyond the scope of this thesis.

Mackey-Glass delay systems [23]:

- The emergence of new periods and the transition to chaos are numerically explained for a specific parameter regime.
- The unpredictability of the model is demonstrated for a specific delay time, accompanied by corresponding tables and numerical characteristics.
- A unidirectionally coupled system is established, and a threshold distinguishing the regions possessing generalized synchronization from those with no synchronization is determined.
- Delta synchronization of chaos is observed below the threshold where generalized synchronization is absent.
- Above the threshold, the coexistence of complete synchronization of unpredictability and generalized synchronization is observed.

Hindmarsh-Rose neural network [24]:

- The chaotic regime is analyzed through interspike intervals and membrane potential, with the external current serving as a control parameter.
- A noise model is developed based on Markov chains and unpredictable functions, implemented in the uncoupled neurons to investigate noise-induced synchronization.
- Unpredictability for all non-zero noise intensities is demonstrated through the numerical degree of unpredictability.

- The existence of identical synchronization for high noise intensities is demonstrated.
- Delta synchronization is observed for non-zero values of noise intensity.
- Coexistence of complete synchronization of unpredictability with identical synchronization is detected.

The novel chaos synchronization method, delta synchronization of Poincaré chaos, is applied to four systems with diverse dynamics, including ordinary, partial, and delay differential equations. In contrast to conventional methods, delta synchronization emphasizes partially synchronized patterns characterized by time sequences of unpredictability. Therefore, in many systems, a unified chaotic dynamic cannot be detected by conventional methods. We demonstrate that these patterns are effectively detected by the delta synchronization method. Moreover, the special case of this approach, complete synchronization of unpredictability, can be classified as a strong-type synchronization, which generally coexists with conventional methods.

1.10 Organization of the thesis

This thesis focuses on the application of delta synchronization of Poincaré chaos to various models. The numerical method introduced as delta synchronization is rooted in the theory of unpredictability. In Chp. 2, theoretical foundations and the numerical implementation of unpredictability are discussed. Building upon this concept, the delta synchronization method is constructed, and definitions and algorithms related to these fields are presented in detail. Additionally, other synchronization methods applied in this thesis, namely generalized and identical synchronization, are also discussed in this chapter.

The application of delta synchronization to gas-discharge semiconductor models is discussed in Chp. 3. This chapter covers the construction of the system with governing equations and modeling approaches, explores the chaotic regime of the system, and examines the application of unpredictability. Using this information, a unidirectionally coupled system is constructed, and the existence of delta synchronization is

demonstrated in the absence of generalized synchronization.

Chp. 4 focuses on the synchronization of chaos in the Mackey-Glass system. The emergence of new periods and the transition to chaos are thoroughly investigated. Unpredictability is demonstrated for the coupled system. The synchronization threshold is analyzed for conventional methods, and the numerical proof of the existence of delta synchronization below the threshold and complete synchronization of unpredictability above it is provided.

Chp. 5 discusses noise-induced synchronization of Hindmarsh-Rose neurons. The chaotic regime is illustrated through interspike interval bifurcation diagrams and the dynamics of membrane potential under different external currents. Markovian noise, constructed based on Markov chains and unpredictable functions, is implemented in the model. While identical synchronization and complete synchronization of unpredictability are demonstrated for high noise intensity domains, the existence of delta synchronization for non-zero noise intensities, even for the lower values, is revealed.

The general results and common features of the models discussed in this thesis are summarized in Chp. 6.

CHAPTER 2

UNPREDICTABILITY AND SYNCHRONIZATION

2.1 Introduction

In this chapter, we will discuss unpredictability, its synchronization, and various chaos synchronization methods in the literature which are used in this thesis. These methods include generalized and identical synchronization. Unpredictability plays a crucial role in the study of chaos in dynamical systems [12–14]. This methodology relies on time sequences, which comprise convergence and separation events. Convergence moments are identified based on the Poincaré recurrence theorem[1], while separation instances record the deviations between trajectories originating from the initial state and the states at convergence moments [12].

Synchronization can be identified by examining commonalities in these sequences, as introduced in Ref. [11]. Delta synchronization of chaos occurs when unpredictable systems share sequences of finite convergence and separation. "Finite convergence" implies that the sequence does not numerically return to its initial state within a sufficiently long simulation. Conversely, complete synchronization of unpredictability is observed when the sequence numerically converges. To distinguish between these two phenomena, we will introduce numerical characteristics and conduct an analysis based on the number of elements in sequences.

Conventional methods have been developed for chaos synchronization [7, 10]. In this thesis, we will employ the approaches of generalized synchronization with an aux-

[1] Poincaré recurrence theorem asserts that certain dynamical systems eventually return to a state arbitrarily close to their initial state for continuous systems [38]. If the phase space volume of a dynamical system remains invariant, as is the case with Hamiltonian systems due to Liouville's theorem, and if the system has bounded trajectories, then, for every open set, orbits intersecting this set will do so infinitely often [110].

iliary system and identical synchronization [4, 5] for comparison with our methods. Studies have shown that delta synchronization of chaos can detect synchronization in specific domains where conventional methods may fail to do so [11, 22–24].

2.2 Unpredictability

The foundational work in mathematical dynamics, originally established by Poincaré [34] and further developed by Birkhoff [111], served as both a starting point and a cornerstone for subsequent explorations and comprehensive examinations of complex dynamics [36, 37, 62, 112, 113]. Poincaré investigated the concept of homoclinic chaos[2] [38], and a Poisson stable trajectory of a strange attractor, an attractor with a fractal structure, is discovered by Lorenz [36]. It's possible that Hilmy was the first to define a quasi-minimal set as the closure of the hull of a Poisson stable motion [114, 115]. In Ref. [115], there's a theorem by Hilmy stating the existence of an uncountable collection of Poisson stable trajectories within a quasi-minimal set. A modification of the Poisson stable points to unpredictable points was introduced in Ref. [12] such that the quasi-minimal set is chaotic.

Fig. (2.1) visualizes where unpredictability occurs as a recurrence. This figure illustrates various types of recurrent motions, including the conservative ones, as well as a novel addition: the unpredictable motion. In the diagram, irregularity increases from left to right, with the unpredictable motion being the most irregular of them all. It is distinctly chaotic, a characteristic that has been theoretically proven [12].

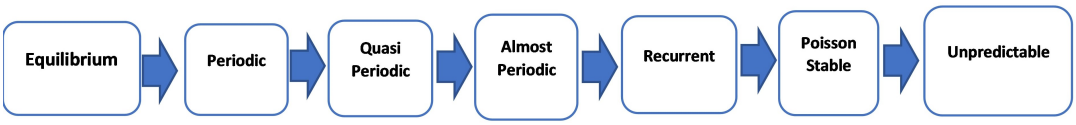

Figure 2.1: The types of recurrence

While this thesis primarily focuses on the numerical implementations of unpredictability, it's important to emphasize that the theoretical framework is constructed based on Refs. [12–14]. It is worth noting that the analysis of unpredictability and synchroniza-

[2] Homoclinic orbit is a trajectory including the intersection of the stable and unstable manifolds [38].

tion in dynamical systems of this study is exclusively carried out through numerical methods.

2.2.1 Theoretical Backgrounds

Let (X, d) be a metric space, where X is a set and d is a metric. $\mathbb{T}$ refer to either the set of real numbers or the set of integers. Then, conditions of a mapping $f : \mathbb{T} \times X \to X$ to be a flow on X are given as follows [116].

(i) $f(0, p) = p$ for all $p \in X$;

(ii) $f(t, p)$ is continuous in the pair of variables t and p;

(iii) $f(t_1, f(t_2, p)) = f(t_1 + t_2, p)$ for all $t_1, t_2 \in \mathbb{T}$ and $p \in X$.

If the conditions (i), (ii), (iii) are satisfied for a mapping $f : \mathbb{T}_+ \times X \to X$, where T_+ denote either the set of non-negative real numbers or the set of non-negative integers, then the mapping is a semi-flow on X [116].

Let f be a flow on X and a point $p \in X$. Also suppose that $\mathcal{U}$ is any neighborhood of p. Then, Poisson stability can be defined for $H_1 > 0$ and $H_2 < 0$ as follows [115].

(i) p is positively Poisson stable if there exists $t \geq H_1$ such that $f(t, p) \in \mathcal{U}$.

(ii) p is negatively Poisson stable if there exists $t \leq H_2$ such that $f(t, p) \in \mathcal{U}$.

(iii) p is Poisson stable if it is both positively and negatively Poisson stable.‘

Let the closure of the trajectory $\mathcal{T}(p) = \{f(t, p) : t \in \mathbb{T}\}$ be denoted by Ω_p for a fixed $p \in X$, i.e., $\Omega_p = \overline{\mathcal{T}(p)}$. The conditions for Ω_p to be a quasi-minimal set are given as follows [115].

(i) p is a Poisson stable point.

(ii) $\mathcal{T}$ is contained in a compact subset of X.

For the positive semi-trajectory $\mathcal{T}^+(p) = \{f(t,p) : t \in \mathbb{T}_+\}$ through p, the closure is $\Omega_p^+ = \overline{\mathcal{T}^+(p)}$. The following theorem is stated in Ref. [114] and can be proved by the methods given in Refs. [114, 115].

Theorem 1. *[12] Suppose that $p \in X$ is positively Poisson stable and $\mathcal{T}^+(p)$ is contained in a compact subset of X. If Ω_p^+ is neither a rest point (fixed point) nor a cycle, then Ω_p^+ contains an uncountable set of motions everywhere dense and positively Poisson stable.*

The following analysis of unpredictability includes semi-flows, but it is also valid for flows. The definition of unpredictability can be given as follows.

Definition 1. *[12] The trajectory through a point $p \in X$ and the point itself are unpredictable if there exists a positive number Δ and the sequences of convergence t_n and separation s_n, both of which diverge to infinity, such that $\lim_{n\to\infty} f(t_n,p) = p$ and $d[f(s_n, f(t_n,p)), f(s_n,p)] \geq \Delta$ for each natural number n.*

The definition of unpredictability states that if, by mistake, a neighboring point $f(t_n,p)$ is chosen instead of the point p, then the distance between these points will satisfy the inequality $d[f(s_n, f(t_n,p)), f(s_n,p)] \geq \Delta$. This illustrates the sensitivity of motion when considering a single trajectory. However, in well-known studies [34–38, 113], sensitivity is often regarded as a property of a system with a specific set of initial data, involving the comparison of the behavior of at least a couple of solutions.

Let's state the following lemmas.

Lemma 1. *[12] If $p \in X$ is an unpredictable point, then $\mathcal{T}_+(p)$ is neither a rest point nor a cycle.*

Proof. [12] Let the number Δ and the sequences t_n, s_n be as in Def. 1. Suppose that there exists a positive number w such that $f(t+w,p) = f(t,p)$ for all $t \in \mathbb{T}_+$. Due to the continuity of $f(t,p)$, there exists a positive number δ such that if $d[p,q] < \delta$ and $0 \leq t \leq w$, then $d[f(t,p), f(t,q)] < \Delta$. Let's fix a natural number n such that $d[f(t_n,p),p] < \delta$. One can find an integer m and a number w_0 satisfying $0 \leq w_0 \leq w$ such that $s_n = mw + w_0$. Then,

$$d[f(s_n, f(t_n,p)), f(s_n,p)] = d[f(w_0, f(t_n,p)), f(w_0,p)] < s_n\,.$$

However, this contradicts with the following equation from the Def. 1.

$$d[f(s_n, f(t_n, p)), f(s_n, p)] = d[f(t_n + s_n, p), f(s_n, p)] \geq s_n \,.$$

Therefore, $\mathcal{T}_+(p)$ is neither a rest point nor a cycle. □

Lemma 2. *[12] If a point $p \in X$ is unpredictable, then every point of the trajectory $\mathcal{T}^+(p)$ is also unpredictable.*

Proof. [12] Let the number Δ and the sequences t_n, s_n be as in Def. 1. Fix an arbitrary point $q \in \mathcal{T}^+(p)$ such that $q = f(\bar{t}, p)$ for some $\bar{t} \in \mathbb{T}_+$. Then, one can verify that

$$\lim_{n\to\infty} f(t_n, q) = \lim_{n\to\infty} (t_n + \bar{t}, p) = \lim_{n\to\infty} f(\bar{t}, f(t_n, p)) = f(\bar{t}, p) = q \,.$$

Now, select a natural number n_0 such that $s_n > \bar{t}$ for each $n \geq n_0$. Let us denote $k_n = s_n - \bar{t}$; then, for $n \geq n_0$, we have

$$\begin{aligned} d[f(t_n + k_n, q), f(k_n, q)] &= d[f(t_n + k_n, f(\bar{t}, p)), f(k_n, f(\bar{t}, p))] \\ &= d[f(t_n + s_n, p), f(s_n, p)] \\ &\geq \Delta \,. \end{aligned}$$

It is evident that $k_n \to \infty$ as $n \to \infty$. Consequently, the point q is unpredictable. □

Remark 1. *The constant Δ is uniform across all points on an unpredictable trajectory.*

Refs. [35,36] states that dynamics on a set $L \subseteq X$ is sensitive if there exists a positive number Δ such that for each $l \in L$ and each positive number δ there exist a point $l_\delta \in L$ and a positive number s_δ such that $d[l_\delta, l] < \delta$ and $d[f(s_\delta, l_\delta), f(s_\delta, l)] \geq \Delta$.

Theorem 2. *[12] The dynamics on Ω_p^+ is sensitive if $p \in X$ is an unpredictable point.*

Proof. Let $\Delta > 0$ denote the unpredictability constant corresponding to the point p. Consider an arbitrary positive number δ, and take a point $r \in \Omega_p^+$.

Firstly, let's examine the case where $r \in \mathcal{T}^+(p)$. According to lemma 2, there exist sequences t_n and s_n diverging to infinity such that $\lim_{n\to\infty} f(t_n, r) = r$ and $d[f(t_n +$

$s_n, r), f(s_n, r)] \geq \Delta$ for each n. Fix a natural number n_0 such that $d[f(t_{n_0}, r), r] < \delta$. In this case, the inequality $d[f(s_{n_0}, f(t_{n_0}, r)), f(s_{n_0}, r)] \geq \Delta$ holds.

Now, suppose that $r \in \Omega_p^+ \setminus \mathcal{T}^+(p)$. One can find a sequence η_m, $\eta_m \to \infty$ as $m \to \infty$, such that $\lim_{m\to\infty} f(\eta_m, p) = r$. According to lemma 2, for each $m \in \mathbb{N}$, there exist sequences u_n and v_n diverging to infinity such that $\lim_{n\to\infty} f(u_n^m, f(\eta_m, p)) = f(\eta_m, p)$ and $d[f(v_n^m, f(u_n^m, f(\eta_m, p))), f(v_n^m, f(\eta_m, p))] \geq \Delta$ for $n \in \mathbb{N}$.

Let m_0 be a natural number such that $d[f(\eta_{m_0}, p), r] < \delta/2$. Suppose that there exists a natural number n_1 such that

$$d[f(v_{n_1}^{m_0}, f(\eta_{m_0}, p)), f(v_{n_1}^{m_0}, r)] \geq \Delta/2 .$$

If this is the case, sensitivity is proved. Otherwise, choose $n_2 \in \mathbb{N}$ satisfying

$$d[f(u_{n_2}^{m_0}, f(\eta_{m_0}, p), f(\eta_{m_0}, p))] < \delta/2$$

so that

$$d[f(u_{n_2}^{m_0}, f(\eta_{m_0}, p)), r] \leq d[f(u_{n_2}^{m_0}, f(\eta_{m_0}, p), f(\eta_{m_0}, p))] + d[f(\eta_{m_0}, p), r] < \delta .$$

It can be confirmed that

$$\begin{aligned} &d[f(v_{n_2}^{m_0}, f(u_{n_2}^{m_0}, f(\eta_{m_0}, p))), f(v_{n_2}^{m_0}, r)] \geq \\ &d[f(v_{n_2}^{m_0}, f(u_{n_2}^{m_0}, f(\eta_{m_0}, p))), f(v_{n_2}^{m_0}, f(\eta_{m_0}, p))] - d[f(v_{n_2}^{m_0}, f(\eta_{m_0}, p)), f(v_{n_2}^{m_0}, r)] \\ &> \Delta/2 \end{aligned}$$

Therefore, the theorem is proved. □

For an unpredictable point p, existence of sensitivity in the set Ω_p^+ has been proven in theorem (2). A similar proof for a flow f can be used to verify the sensitivity in Ω_p.

Based on the aforementioned lemmas and theorems, following definition is proposed.

Definition 2. *The dynamics on the quasi-minimal set Ω_p is called Poincaré chaotic if p is an unpredictable point.*

Thus, chaos originates from a single function, extending the spectrum of possibilities beyond equilibrium, periodic, quasi-periodic, almost periodic, recurrent functions, and Poisson stable motion to include unpredictable motion as a new element.

2.2.2 Numerical Implementation

The numerical existence of unpredictability is demonstrated in various models, as seen in Refs. [11, 22–24]. This method relies on identifying sequences of convergence and separation within a model, requiring a sufficiently long simulation time to accumulate an adequate amount of data.

Let's elaborate on Def. (1), which will be applied numerically to the corresponding models in this thesis. In Def. (1), each return of a trajectory to its initial state is denoted by n. We introduce a non-increasing sequence, δ_n, which represents the maximum possible distance between the initial point p and $f(t_n, p)$, satisfying $d[p, f(t_n, p)] \leq \delta_n$.

Then, we define the moments t_n that meet the conditions $d[p, f(t_n, p)] \leq \delta_n$ and $\lim_{n\to\infty} f(t_n, p) = p$ as the sequences of convergence. These moments represent when trajectories return close to their initial state.

On the other hand, the sequence of separation, denoted as s_n, comprises moments that satisfy $d[f(s_n, f(t_n, p)), f(s_n, p)] \geq \Delta$. These moments capture the times at which trajectories, starting from p and $f(t_n, p)$, diverge from each other. Corresponding illustration is given in Fig. (1.1)

In addition to existence of the sequences, a numerical characteristic called degree of numerical unpredictability to measure the strength and presence of unpredictability have been developed and applied various models [11, 22–24]. This degree of numerical unpredictability, denoted as α_k for a finite number k, is defined as follows:

$$\alpha_k = \frac{min_{1,2,\ldots,k}\delta_n}{\Delta}\,. \tag{2.1}$$

The unpredictability of the motion is confirmed when α_k has a small value that converges to zero as k becomes larger. Numerically, smaller α_k values indicate stronger chaotic behavior. This can be illustrated using the following analogy: If the simulation begins with a point arbitrarily close to the initial point, $f(t_n, p)$, rather than the initial point, $f(0, p)$, the error can be expressed as $1/\alpha_k$. Therefore, a smaller α_k implies a stronger degree of chaos.

It's important to note that in numerical simulations, the number of elements in the

sequence of convergence t_n and the sequence δ_n are both equal to n. However, the number of elements in the sequence of separation does not necessarily have to be n. This discrepancy can occur when the time values in t_n approach the total simulation time, causing the simulation to end before the trajectory diverges. In Equation (2.1), k represents the number of elements in the sequence of separation.

Consider a differential equation $\dot{x} = f(x)$. Let the simulation of this equation be in a time domain $T \in [T^i, T^f]$ with the time difference ΔT. The algorithm for unpredictability, as described in [22, 24], is provided in Algorithm (1).

In this algorithm, δ, $\Delta\delta$, and Δ are constants that must be chosen based on the scale of the motion. δ should be a small number, while a large number Δ satisfies $\Delta \gg \delta$. The decrement of δ at each iteration is indicated by $\Delta\delta$. The algorithm finds the corresponding values of t_n, s_n, δ_n and the degree of numerical unpredictability α. It is important to note that if the numbers of elements of t_n and s_n are not same, the 21st. line should take the last δ_n value at which s_n exists.

Transient time should not be considered in the algorithm. Then, the existence of the sequences in which the time values cover the entire simulation, and small α value confirms the unpredictability in a model.

This algorithm is versatile and applicable to various types of differential equations. It has been successfully applied to ordinary and partial differential equations in Ref. [11, 22, 24], and to delay differential equations in Ref. [23]. The dimension of the differential equations, denoted by d, must satisfy $d \geq 1$. Additionally, the unpredictability can be applied to stochastic systems, as demonstrated in Ref. [24].

2.3 Synchronization through Unpredictability

Unpredictability analysis centers around two key sequences: sequences of convergence and separation. Each time a trajectory returns to its initial state, these sequences capture the moments of convergence and divergence. These sequences are sufficient to demonstrate chaotic behavior over an extended simulation.

Similarly, synchronization of chaos among dynamical systems can be detected using

Algorithm 1: Algorithm for Unpredictability

```
Input: δ
Input: Δδ
Input: Δ
n = 0;
q = 0;
for T = T^i + ΔT : ΔT : T^f do
    if ‖x(T) − x(T^i)‖ < (δ − n ∗ Δδ) then
        n = n + 1;
        t_n = T    % Sequence of convergence;
    end
end
δ_last = δ − n ∗ Δδ;
for T = T^i + ΔT : ΔT : T^f do
    for i = 1 : 1 : n do
        if ‖x(t_i + T) − x(T)‖ > Δ then
            if T > q then
                s_i = T    % Sequence of separation;
                q = T;
                break;
            end
        end
    end
end
α = δ_last / Δ    % Degree of numerical unpredictability
```

a similar analysis. For each return of a trajectory to its initial state, the essential time values for synchronization are the same as those used in the unpredictability analysis, specifically the moments of convergence and divergence.

In contrast, other synchronization methods in the literature, such as generalized, identical, and phase synchronization, focus on fully synchronized systems where corresponding parameters follow precisely the same trajectory. One drawback of these methods is that they conclude no synchronization at all when fully synchronized systems are absent. However, unpredictability characterizes chaos primarily by the significant moments of a trajectory, and synchronization of these moments reveals chaos synchronization.

Let the unidirectionally coupled systems be given as

$$\dot{x} = f(x)\,, \tag{2.2a}$$

$$\dot{y} = g(y, h(x))\,, \tag{2.2b}$$

where these two systems, (2.2a) and (2.2b), are called drive and response systems[3], respectively. Suppose that both systems have unpredictable solutions. Then, definition of delta synchronization of chaos, as in [11, 22–24], can be given as follows.

Definition 3. *[11] The systems 2.2a and 2.2b with unpredictable motions $x(t)$ and $y(t)$ admit the delta synchronization of chaos, if there exist positive numbers $\delta, \Delta_1, \Delta_2$, for $\delta < \Delta_{1,2}$, the sequence of finite convergence u_n and sequence of separation v_n such that $\|x(u_n) - x(0)\| + \|y(u_n) - y(0)\| = \delta_n \leq \delta, \quad \|x(u_n + v_n) - x(v_n)\| \geq \Delta_1$ and $\|y(u_n + v_n) - y(v_n)\| \geq \Delta_2, n = 1, 2, \ldots$.*

Here, the distance is computed by the Euclidean norm $\|.\|$. The definition contains two Δ values, which are Δ_1 and Δ_2 corresponding to systems (2.2a) and (2.2b), respectively. To establish the presence of DSC, the values Δ_1 and Δ_2 are set equal to the values used in the unpredictability analysis.

For DSC to exist, two conditions must be met. First, there must be u_n values that satisfy the inequality $\|x(u_n) - x(0)\| + \|y(u_n) - y(0)\| = \delta_n \leq \delta$, where δ decreases

[3] For the analysis of synchronization through unpredictability, systems (2.2a) and (2.2b) do not have to be unidirectionally coupled. They can be bidirectionally coupled or uncoupled as well. In those cases, the following definition, algorithm and analysis do not change.

for each n. Then, the presence of v_n values that simultaneously satisfy the inequalities $\|x(u_n + v_n) - x(v_n)\| \geq \Delta_1$ and $\|y(u_n + v_n) - y(v_n)\| \geq \Delta_2$ demonstrates the existence of DSC.

In the context of DSC, synchronization doesn't necessitate $\lim_{n\to\infty} \delta_n = 0$. Instead, we refer to u_n as a sequence of *finite* convergence. However, sequence of finite convergence should encompass moments spanning the entire simulation, not just a portion of it. The presence of both u_n and v_n confirms the system exhibits DSC.

The finite convergence property of DSC categorizes it as a form of weak synchronization. Notably, in numerical simulations, the sequences used for unpredictability analysis always have more elements than those for DSC due to this finite convergence. However, this unique feature gives our method the ability to detect weak synchronization patterns that other methods may miss.

In various studies [11, 22, 23], the presence of DSC has been observed in regions where generalized synchronization does not exist. These models involve drive-response systems, for which the auxiliary systems method does not confirm generalized synchronization. A similar phenomenon is seen in Ref. [24], which explores noise-induced synchronization. In this case, identical synchronization is compared to DSC, and the results demonstrate that DSC exists even when identical synchronization is absent.

A special form of the DSC, known as complete synchronization of unpredictability, differentiate from the DSC with its complete convergence. In this type, the convergence of u_n series is evident, leading to δ_n approaching zero as n becomes large in numerical simulations.

Complete synchronization of unpredictability has been observed in regions where other synchronization methods like generalized and identical synchronization exist [23, 24]. Furthermore, numerical studies reveal that complete synchronization of unpredictability features sequences with a number of elements that are nearly equal to the number of elements in the unpredictability sequences.

Additionally, a unique numerical characteristic of DSC, termed the degree of numerical synchronization, can be defined to indicate the presence and strength of synchro-

nization [11]. It is calculated as follows.

$$\alpha_k^{sync} = \frac{\delta_k}{min(\Delta_1, \Delta_2)} \,. \tag{2.3}$$

DSC is confirmed for $\alpha_k^{sync} < 1$ with sufficiently large sequences u_n and v_n covering the entire simulation. Smaller α_k^{sync} indicates stronger synchronization since smaller values imply more common time values in the sequence of finite convergence and separation. Complete synchronization of unpredictability is achieved when $\alpha_k^{sync} \to 0$ as $k \to \infty$.

Let the Equations (2.2a) and (2.2b) be numerically solved in a time domain $T \in [T^i, T^f]$ with the time difference ΔT. The synchronization through unpredictability can be applied to the systems simultaneously by using Algorithm (2).

The values δ and $\Delta\delta$ must be common in unpredictability analyses of Eqs. (2.2a) and (2.2b), and the synchronization analysis of unpredictability. For consistency, the values Δ_1 and Δ_2 must come from the unpredictability analyses of Eqs. (2.2a) and (2.2b), respectively. As in the numerical unpredictability analysis, if the numbers of elements of t_n and s_n are not same, the 21$^{\text{st.}}$ line should take the last δ_n value that s_n exists.

In Algorithm (2), the conditions at the at 4$^{\text{th.}}$ and 12$^{\text{th.}}$ lines define the process of identifying sequences of finite convergence and separation, as per Def. (3). According to the algorithm, the time values found in synchronization analysis do not have to be contained in the unpredictability sequences.

Numerical studies have shown that these values can differ for coupled systems [11, 22, 23], whereas they tend to be identical for uncoupled systems [24]. The reason is even though driven systems differentiate from drive systems by a small perturbation and synchronization still occurs, this small difference leads to a slight time disparity between the elements of sequences in unpredictability and synchronization analyses. In contrast, uncoupled systems involve two identical systems initiated with different initial conditions, resulting in no observable difference in these models.

The method has been numerically tested on various models. However, although the

numerical implementation based on the Algorithm (2) can be easily implemented in the corresponding models, theoretical aspects of the method have not been developed yet.

Algorithm 2: Algorithm for Delta Synchronization of Chaos

```
Input: δ
Input: Δδ
Input: Δ_1
Input: Δ_2
n = 0;
q = 0;
for T = T^i + ΔT : ΔT : T^f do
    if ‖x(T) − x(T^i)‖ + ‖y(T) − y(T^i)‖ < (δ − n ∗ Δδ) then
        n = n + 1;
        u_n = T    % Sequence of finite convergence;
    end
end
δ_last = δ − n ∗ Δδ;
for T = T^i + ΔT : ΔT : T^f do
    for i = 1 : 1 : n do
        if ‖x(u_i + T) − x(T)‖ > Δ_1 && ‖y(u_i + T) − y(T)‖ > Δ_2 then
            if T > q then
                v_i = T    % Sequence of separation;
                q = T;
                break;
            end
        end
    end
end
α^sync = δ_last / min(Δ_1, Δ_2)    % Degree of numerical synchronization
```

2.4 Identical Synchronization

Identical synchronization analyze the phenomenon between systems initiated with different sets of initial conditions [7]. Let two systems be given as follows.

$$\dot{x} = f(x)\,, \tag{2.4a}$$

$$\dot{y} = g(y, x)\,, \tag{2.4b}$$

where Equations (2.4a) and (2.4b) are drive and response systems, respectively. The variable y of the response system can be subjected to continuous control or to replacement of variables such as decomposition of drive system into subsystems and using the new variables.

Identical synchronization between these systems occurs if there are sets of initial condition $I_x \subset \mathbb{R}^d$ for the drive and $I_y \subset \mathbb{R}^r$ for the response, such that for all $x(0) \in I_x$ and $y(0) \in I_y$

$$\lim_{t\to\infty} \|y(t) - x(t)\| = 0\,. \tag{2.5}$$

If the same initial conditions are chosen for the drive and response systems, synchronization will occur such that $x(t) = y(t)$ for all $t > 0$. The stability of the synchronization can be tested by conditional Lyapunov exponents.

Let the difference between the drive and response systems be $\delta(x, y) \equiv y - x \neq 0$. Then, evolution of $\delta(x, y)$ in time can be given as follows.

$$\dot{\delta}(x, y) = g(y, x) - f(x)\,. \tag{2.6}$$

Asymptotically stable synchronization is achieved if the all Lyapunov exponents of Equation (2.6) are negative for $y = x$. Since these Lyapunov exponents are computed for a particular state of the drive system, Eq. (2.6), they are called conditional Lyapunov exponents.

These Lyapunov exponents can be calculated by linearizing Equation (2.6) around the synchronized state $y = x$,

$$\dot{\delta}(x, y) = J(x)\delta(x, y)\,, \tag{2.7}$$

with the Jacobian

$$J(x) = \left.\frac{\partial g(y, x)}{\partial y}\right|_{y=x}\,, \tag{2.8}$$

of response system vector field. Subsequently, procedures to find Lyapunov exponents are fallowed, and stability of synchronization is determined [7]. Alternatively, Lyapunov functions [7] can be used to determine the stability of the synchronization instead of Lyapunov exponents [117].

2.5 Generalized synchronization

Identical synchronization is considered when the response is identical or nearly identical to the drive system. On the other hand, generalized synchronization is a tool for studying the synchronization of nonidentical chaotic systems. Systems amenable to generalized synchronization can be classified into two categories:

1. Similar Nature Systems: In this case, the systems share the same underlying physical structure but exhibit individual differences. For instance, the drive and response systems may both be electric circuits, but they have distinct element values (e.g., capacitance, resistance) in each system.

2. Different Nature Systems: Here, the systems have different physical structures or designs. For example, both the drive and response systems could be electric circuits, but with distinct circuit designs. Additionally, systems can differ conceptually, such as biological neurons and optical devices.

Let a unidirectionally coupled system be given as follows.

$$\dot{x} = f(x)\,, \tag{2.9a}$$

$$\dot{y} = g(y, h(x))\,, \tag{2.9b}$$

where these two equations, (2.9a) and (2.9b), define drive and response systems, respectively. Generally, $x(t) = y(t)$ is not achieved for all t due to the different nature of the drive and response systems. However, synchronization can still be achieved for nonidentical systems since the dynamic of the response can be completely predicted by the drive. This is known as the generalized synchronization [3].

Generalized synchronization is achieved if the initial condition sets I_x and I_y exist

such that $x(0) \in I_x$ and $y(0) \in I_y$, and the following condition is satisfied

$$\lim_{t\to\infty} \|y(t) - \phi[x(t)]\| = 0\,, \tag{2.10}$$

with $\phi[x(t)]$ a functional determining the phase space trajectory of $y(t)$ from the trajectory of $x(t)$ [7]. When the functional is identity, $\phi[x(t)] = x(t)$, identical synchronization is recovered.

Detecting generalized synchronization can be challenging in various situations, leading to the development of specific criteria and algorithms for this purpose. There are three primary methods for identifying generalized synchronization [7]:

- Analyses of conditional Lyapunov exponents [4].
- Application of the auxiliary system approach [5].
- Utilization of statistical predictability estimations [3].

The auxiliary system approach is considered and utilized in this thesis. It relies on the predictability aspect of synchronization, which means that if two identical replicas of the response systems, starting from distinct initial conditions within the synchronization basin of attraction, are both influenced by the same drive system, they should ultimately reach the same state once transient behaviors have subsided. To achieve this, the auxiliary system approach involves employing an extra response system that mirrors the original response system and operates independently of it.

Let us call the identical copy of the response system given in Equation (2.9b) auxiliary system and denote it by $y'(t)$. For $x_0 \in I_x$ and $y(0), y'(0) \in I_y$, the condition for the generalized synchronization can be given as follows.

$$\lim_{t\to\infty} \|y(t) - y'(t)\| = 0\,, \tag{2.11}$$

which is called the asymptotic stability condition. This condition is examined after the transient regime in the numerical simulations.

Numerically, parametric plots of the auxiliary system versus the can be a test to observe the presence of generalized synchronization. If the motion takes place on $y(t) = y'(t)$ line, existence of the generalized synchronization is confirmed.

CHAPTER 3

DELTA SYNCHRONIZATION OF POINCARÉ CHAOS IN GAS DISCHARGE-SEMICONDUCTOR SYSTEMS

3.1 Introduction

A gas discharge semiconductor system (GDSS) is a plasma system that combines gas discharge with a high-ohmic semiconductor barrier. In this study, a one-dimensional fluid model using the drift-diffusion approximation is being discussed. This model considers only electrons and ions as plasma species. In the existing literature, this particular GDSS model is referred to as a simple fluid model or a local field approximation [45, 118–120]. It focuses primarily on ionization processes that occur in regions with weak electric fields within the discharge gap. Despite its omission of non-local ionization effects, this model can still provide a qualitative understanding of the fundamental behaviors of discharge systems.

Since our model is one-dimensional, temporal oscillations of plasma variables between Townsend discharge and the normal glow discharge (i.e., subnormal regime) occur only along the direction perpendicular to the gas discharge and semiconductor layers. In the transverse dimension, the system exhibits spatial homogeneity. Previous literature [53–57] has investigated the transition of GDSSs from regular periodic behavior to fully chaotic states in subnormal oscillations.

In this study, our focus is on the regime where chaotic oscillations occur. We establish unidirectional coupling between GDSSs to explore chaos synchronization. The unperturbed system is referred to as the drive system, and we use the discharge potential of the drive system as a perturbation for the response system. Although the coupled system (comprising the drive and response systems) does not exhibit gener-

alized synchronization as indicated by [53], our aim is to identify a more general form of synchronization. We have demonstrated that both the drive and response systems exhibit Delta Synchronization of Chaos (DSC). By employing the DSC method in the coupled system, we show that the two models behave in unison, characterized by a common sequence of finite convergence and a sequence of separation that we have numerically determined. The research related to this chapter is published in Ref. [11].

3.2 Fluid Modeling of Plasma

Velocity distribution function $f(\mathbf{r}, \mathbf{v}, t)$ can be used for the description of plasma species. The function yields the probability of finding particles at a specific position and velocity of a six dimensional phase space $(\mathbf{r}, \mathbf{v})$ [44, 121]. According to the kinetic theory of plasmas, the Boltzmann equation is employed to describe the time evolution of $f(\mathbf{r}, \mathbf{v}, t)$ under the influence of external forces.

The kinetic Boltzmann[1] equation can be given as

$$\frac{\partial f_j}{\partial t} + \boldsymbol{\nabla}_{\mathbf{r}} \cdot \mathbf{v} f_j + \frac{q_j}{m_j} \boldsymbol{\nabla}_{\mathbf{v}} \cdot [(\mathbf{E} + \mathbf{v} \times \mathbf{B}) f_i] = \sum_k C_k f_k \,, \tag{3.1}$$

where each plasma species are represented as j. The quantity of particles within the volume $d\mathbf{r}d\mathbf{v}$ can be determined using the expression $f_j d\mathbf{r}d\mathbf{v}$. In this context, $\mathbf{E}$ and $\mathbf{B}$ denote the local electric and magnetic fields, respectively. The particle's charge and mass are represented as q_j and m_j, respectively. Any elastic or inelastic collisions experienced by a particle are described by the operator C_k corresponding to the species k.

Due to the computational inefficiency of solving the Boltzmann equation directly, Eq.(3.1) can be multiplied by the velocity $\mathbf{v}$ with different power orders and can be integrated along the velocity instead. The resulting equations, corresponding to different orders of velocity power, yield moments of the Boltzmann equation. These moments and functional integrals are used to define macroscopic quantities such as plasma particle number density, velocity, and energy. As in Ref. [44], these equations are then coupled with Maxwell's equations to establish a self-consistent plasma fluid theory.

[1] Vectors are represented by bold characters.

The zeroth order moment of the Boltzmann equation can be obtained by multiplying Eq.(3.1) by $\mathbf{v}^0 = 1$ and integrating over the velocity as follows.

$$\int \frac{\partial f_j}{\partial t}\,\mathrm{d}\mathbf{v} + \int \boldsymbol{\nabla}_{\mathbf{r}} \cdot \mathbf{v} f_j\,\mathrm{d}\mathbf{v} + \frac{q_j}{m_j}\int \boldsymbol{\nabla}_{\mathbf{v}} \cdot [(\mathbf{E} + \mathbf{v} \times \mathbf{B}) f_j]\,\mathrm{d}\mathbf{v} = \int \sum_k C_k f_k\,\mathrm{d}\mathbf{v}\,. \tag{3.2}$$

Let us introduce the particle density,

$$n_j(\mathbf{r}, t) = \int f_j(\mathbf{r}, \mathbf{v}, t)\,\mathrm{d}\mathbf{v}\,, \tag{3.3}$$

and the average fluid velocity,

$$\langle \mathbf{v} \rangle = u_j(\mathbf{r}, t) = \frac{1}{n_j(\mathbf{r}, t)} \int \mathbf{v} f_j(\mathbf{r}, \mathbf{v}, t)\,\mathrm{d}\mathbf{v}\,. \tag{3.4}$$

The following term vanishes by the Gauss theorem.

$$\frac{q_j}{m_j}\int \boldsymbol{\nabla}_{\mathbf{v}} \cdot [(\mathbf{E} + \mathbf{v} \times \mathbf{B}) f_j]\,\mathrm{d}\mathbf{v} = 0\,. \tag{3.5}$$

We can see this by separating the equation as follows [121].

$$\int (\mathbf{E} \cdot \boldsymbol{\nabla}_{\mathbf{v}}) f_j d\mathbf{v} = \int \boldsymbol{\nabla}_{\mathbf{v}} \cdot (f\mathbf{E}) d\mathbf{v} = \oint_{S_v} f\mathbf{E} \cdot d\mathbf{s}_v = 0\,, \tag{3.6}$$

The reason last term vanishes is that while the surface area increases as v^2, all physical distributions approaches zero faster such as Maxwellian distribution which approaches zero as e^{-v^2}.

The second term of Eq. (3.5) vanishes as follows.

$$\begin{aligned}\int ((\mathbf{v} \times \mathbf{B}) \cdot \boldsymbol{\nabla}_{\mathbf{v}}) f_j d\mathbf{v} &= \int \boldsymbol{\nabla}_{\mathbf{v}} \cdot (f(\mathbf{v} \times \mathbf{B})) d\mathbf{v} - \int f \boldsymbol{\nabla}_{\mathbf{v}} \cdot (\mathbf{v} \times \mathbf{B}) d\mathbf{v} \\ &= \oint_{S_v} f(\mathbf{v} \times \mathbf{B}) \cdot d\mathbf{s}_v - \int f \boldsymbol{\nabla}_{\mathbf{v}} \cdot (\mathbf{v} \times \mathbf{B}) d\mathbf{v} = 0\end{aligned} \tag{3.7}$$

Here, first integral vanishes as in Eq. (3.6). The second integral also vanishes since $(\mathbf{v} \times \mathbf{B})$ is perpendicular to $\boldsymbol{\nabla}_{\mathbf{v}}$.

Let $S_j = \sum_k n_k \langle C_k \rangle$, which represents the inelastic collisions influencing the population of species. Then, as in Ref. [44], Eq.(3.2) becomes

$$\frac{\partial n_j}{\partial t} + \boldsymbol{\nabla} \cdot (n_j \mathbf{u}_j) = S_j\,. \tag{3.8}$$

which is the continuity equation.

For the first order moment, Eq.(3.1) is multiplied by $\mathbf{v}^1 = \mathbf{v}$ and integrated over the velocity as follows.

$$\int \mathbf{v}\frac{\partial f_j}{\partial t}\,\mathrm{d}\mathbf{v} + \int \mathbf{v}\boldsymbol{\nabla}_{\mathbf{r}}\cdot\mathbf{v}f_j\,\mathrm{d}\mathbf{v} + \frac{q_j}{m_j}\int \mathbf{v}\boldsymbol{\nabla}_{\mathbf{v}}\cdot[(\mathbf{E}+\mathbf{v}\times\mathbf{B})f_j]\,\mathrm{d}\mathbf{v} = \int \sum_k \mathbf{v}C_k f_k\,\mathrm{d}\mathbf{v}\,. \tag{3.9}$$

After taking the necessary steps as in Ref. [45], Eq.(3.9) turns into the following equation, which corresponds to the fundamental principle of momentum conservation.

$$m_j n_j \frac{\mathrm{d}\mathbf{u}_j}{\mathrm{d}t} = q_j n_j(\mathbf{E}+\mathbf{u}_j\times\mathbf{B}) - \boldsymbol{\nabla}p_j - \boldsymbol{\nabla}\cdot\pi_j + \mathbf{R}_j\,, \tag{3.10}$$

where $\pi_j = \mathbf{P}_i - p_i I$ is the traceless pressure tensor such that $\mathbf{P}_i$ is the pressure tensor, p_i is the partial pressure corresponding to the thermal velocity and I is the identity matrix [45]. $\mathbf{R}_j/m_j = \sum_k n_k\langle C_k\mathbf{v}\rangle$ is the rate of momentum exchange through collisions among different species.

The second order moment can be found by multiplying both side of Eq.(3.1) by $\mathbf{v}^2$ and integrating over velocity as follows.

$$\int v^2\frac{\partial f_j}{\partial t}\,\mathrm{d}\mathbf{v} + \int v^2\boldsymbol{\nabla}_{\mathbf{r}}\cdot\mathbf{v}f_j\,\mathrm{d}\mathbf{v} + \frac{q_j}{m_j}\int v^2\boldsymbol{\nabla}_{\mathbf{v}}\cdot[(\mathbf{E}+\mathbf{v}\times\mathbf{B})f_j]\,\mathrm{d}\mathbf{v} = \int \sum_k v^2 C_k f_k\,\mathrm{d}\mathbf{v}\,. \tag{3.11}$$

By manipulating this equation as in Ref. [45] and using the following Maxwellian distribution function

$$F_j(v) = \left(\frac{m_j}{2\pi k_B T_j}\right)^{3/2}\exp\left(-\frac{m_j v^2}{2k_B T_j}\right) \tag{3.12}$$

with $k_B T_j = \dfrac{p_j}{n_j}$, where p_j is the partial pressure and k_B is the Boltzmann constant, we end up with the following energy balance equation

$$\frac{3}{2}n_j\frac{\mathrm{d}}{\mathrm{d}t}(k_B T_j) + p_j\boldsymbol{\nabla}\cdot\mathbf{u}_j = -\pi_j\boldsymbol{\nabla}\cdot\mathbf{u}_j - \boldsymbol{\nabla}\cdot\mathbf{q}_j + Q_j\,. \tag{3.13}$$

Here, $\mathbf{q_j}$ is heat flow vector and Q_j, rate of heat exchange, is responsible for elastic and inelastic collisions such that $\mathbf{q}_i = n_i\langle\frac{1}{2}m_i w^2\mathbf{w}\rangle$ where w is the thermal velocity[2]. Although Eqs. (3.8), (3.10), (3.13) define the dynamics of species in a plasma, more equations are required to define the dynamics comprehensively.

[2] A more detailed analysis can be found in Refs. [44, 45]

3.2.1 Two-fluid model

The fluid equations (3.8), (3.10), (3.13), which were derived previously, are employed to describe a plasma consisting of electrons and a single species of ions. These equations collectively illustrate the behavior of two coupled fluid components. Let us assume that viscosity effects are negligible.

For the electrons, fluid equations can be given as follows.

$$\begin{aligned} \frac{\partial n_e}{\partial t} + \boldsymbol{\nabla} \cdot (n_e \mathbf{u}_e) &= S_e \,, \\ m_e n_e \frac{\mathrm{d}\mathbf{u}_e}{\mathrm{d}t} &= q_e n_e (\mathbf{E} + \mathbf{u}_e \times \mathbf{B}) - \boldsymbol{\nabla} p_e + \mathbf{R}_{e,i} \,, \\ \frac{3}{2} n_e \frac{\mathrm{d}}{\mathrm{d}t}(k_B T_e) + p_e \boldsymbol{\nabla} \cdot \mathbf{u}_e &= -\boldsymbol{\nabla} \cdot \mathbf{q}_e + Q_{e,i} \,. \end{aligned} \tag{3.14}$$

For the ions, fluid equations become

$$\begin{aligned} \frac{\partial n_i}{\partial t} + \boldsymbol{\nabla} \cdot (n_i \mathbf{u}_i) &= S_i \,, \\ m_i n_i \frac{\mathrm{d}\mathbf{u}_i}{\mathrm{d}t} &= q_i n_i (\mathbf{E} + \mathbf{u}_i \times \mathbf{B}) - \boldsymbol{\nabla} p_i + \mathbf{R}_{e,i} \,, \\ \frac{3}{2} n_i \frac{\mathrm{d}}{\mathrm{d}t}(k_B T_i) + p_i \boldsymbol{\nabla} \cdot \mathbf{u}_i &= -\boldsymbol{\nabla} \cdot \mathbf{q}_i + Q_{e,i} \,. \end{aligned} \tag{3.15}$$

Within the provided equations, n denotes the particle number density, while S represents the rate at which particles are either created or destroyed. $\mathbf{R}$ and Q signify the momentum and rates of energy exchange, respectively. m corresponds to the mass of the particles, and p is defined as the pressure, where $p = nk_BT$. The electron and ion species are indicated by the subscripts e and i, respectively.

In order to describe a plasma system comprehensively, governing the behavior of electric and magnetic fields requires the "two-fluid" equations to be considered with Maxwell's equations [44], which can be given as follows.

$$\begin{aligned} \epsilon_0 \boldsymbol{\nabla} \cdot \mathbf{E} &= \sigma \,, \\ \boldsymbol{\nabla} \times \mathbf{E} &= -\frac{\partial \mathbf{B}}{\partial t} \,, \\ \boldsymbol{\nabla} \cdot \mathbf{B} &= 0 \,, \\ \frac{1}{\mu_0} \boldsymbol{\nabla} \times \mathbf{B} &= \mathbf{j} + \epsilon_0 \frac{\partial \mathbf{E}}{\partial t} \end{aligned} \tag{3.16}$$

where σ and j stand for the charge and current densities, respectively. It is important to note that the spatial distribution of electric charges and the flow of electric current within the plasma system can be obtained by σ and j in the Maxwell's equations.

3.2.2 Drift-Diffusion Approximation

Drift diffusion approximation considers weakly ionized low temperature gas discharge plasmas. The discharge is distant from a state of local thermodynamic equilibrium, indicating that the temperature of electrons is notably higher than the temperatures of other species. It is assumed that the background gas temperature is equivalent to temperature of all heavy particles. Then, the total pressure is expressed as $p = Nk_bT$, where $N = \sum_i n_i$ for all species i.

When the inertia terms are neglected on the left hand side of the momentum conservation equation (3.10), which is also included in Eqs.(3.14) and (3.15), the particle flux density in the absence of magnetic field ($\mathbf{B} = 0$) can be found as follows:

$$\Gamma_k = n_k \mathbf{u}_k = sgn(q_k)\mu_k n_k \mathbf{E} - D_k \boldsymbol{\nabla} n_k \,, \tag{3.17}$$

where k denotes the species of particles: electrons, ions, and neutral species. Here, the particle mobility and diffusion coefficients are given as $\mu_k = |q_k|/(m_k\nu_k)$ and $D_k = k_B T_k \mu_k / q_k$, where ν_k is the collision frequency. For the electrons and ions, Eq.(3.17) can be given as

$$\begin{aligned} \Gamma_e &= n_e \mathbf{u}_k = -\mu_e n_e \mathbf{E} - D_e \boldsymbol{\nabla} n_e \,, \\ \Gamma_i &= n_i \mathbf{u}_k = \mu_i n_i \mathbf{E} - D_i \boldsymbol{\nabla} n_i \,, \end{aligned} \tag{3.18}$$

where subscripts e and i represent electrons and ions, respectively.

Let us substitute Eq.(3.17) into the first equations of Eqs. (3.14) and (3.15), then the two-fluid equations with drift-diffusion approximation are given as [44]

$$\frac{\partial n_k}{\partial t} + \boldsymbol{\nabla} \cdot (sgn(q_k)\mu_k n_k \mathbf{E} - D_k \boldsymbol{\nabla} n_k) = S_k \tag{3.19}$$

It is important to note that this equation is coupled with the Poisson equation for the electric field $\mathbf{E}$ to build a self-consistent model. Poisson equation is given as

$$-\epsilon_0 \frac{\partial^2 \varphi}{\partial x^2} = \sum_k q_k n_k \,, \tag{3.20}$$

where φ is the potential.

3.3 Simple Fluid Model

We have discussed the governing equations of the glow discharge as a fluid model derived from the moments of the Boltzmann equation, which are continuity, momentum conservation and energy equations. Additionally, to ensure a comprehensive model for the electric field distribution, these equations are coupled with the Poisson equation. Two-fluid equations with drift-diffusion approximation are derived by transforming the momentum equation such that particle flux densities are taken into account.

Electron transport and collisional reaction rate coefficients in the fluid equations are responsible for the particle collisions dynamics. Thus, determining these coefficients is important for the accuracy of the model. In this chapter, local field approximation (LFA) is considered for the description of electrons' transport and rate coefficients [44, 118] such that they are described as functions of the local reduced electric field E/p, where E is the magnitude of the electric field and p is the pressure. Furthermore, mobility and diffusion (transport coefficients) can be taken constant by using the Einstein relation $D/\mu = k_B T/e$. A fluid model of gas discharge plasma constructed on this approximation is called simple fluid model.

Then, the equations of the model can be given as follows [44].

$$\begin{aligned} \frac{\partial n_k}{\partial t} + \boldsymbol{\nabla} \cdot \boldsymbol{\Gamma}_k &= S_k \,, \\ \boldsymbol{\Gamma}_k = sgn(q_k)\mu_k n_k \mathbf{E} - D_k \boldsymbol{\nabla} n_k \,, \\ \epsilon_0 \boldsymbol{\nabla} \cdot \mathbf{E} &= \sum_k q_k n_k \,, \\ \mathbf{E} &= -\boldsymbol{\nabla}\varphi \,, \end{aligned} \tag{3.21}$$

for each species k. For both the electrons and ions, the source term is defined as $S_k = \alpha|\Gamma_e| - \beta n_e n_i$, where $\alpha = \alpha(E)$ is the first Townsend coefficient, which is the rate coefficient of electron impact ionization, and β is the electron-ion recombination coefficient [45]. Additionally, the electric potential is denoted as φ.

3.4 Description of the Gas-Discharge Semiconductor Model

The present study examines a DC-driven planar gas discharge system, in which one of the electrodes is constructed from a high-ohmic semiconductor. This system features a large aspect ratio, meaning that the gap between the electrodes is much smaller than the system's transverse dimensions. Such a gas discharge-semiconductor system has been previously explored both experimentally and numerically, as documented in various references [48, 54–56, 119, 120, 122–133]. This system is schematically represented in Fig. (3.1). In the diagram, an external circuit, including a resistor and a supplied voltage source, is connected to the gas discharge gap and the GaAs semiconductor layer, both of which are sandwiched between two planar electrodes.

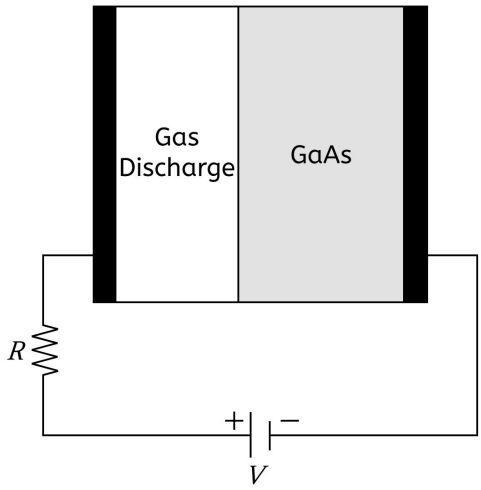

Figure 3.1: The schematic illustration of a planar gas discharge coupled with a semiconductor layer.

A spatially one-dimensional model is developed for the analysis. This model, also known as DC discharge plasma model, extends in a direction perpendicular to the electrode layers and does not consider spatial variations in the parallel direction to the layers (transverse direction). In other words, our focus is on temporal oscillations occurring in a transversely homogeneous mode. The one-dimensional model is also based on a simple fluid model for gas discharge in nitrogen, akin to those employed in numerous numerical investigations of GDSSs [54,55,57,120,127,128,131,133,134]. Within this model, two plasma species, namely the electrons and the positive ions,

are considered, and two types of ionization processes take place: electron impact ionization within the bulk of the gas and secondary electron emission from the cathode surface.

The mobility coefficients are given as approximation by $\mu_e p = 2\times10^5$ cm^2 Torr V^{-1}s^{-1} and $\mu_i p = 699$ cm^2 Torr V^{-1}s^{-1}. The corresponding diffusion coefficients, D_e and D_i, are determined by the Einstein relation, which is $D/\mu = k_B T/e$. The ionization rate can be expressed as a function of the reduced electric field by Townsend formula such that $\alpha = Ap\exp(-Bp/|E|)$, where p is the pressure of the gas and constants A, B are $A = 12$ cm^{-1}Torr^{-1} and $B = 343$ V cm^{-1}Torr^{-1} [135].

The anode and cathode ends of the gas discharge are positioned at $x = 0$ and $x = d$, respectively. The semiconductor layer extends up to $d = d_g + d_s$, where d_g and d_s represent the lengths of the discharge gap and the semiconductor layer, respectively. Boundary conditions for ions and electrons at the anode ($x = 0$) are determined by the following equations.

$$n_\mathrm{i} = 0 \text{ and } \frac{\partial n_\mathrm{e}}{\partial x} = 0, \tag{3.22}$$

The boundary conditions for the cathode ($x = d$) can be given as follows.

$$\frac{\partial n_\mathrm{i}}{\partial x} = 0 \text{ and } \mu_\mathrm{e} n_\mathrm{e} = \gamma \mu_\mathrm{i} n_\mathrm{i}, \tag{3.23}$$

where γ is the secondary emission coefficient.

To complete the system of equations, the external circuit equation is integrated into the GDSS model to account for the semiconductor layer. It is given as

$$\tau_\mathrm{s} \frac{\partial U(t)}{\partial t} = U_t - U(t) - R_\mathrm{s} J(t)\,. \tag{3.24}$$

Here, $U(t)$ denotes the discharge voltage, $U_\mathrm{t} = U(t) + U_s(t)$ represents the total stationary voltage, $R_\mathrm{s} = d_\mathrm{s}/\sigma_\mathrm{s}$ is the resistance of the semiconductor, $C_\mathrm{s} = \epsilon_\mathrm{s}\epsilon_0/d\mathrm{s}$ is the capacitance per area, and $\tau_\mathrm{s} = C_\mathrm{s} R_\mathrm{s} = \epsilon_\mathrm{s}\epsilon_0/\sigma_\mathrm{s}$ is the Maxwell time scale of the semiconductor with dielectric constant ϵ_s, conductivity σ_s, and permittivity of free space ϵ_0. In addition to the total current density $J(t)$, the currents of species can be given for electrons and positive ions as $\mathbf{J}_e = -\mu_e n_e \mathbf{E}$ and $\mathbf{J}_i = \mu_i n_i \mathbf{E}$, respectively.

The input parameters are defined same as in the experiment [48] and in theoretical works [54, 56, 57], which are demonstrated in Table (3.1).

Table 3.1: Input parameters of the one-dimensional simple fluid model

Description	**Input parameters**
Pressure of nitrogen gas	$p = 40$ mbar
Gas temperature	$T_{\mathrm{g}} = 297\,\mathrm{K}$
Discharge gap width	$d_g = 1.4$ mm
GaAs layer width	$d_{\mathrm{s}} = 1.5$ mm
GaAs dielectric constant	$\epsilon_{\mathrm{s}} = 13.1$
GaAs conductivity	$\sigma_{\mathrm{s}} = (2.6 \times 10^5\,\Omega\,\mathrm{cm})^{-1}$
Secondary emission coefficient	$\gamma = 0.08$
Electron mobility coefficient	$\mu_{\mathrm{e}} p = 2 \times 10^5\ \mathrm{cm}^2\,\mathrm{Torr}\,\mathrm{V}^{-1}\mathrm{s}^{-1}$
Ion mobility coefficient	$\mu_{\mathrm{i}} p = 699\ \mathrm{cm}^2\,\mathrm{Torr}\,\mathrm{V}^{-1}\mathrm{s}^{-1}$

The applied total voltage U_t and the semiconductor resistance R_s serve as control parameters. By appropriately adjusting these two parameters, we restrict the discharge system to operate in the regime where it corresponds to the transition from Townsend to glow discharge.

Our model is initially developed in dimensionful units, but the results are presented in terms of dimensionless parameters. The process of nondimensionalization for this model is primarily conducted as outlined in [56, 133]. The corresponding expressions to transform the results into a dimensionless parameters are as follow.

$$\boldsymbol{U} = \frac{U}{E_0 X_0}\,, \quad \boldsymbol{J} = \frac{J}{e n_0 X_0 / t_0}\,, \quad \boldsymbol{\tau} = \frac{t}{t_0}\,, \quad \boldsymbol{R_s} = \frac{R_s}{E_0 t_0 / e n_0}\,, \tag{3.25}$$

where the intrinsic parameters are

$$\begin{gathered} X_0 \approx 2.78 \times 10^{-5}\ m, \ \ t_0 \approx 4.05 \times 10^{-11}\ s, \\ n_0 \approx 2.05 \times 10^{18}\ m^{-3}, \ \ E_0 \approx 1.03 \times 10^{6}\ V/m. \end{gathered} \tag{3.26}$$

3.5 Periodic and Chaotic Oscillations

In this section, we use a bifurcation diagram presented in Fig. (3.2) to unveil the regions of regularity and chaos. Similar diagrams have been explored in previous studies such as [54, 120, 133]. Within this diagram, the bifurcation curve, determined

as a function of two control parameters, U_t and R_s, serves to distinguish the stable stationary solutions from the unstable ones, where temporal oscillations occur. Left side of the curve in Fig. (3.2) covers the stable stationary solutions such as point (a), while right side includes unstable ones such as (b), (c), (d).

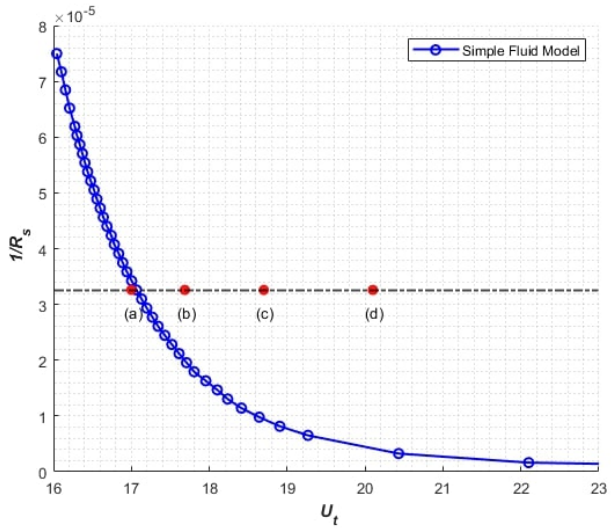

Figure 3.2: Bifurcation diagram separating stable stationary region from unstable region. Points denoted by (a), (b), (c) and (d) indicate regimes with $U_t = 17.04$, 17.68, 18.71 and 20.11 at $R_s = 30709$, respectively.

In this figure, the horizontal line corresponds to calculations with a constant semiconductor resistance value $R_s = 30709$, while the total applied potential U_t varies. Different U_t values are marked as points (a), (b), (c), and (d), and the corresponding phase portraits are also provided in Fig. (3.3).

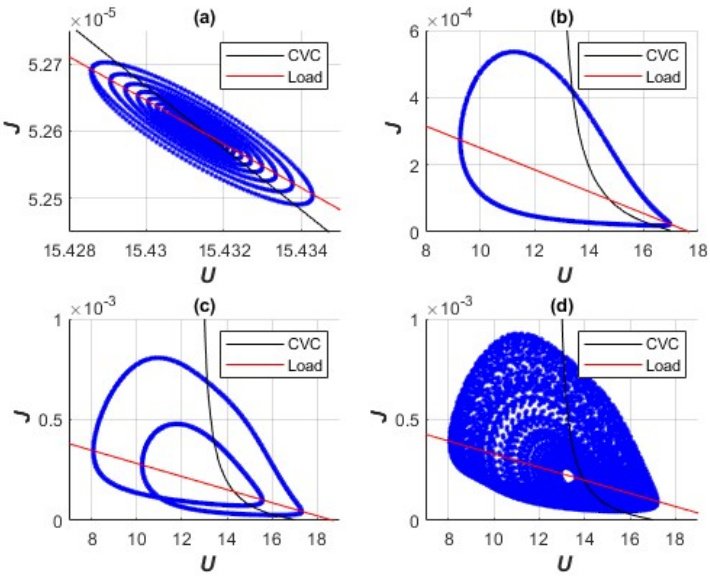

Figure 3.3: Phase portraits of trajectories in the $\boldsymbol{U}$-$\boldsymbol{J}$ plane, computed for corresponding (a), (b), (c) and (d) points in figure (3.2).

In Fig. (3.3), while the trajectory of oscillations has an inward spiral converging to a stationary point in (a), the stationary state is unstable and develops into a limit cycle in (b). A new periodic trajectory emerges with the doubled period in (c). This period-doubling bifurcation is considered as a route to temporal chaos [136–138] as it is verified by the chaotic patterns of (d). The two curves on each plot represent the load (red curve) $\boldsymbol{U} = \boldsymbol{U_t} - \boldsymbol{R_s J}$ and current-voltage characteristic (CVC) of gas discharge (black curve) $\boldsymbol{U} = \boldsymbol{U}(\boldsymbol{J})$. The intersection point of the CVC and load curves represents the stationary solution, or equilibrium point.

In the next section, the drive and response systems are configured as the coupled GDS systems using the bifurcation points $\boldsymbol{U_t}$, $\boldsymbol{R_s}$ specified at regime point (d) in Fig. (3.2), along with the corresponding phase portrait in Fig. (3.3)-(d).

3.6 Delta synchronization of chaos in the coupled GDSS

In this section, we conduct simulations for both the drive and response systems, where the response system is established using the voltage of the drive system as a perturba-

tion. Both systems, characterized by the values ($\boldsymbol{U_t}, \boldsymbol{R_s}$) specified at regime point (d) in Fig. (3.2), exhibit chaotic solutions. The method for detecting chaos, as discussed in Chp.2, is referred to as unpredictability.

Moreover, besides the existence of sequences of convergence and separation separately in both systems, we will demonstrate that they have common corresponding finite convergence and separation sequences, indicating that the coupled system exhibits delta synchronization of chaos (DSC). However, it's important to note that the system lacks generalized synchronization. Therefore, the DSC method offers a broader approach to chaos synchronization.

The data for the drive, response, and synchronized systems are computed in the same simulation, ensuring that the time values align across all different analyses. Consequently, the sequences u_n and v_n for the synchronized system, as well as t_n and s_n for the drive and response systems, are obtained within the same numerical analysis.

Based on the modeling approaches in previous sections, the drive system can be described as follows.

$$\begin{aligned}
&\frac{\partial n_k}{\partial t} + \frac{\partial \Gamma_k}{\partial x} = S_k \,, \\
&\Gamma_k = \mathrm{sgn}(q_k)\mu_k n_k E - D_k \frac{\partial n_k}{\partial x} \,, \\
&-\epsilon_0 \frac{\partial^2 \varphi}{\partial x^2} = \sum_k q_k n_k \,, \\
&\tau_\mathrm{s} \frac{\partial U(t)}{\partial t} = U_t - U(t) - R_\mathrm{s} J(t) \,,
\end{aligned} \tag{3.27}$$

with the boundary conditions

$$\begin{aligned}
\text{Anode } (x=0): \quad & n_i = 0 \,, \quad \frac{\partial n_e}{\partial x} = 0 \,, \quad \varphi = 0 \,, \\
\text{Cathode } (x=d): \quad & \frac{\partial n_i}{\partial x} = 0 \,, \quad \mu_e n_e = \gamma \mu_i n_i \,, \quad \varphi = -U \,.
\end{aligned} \tag{3.28}$$

The values of U, obtained from the solution of Eq.(3.27), are incorporated into the response system as a perturbation. This perturbation term constitutes the sole distinction between the drive and response systems. Here are the governing equations for

the response system.

$$
\begin{aligned}
&\frac{\partial \tilde{n}_k}{\partial t} + \frac{\partial \tilde{\Gamma}_k}{\partial x} = \tilde{S}_k \,, \\
&\tilde{\Gamma}_k = \mathrm{sgn}(q_k)\mu_k \tilde{n}_k \tilde{E} - D_k \frac{\partial \tilde{n}_k}{\partial x} \,, \\
&-\epsilon_0 \frac{\partial^2 \tilde{\varphi}}{\partial x^2} = \sum_k q_k \tilde{n}_k \,, \\
&\tau_{\mathrm{s}} \frac{\partial V(t)}{\partial t} = V_t - V(t) - R_{\mathrm{s}} \tilde{J}(t) + \delta U(t) \,,
\end{aligned}
\tag{3.29}
$$

with the boundary conditions

$$
\begin{aligned}
\text{Anode } (x=0): \quad & \tilde{n}_i = 0 \,, \quad \frac{\partial \tilde{n}_e}{\partial x} = 0 \,, \quad \tilde{\varphi} = 0 \,, \\
\text{Cathode } (x=d): \quad & \frac{\partial \tilde{n}_i}{\partial x} = 0 \,, \quad \mu_e \tilde{n}_e = \gamma \mu_i \tilde{n}_i \,, \quad \tilde{\varphi} = -V \,.
\end{aligned}
\tag{3.30}
$$

To determine the convergence sequence t_n, we place a circle with a radius δ_n, centered at the initial point. In the $\boldsymbol{U}(\tau) - \boldsymbol{J}(\tau)$ phase portraits, the horizontal $\boldsymbol{U}$-axis and the vertical $\boldsymbol{J}$-axis have different scales, with $\boldsymbol{U} \in [8, 18]$ and $\boldsymbol{J} \in [0, 10^{-3}]$. The $\boldsymbol{U}$-axis is selected as the reference for δ_n, and the $\boldsymbol{J}$-axis is rescaled by multiplying it by 10^4 within the circle equation. In other words, the circles for each n value are defined by the equation: $\sqrt{(\boldsymbol{U}(\tau) - \boldsymbol{U}(0))^2 + ((\boldsymbol{J}(\tau) - \boldsymbol{J}(0)) \times 10^4)^2} = \delta_n$.

Then, we identify the time values that satisfy $\|\phi(t_n) - \phi(0)\| < \delta_n$, where $\phi(\tau) = (\boldsymbol{U}(\tau), \boldsymbol{J}(\tau) \times 10^4)$ with $\tau(t) = t/t_0$. The radii δ_n become smaller with each iteration. After obtaining the t_n values, we derive the s_n sequence for a specific Δ such that it satisfies $\|\phi(t_n + s_n) - \phi(s_n)\| \geq \Delta$ for each n.

In the drive system, we set $\boldsymbol{U}_t = 20.11$ and $\boldsymbol{R}_s = 30709$. As demonstrated in the previous section, this system exhibits chaotic behavior. The chaotic solution of the drive system is illustrated in Fig. (3.4). The simulation time is $\tau_{\text{end}} = 1.61 \times 10^8$ with a time step of $\Delta\tau = 823.33$. There are 173 t_n values for this system in the range $t_n \in [1.27 \times 10^5, 1.46 \times 10^8]$, and the radii decrease at each step by 0.001, taking the following values: $\delta_n = 0.18, 0.1790, ..., 0.0080$. For $\Delta = 7.2$, there are 173 s_n values in the range $s_n \in [4.12 \times 10^3, 1.45 \times 10^7]$.

It is important to note that the t_n and s_n sequences consist of time values in dimensionless units, as defined in the previous section. The presence of the sequences t_n

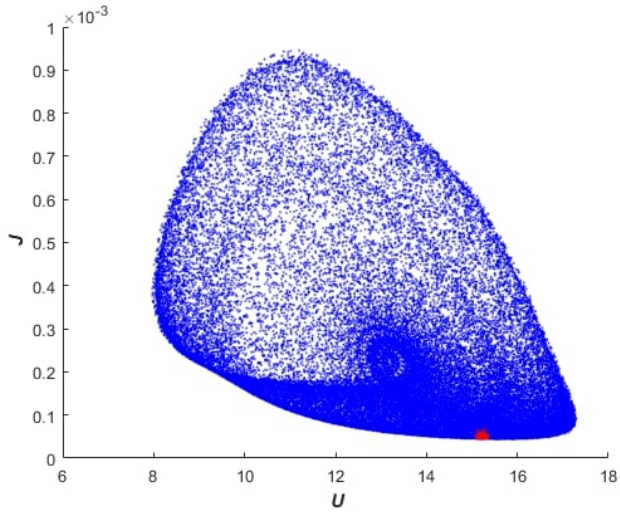

Figure 3.4: $\boldsymbol{U} - \boldsymbol{J}$ plot of the drive system at $\boldsymbol{U}_t = 20.11$ and $\boldsymbol{R}_s = 30709$

and s_n demonstrates that the system exhibits unpredictable behavior and is chaotic. The degree of numerical unpredictability for the drive system is $\alpha \simeq 0.001$. The data points $(\boldsymbol{U}(t_n), \boldsymbol{J}(t_n))$ are indicated by the red markers in Fig. (3.4), and the corresponding t_n, s_n, and δ_n values are provided in Table (3.2).

Based on the results from this simulation, we have demonstrated that for the drive GDSS, the degree of unpredictability is given by $\alpha = \frac{\min_{n=1,2,..,173}\delta_n}{\Delta} = \frac{0.008}{7.2} = 0.001111....$ This value is relatively small. Meanwhile, the dimensionless time length of the simulation is $\tau_{\text{end}} = 1.61 \times 10^8$, which is quite large. According to the assumptions stemming from Def. (1), one can conclude that the unpredictability of the solution for the drive system is confirmed.

In the response system, we use the same parameters as in the drive system, with $\boldsymbol{V}_t = 20.11$ and $\boldsymbol{R}_s = 30709$. The only difference between the response system and the drive system is the presence of the perturbation term $\delta U(t)$ coming from the drive system. We choose a nonzero constant $\delta = 0.047$. The chaotic solution of this system is depicted in Fig. (3.5), and the simulation time and time difference match those of the drive system.

There are 172 t_n values for this system in the range $t_n \in [1.38 \times 10^5, 1.60 \times 10^8]$, with radii decreasing at each step, mirroring the values used in the drive system. For $\Delta = 2.8$, there are 172 s_n values in the range $s_n \in [1.65 \times 10^4, 9.02 \times 10^5]$. The red

Table 3.2: Sequences of convergence t_n and divergence s_n with δ_n values for the drive system.

n	t_n	s_n	δ_n
1	126793	4117	0.180
2	222299	4940	0.179
3	270052	5763	0.178
4	317805	6587	0.177
5	364735	7410	0.176
	⋮		
	⋮		
169	134574915	14129164	0.012
170	136979861	14187620	0.011
171	137969504	14429679	0.010
172	138725321	14477433	0.009
173	145558959	14513659	0.008

marked data points in Fig. (3.5) represent $(\boldsymbol{V}(t_n), \boldsymbol{J}(t_n))$.

The existence of the t_n and s_n sequences in the response system indicates that it also exhibits unpredictable behavior. The degree of numerical unpredictability for the response system is $\alpha \simeq 0.003$. The corresponding t_n, s_n, and δ_n values are provided in Table (3.3).

Based on the data of the simulations, one can conclude that the degree of unpredictability has a value of $\alpha = \frac{\min_{n=1,2,..,172}\delta_n}{\Delta} = \frac{0.009}{2.8} = 0.00321....$ This value is relatively small. Additionally, the dimensionless time parameter has a large value, $\tau_{\text{end}} = 1.61 \times 10^8$. These findings confirm the unpredictability of the solution for the response GDSS as in the drive system.

Since both the drive and response systems exhibit unpredictable solutions, the examination of DSC between the systems proceeds as follows. We aim to find common u_n and v_n sequences in both systems such that $\|x(u_n) - x(0)\| + \|y(u_n) - y(0)\| < 2 \times \delta_n$, where δ_n values are taken the same as in the drive and response systems. Here,

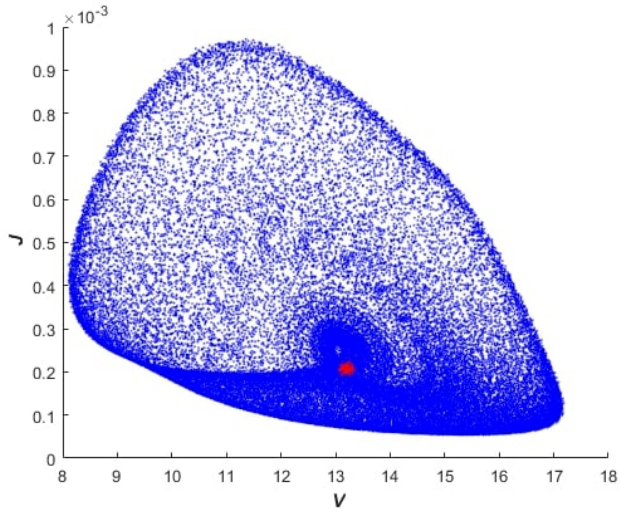

Figure 3.5: $\boldsymbol{V} - \boldsymbol{J}$ plot of the response system at $\boldsymbol{V}_t = 20.11$ and $\boldsymbol{R}_s = 30709$

$x(\tau) = (\boldsymbol{U}^{drive}(\tau), \boldsymbol{J}^{drive}(\tau))$ and $y(\tau) = (\boldsymbol{V}^{resp.}(\tau), \boldsymbol{J}^{resp.}(\tau))$. We set $\Delta_1 = 7.2$ and $\Delta_2 = 2.8$ to ensure sufficient separation.

In Fig. (3.6), both the drive and response GDSSs are depicted. The blue and red data points correspond to the drive and response systems, respectively. The green data points represent $(\boldsymbol{U}(u_n), \boldsymbol{J}(u_n))$, and the yellow data points represent $(\boldsymbol{V}(u_n), \boldsymbol{J}(u_n))$, where u_n values are the same in both systems. The $x(0)$ and $y(0)$ values are also same as the unpredictability analysis to maintain consistency.

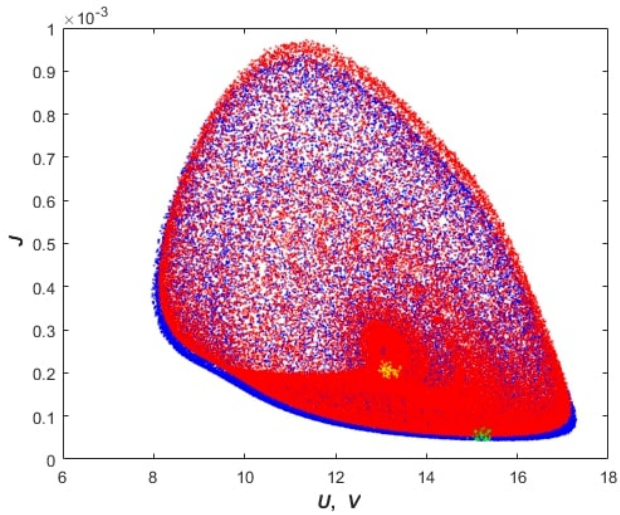

Figure 3.6: $\boldsymbol{U}, \boldsymbol{V} - \boldsymbol{J}$ plot of both drive (blue) and response (red) systems

Table 3.3: Sequences of convergence t_n and divergence s_n with δ_n values for the response system.

n	t_n	s_n	δ_n
1	138319	16467	0.180
2	139143	17290	0.179
3	199246	18113	0.178
4	200069	18937	0.177
5	200892	19760	0.176
	⋮		
	⋮		
168	108691070	862026	0.013
169	121822358	894960	0.012
170	140256714	899076	0.011
171	152259217	900723	0.010
172	159626373	901546	0.009

There are 53 u_n values and 52 v_n values, as listed in table (3.4). The degree of synchronization is calculated as $\alpha^{sync} \simeq 0.046$. The analysis demonstrates that both systems approach their initial points at the same time values, u_n, within a given radius, and they diverge from these points at the same time values, v_n.

The latest numerical data for the coupled GDSSs reveals a degree of synchronization, $\alpha_{52}^{sync} = \frac{\delta_{52}}{min(\Delta_1,\Delta_2)} = \frac{0.129}{2.8} = 0.0460714...$, which is a finite number. Additionally, the large dimensionless computational time, $\tau_{\text{end}} = 1.61 \times 10^8$, suggests that the Def. (3) of DSC has been numerically satisfied.

The phenomenon in which both systems share the same u_n and v_n values reveals a new type of synchronization, which we have termed "delta synchronization of chaos [11]." This approach differs from generalized synchronization, and we will demonstrate that even in the absence of generalized synchronization, we can observe synchronization between the drive and response systems using this method.

One widely accepted method for identifying synchronized chaotic motion is general-

Table 3.4: Common u_n, v_n and δ_n values of drive and response systems

n	u_n	v_n	δ_n
1	2104431	73276	0.180
2	3140180	74099	0.179
3	3977506	74923	0.178
4	5158984	75746	0.177
5	5159808	76569	0.176
	⋮		
	⋮		
49	147159511	10672001	0.132
50	147207265	10692585	0.131
51	147703732	10695055	0.130
52	148084111	11110013	0.129
53	160175533	-	0.128

ized synchronization [4,5], as elaborated in Chp.2. We will adopt the auxiliary system approach of generalized synchronization to compare our findings with this method. A similar analysis was conducted in Ref. [53], revealing that this coupled system does not exhibit generalized synchronization.

In auxiliary system approach, the asymptotic stability condition given in Eq.(2.11) should be satisfied to verify existence of generalized synchronization. It is important to note that the transient solutions are ignored in this process. The discharge voltages of the response and auxiliary systems will be considered in the application of Eq.(2.11).

Consider the drive and response systems defined in Equations (3.27) and (3.29), respectively. The auxiliary system is an exact replica of the response system, with the only distinction being its initialization with different initial conditions. The equations

for the auxiliary system are as follows.

$$
\begin{aligned}
&\frac{\partial \bar{n}_k}{\partial t} + \frac{\partial \bar{\Gamma}_k}{\partial x} = \bar{S}_k \,, \\
&\bar{\Gamma}_k = \mathrm{sgn}(q_k)\mu_k \bar{n}_k \bar{E} - D_k \frac{\partial \bar{n}_k}{\partial x} \,, \\
&-\epsilon_0 \frac{\partial^2 \bar{\varphi}}{\partial x^2} = \sum_k q_k \bar{n}_k \,, \\
&\tau_{\mathrm{s}} \frac{\partial W(t)}{\partial t} = W_t - W(t) - R_{\mathrm{s}} \bar{J}(t) + \delta U(t) \,,
\end{aligned}
\tag{3.31}
$$

with the boundary conditions

$$
\begin{aligned}
&\bar{n}_i = 0 \,, \\
&\frac{\partial \bar{n}_k}{\partial x} = 0 \,, \\
&\mu_e \bar{n}_e = \gamma \mu_i \bar{n}_i \,, \\
&\bar{\varphi}_0 = 0 \,, \quad \bar{\varphi}_{d_g} = -W \,,
\end{aligned}
\tag{3.32}
$$

where $\boldsymbol{W}_t = 20.11$, $\boldsymbol{R}_s = 30709$ and $\delta = 0.047$ as in the response system.

The solutions of $\boldsymbol{V}$ and $\boldsymbol{W}$ are depicted in the $\boldsymbol{V} - \boldsymbol{W}$ plot shown in Fig. (3.7). Since the plot is not confined to the $\boldsymbol{V} = \boldsymbol{W}$ line, the asymptotic stability condition given in Eq. (2.11) is not satisfied. Consequently, the drive and response systems do not exhibit generalized synchronization.

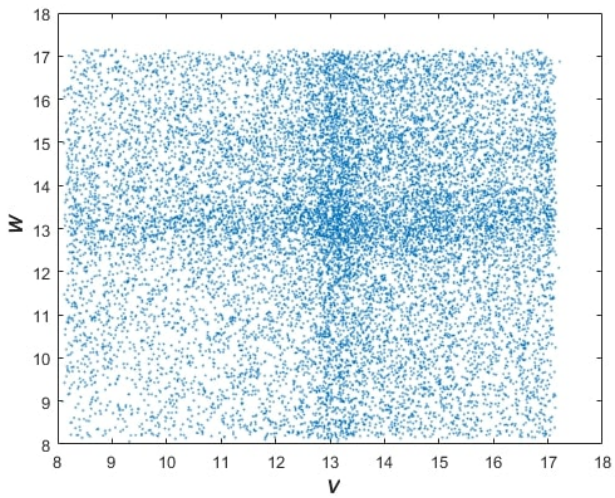

Figure 3.7: $\boldsymbol{W} - \boldsymbol{V}$ plot at $\boldsymbol{W}_t = 20.11$, $\boldsymbol{R}_s = 30709$

These findings indicate that synchronization can still occur between the drive and

response systems, even in the absence of generalized synchronization, and this synchronization can be detected using the DSC method.

3.7 Discussion

A gas-discharge semiconductor system is constructed through the use of a two-fluid model. The simple fluid model of the system is formulated using the drift-diffusion approximation. The governing equations of the system are derived to provide a comprehensive analysis.

We have applied the delta synchronization of chaos to a specific chaotic regime of the GDSSs, which are described within the corresponding parametric regime. A bifurcation diagram was used to differentiate the stable stationary regions from the unstable regions where temporal oscillations occur. We considered the Poincaré chaotic regime in the parameter space and established the drive and response systems, unidirectionally coupled by perturbing the response system with the unpredictable solution of the drive system. Unpredictability was numerically demonstrated in both GDSSs.

The existence of a common sequence of finite convergence, denoted as u_n, and a sequence of separation, denoted as v_n, for the drive and response systems, demonstrates that these systems exhibit delta synchronization of chaos. The common sequence of finite convergence indicates that the unpredictable motions of both systems approach their initial points at the same moments. Simultaneously, the common sequence of separation shows that the trajectories, which start converging at moments u_n and the initial moment u_0 in both systems, diverge from each other at the same moments v_n. The numerical values of these common sequences u_n and v_n are presented in a table for each n.

Additionally, it was shown that the coupled GDSSs do not exhibit generalized synchronization when using the auxiliary system approach. Thus, DSC is revealed as a more general synchronization method than generalized synchronization.

The primary novelty of this research lies in demonstrating that systems that do not exhibit canonical types of synchronization can still be considered synchronized based

on their chaotic characteristics, which can be identified using the delta synchronization approach.

3.8 Further analysis on gas-discharge systems

In this study, a one-dimensional simple fluid model with a drift-diffusion approximation for electron and ion particle fluxes was employed. This model, which is qualitatively sufficient to describe the fundamental properties of a nitrogen gas discharge system, successfully confirmed the existence of delta synchronization of chaos. It's noteworthy that this synchronization method was demonstrated even though the system did not exhibit generalized synchronization, as discussed in this chapter and Ref. [11].

To further advance the analysis of the semiconductor gas discharge system in terms of chaos synchronization, a more realistic and advanced one-dimensional fluid model was developed [22]. This model, known as the "extended fluid model" or "local mean energy approximation" (LMEA) model [58], was employed in the same system. While the details of this study are not presented in the current thesis, the results will be briefly mentioned due to their significance for the development of the delta synchronization method. This approach provides a more comprehensive understanding of the dynamics of the system, and its outcomes can contribute to the refinement of delta synchronization techniques, as discussed in the reference [22].

The comparison between these two modeling approaches is summarized as follows.

1. Types of particles:
    - In the simple fluid model, only two kinds of particles, electrons, and ions, are taken into consideration.
    - The extended fluid model includes a total of seven different particle species, including electrons, ions, excited molecules, and ground state molecules.
2. Plasma chemical reactions:
    - In the simple fluid model, the only occurring reactions involve electron

impact ionization and secondary electron emission from the cathode surface.

- The extended fluid model broadens the scope by including a range of reactions. These include direct ionization, secondary emission from the wall, elastic collisions, electron-induced excitations, vibrations, rotations, collisions between molecules, and relaxation reactions.

3. Governing equations:

   - The simple fluid model solves a simplified set of equations, specifically the two-fluid equations using the drift-diffusion approximation. It also incorporates Poisson's equation to ensure self-consistency in the model.
   - The extended fluid model introduces a more complex set of equations. It includes continuity equations for each of the seven particle species and Poisson's equation to determine the electric field profile. Moreover, it includes the electron energy equation.

4. Electron kinetic coefficients:

   - In the simple fluid model, electron transport coefficients as diffusion and mobility are assumed to be constants. The ionization rate coefficient, also known as the Townsend ionization coefficient, is defined based on the local electric field. This approach leads to the simple fluid model being referred to as the "local field approximation" (LFA).
   - The extended fluid model takes a different approach. It defines electron transport coefficients (diffusion and mobility) and rate coefficients for electron-induced plasma chemical reactions as functions of mean electron energy, derived from a separate online electron Boltzmann solver.

5. Nonlocality of electrons:

   - The simple fluid model neglects the nonlocal ionization events that occur in regions with a weak electric field. This is because the ionization rate is exclusively defined as a function of the local electric field, which increases with electric field strength.

- In contrast, the extended fluid model explicitly incorporates the nonlocality of electrons. It describes ionization events by defining transport and rate coefficients as functions of mean electron energy rather than relying on the local electric field. This means that ionization can occur independently of the electric field strength in a specific region within the discharge tube.

6. Practical importance:

   - In various industrial plasma devices such as energy-saving lamps, projectors, and flat plasma display panels, instability and chaotic oscillations are undesirable. Addressing and comprehending these erratic behaviors using advanced and realistic fluid models is crucial. This approach is particularly relevant when considering factors such as computational efficiency and speed. Given that the extended fluid model offers greater sophistication compared to the simple fluid model, utilizing this modeling approach in our analyses enables us to draw more precise conclusions about these practical applications.

It is important to emphasize that the comparisons presented above primarily pertain to the electron dynamics within the models. Electron behavior is the least precisely known aspect in these models due to the nonlocal characteristics of electrons in gas discharge systems. The choice of approximations, whether it's the Local Field Approximation (LFA) or the Local Mean Energy Approximation (LMEA), significantly influences the accuracy of these models.

The chaos synchronization analyses, employing this modeling approach, are carried out, in Ref. [22], in a manner similar to the simple fluid model discussed in this chapter. The results reveal that the systems in the detailed model exhibit unpredictability, and the delta synchronization of chaos is observed in the model in the absence of generalized synchronization. Furthermore, the research in Ref. [22] demonstrates that more complex and realistic models yield even more unpredictable and synchronous behaviors, and the delta synchronization approach allows us to detect and compare the intensity of synchronization across different approaches.

CHAPTER 4

REVEALING CHAOS SYNCHRONIZATION BELOW THE THRESHOLD IN COUPLED MACKEY-GLASS SYSTEMS

4.1 Introduction

Time-delay systems play a vital role in the field of chaos synchronization, particularly in applications related to secure communication [67–69]. The current study focuses on the concept of delta synchronization of chaos (DSC) within the context of Mackey-Glass systems. These systems are described by first-order delay differential equations and were initially developed to model blood production. Notably, they exhibit chaotic behaviors for specific parameter regimes [59, 72].

Researchers have employed electronic circuit implementations of these models, enabling experimental investigations into the synchronization of chaotic systems [64–66]. This practical approach offers insights into real-world applications of chaos synchronization, including secure communication.

The synchronization behavior of unidirectionally coupled Mackey-Glass drive response systems has been a subject of investigation, with previous studies highlighting specific synchronization thresholds [65, 73–76]. For instance, the research Ref. [75] has indicated that coupled systems achieve generalized and complete synchronization only above a particular threshold. In this chapter, we aim to explore the synchronized behavior of Mackey-Glass drive-response systems [23], using parameters identical to those in Ref. [75], on both sides of this threshold. We employ the DSC to assess synchronization behavior.

Additionally, Ref. [73] discusses the existence of synchronization when the coupling

parameter exceeds a certain threshold, while also considering different delay times in the drive and response systems. Ref. [74] offers both analytical and numerical insights into the relationship between synchronization thresholds and delay times. Furthermore, in Ref. [76], synchronization regimes and stability conditions of two linearly and nonlinearly coupled Mackey-Glass systems are comprehensively analyzed. These studies collectively contribute to our understanding of synchronization phenomena in Mackey-Glass systems under various conditions.

This chapter's primary motivation is to show the occurrence of synchronous chaotic behavior in drive-response Mackey-Glass systems, specifically within regions that lack generalized synchronization. It is discussed in prior research that synchronization in these systems is sensitive to the coupling constant between the Mackey-Glass systems, leading to a distinct synchronization threshold. Previous studies consistently indicate that synchronization is present on one side of this threshold while absent on the other [65, 73–76]. Moreover, there is evidence that both generalized and complete synchronization coexist on the same side of the threshold [73, 75].

In our investigation, we make a novel observation: synchronization can occur and be identified by the DSC method even below the synchronization threshold, where no synchronization was previously detected. Additionally, in the region where generalized synchronization is known to exist, we find the coexistence of complete synchronization of unpredictability, a special case of DSC. These findings align with similar results obtained in Refs. [11,22], underscoring the significance of our synchronization research and providing a robust basis for the DSC method.

The numerical characteristics of our method have been rigorously analyzed to substantiate our argument. In this study, we have demonstrated that synchronization of unpredictability serves as evidence for the existence of chaos synchronization. Our findings suggest that uncovering synchronous dynamics in regions previously considered asynchronous for coupled systems may have implications for the field of secure communication.

Furthermore, we have observed the coexistence of both complete synchronization of unpredictability and generalized synchronization above the synchronization threshold. This insight adds an intriguing layer to our understanding of complex synchro-

nization phenomena. The findings of this research, which is covered in this chapter, is published in Ref. [23].

4.2 Mackey-Glass System

Mackey-Glass equation is a delay differential equation with the form [72]

$$\frac{\mathrm{d}x(t)}{\mathrm{d}t} = F(x(t), x(t-\tau))\,, \tag{4.1}$$

where τ is the delay time. To be well-posed, a problem represented in this form requires initial data, which includes the values of the function $x(t)$ over an interval of time τ. In numerical computations, the function $x(t)$ in the interval $t \in [0, \tau]$ is called history of the system. Delay equations depict systems in which a stimulus results in a response that is delayed in time. Practical examples of such systems can be found in various fields, including control theory, economics, population biology, physics, and others.

The equation describing the Mackey-Glass system is as follows:

$$\frac{dx}{dt} = f(x, x_\tau) \equiv \frac{a x_\tau}{1 + (x_\tau)^b} - cx\,. \tag{4.2}$$

In this equation, $x_\tau \equiv x(t-\tau)$ represents the time-delay variable. The parameters τ, a, b, and c are all real numbers greater than zero, with τ representing the delay time.

The model originally defines the blood production. In this context, $x(t)$ represents the concentration of blood at the time t, while $x(t-\tau)$ is the concentration when the body signals the need for more blood [72]. Patients with leukemia may experience a significantly large time delay τ, leading to oscillations in the concentration of blood. When τ is even larger, the concentration can vary chaotically, as originally demonstrated by Mackey and Glass [59].

The dynamical behavior of the Mackey-Glass system has been extensively explored, particularly focusing on periodic and chaotic oscillations, by varying its parameters [59,72–75,139]. Different parameter settings in the model lead to variations in several crucial characteristics. These include the delay time (τ) determining the transition to chaotic regimes, the stability and oscillatory patterns exhibited by the model, the

occurrence of bifurcation cascades, and the impact of perturbations applied to the system [139–142]. In this study, we specifically consider the input parameters used in Refs. [73, 75], where a, b, and c are fixed at 2, 10, and 1, respectively [1].

4.3 Transition to chaos

The transition from periodic oscillations to chaotic ones in the Mackey-Glass system is achieved by adjusting the delay time τ. An increase in τ results in the emergence of new periods through period-doubling bifurcations, while periodic behaviors vanish, leading to a complete shift to chaotic states. This local change in stability is referred to as Hopf bifurcation [143, 144].

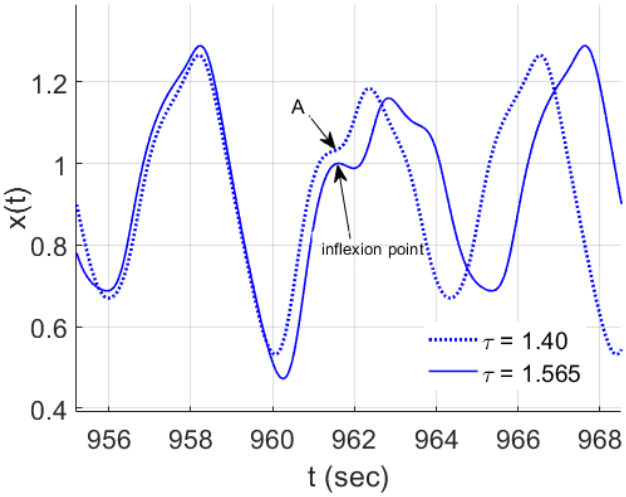

Figure 4.1: Time oscillations of variable x at $\tau = 1.40$ and $\tau = 1.565$. Point A at $\tau = 1.40$ evolves into an inflexion point at $\tau = 1.565$.

This transition is evident when analyzing the emergence of new periods. Fig. (4.1) illustrates the temporal oscillations of variable x at two different values of τ, specifically $\tau = 1.40$ and $\tau = 1.565$. At $\tau = 1.40$, point A takes on a certain characteristic, but it transforms into an inflection point at $\tau = 1.565$. The formation of an inflection point within the waveform corresponds to the emergence of a new period along the curve $f(x, x_\tau) = 0$ as seen in the return map shown in Fig. (4.2).

[1] Another common parameter set in the literature is achieved by scaling these parameters as $a = 0.2$, $b = 0.1$ and $c = 10$.

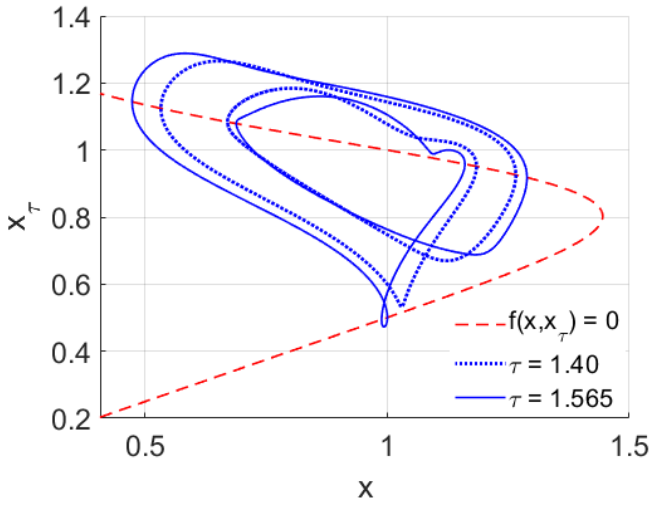

Figure 4.2: Emerging of a new period along the curve $f(x, x_\tau) = 0$.

To identify the initiation of a new period's formation, Fig. (4.3) presents the results at several values of τ, namely $\tau = 1.40, 1.456, 1.49, 1.565$. It's worth noting that at $\tau = 1.456$, point A intersects the curve $f(x, x_\tau) = 0$, representing the birth of a new period. At $\tau = 1.49$ and $\tau = 1.565$, point A becomes the maximum of the corresponding waveform and intersects the solution of the curve $f(x, x_\tau) = 0$ at an additional intersection point, representing a local minimum within this new periodic motion.

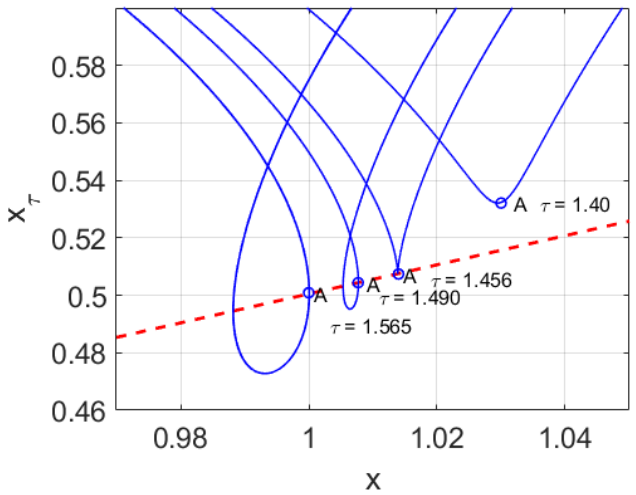

Figure 4.3: The beginning of a new period formation along the curve $f(x, x_\tau) = 0$. Calculations are carried out at $\tau = 1.40, 1.456, 1.49$, and 1.565.

The point A occurs when both the first and second derivatives of the function are equal to zero ($\frac{\mathrm{d}x}{\mathrm{d}t} = \frac{\mathrm{d}^2x}{\mathrm{d}t^2} = 0$). This particular scenario is depicted in Fig. (4.4). It's noteworthy that the intersection point of the first and second derivatives along the y axis corresponds to point A in the solution $x(t)$.

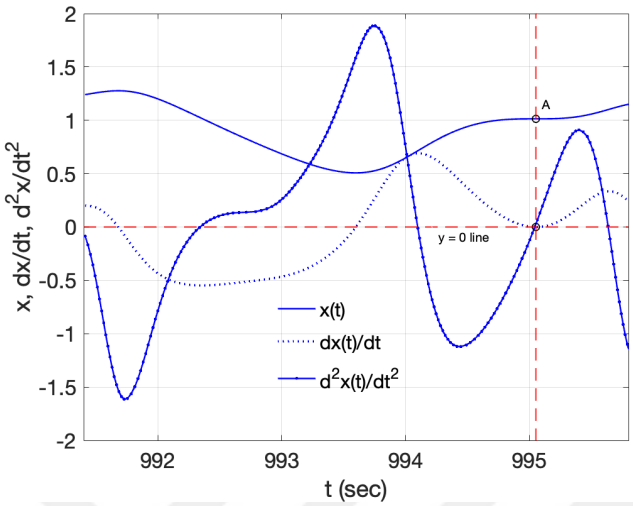

Figure 4.4: Time oscillations of x, $\frac{\mathrm{d}x}{\mathrm{d}t}$, $\frac{\mathrm{d}^2x}{\mathrm{d}t^2}$, where the intersection point of $\frac{\mathrm{d}x}{\mathrm{d}t}$ and $\frac{\mathrm{d}^2x}{\mathrm{d}t^2}$ along the y-axis corresponds to the point A on the solution x.

The diagram in Fig. (4.5), depicting the onset of the period-doubling bifurcation cascade in the $x(t)$ and τ plane, is obtained by considering local maxima (peaks) of oscillations against the delay time. It's important to note that a single new branch emerges suddenly at $\tau = 1.475$, and this birth is dependent on the chosen values of constants a and b [140–142].

It's worth mentioning that more typical bifurcations, excluding the abrupt emergence and disappearance of branches, can be achieved by selecting appropriate constant values. Different bifurcation diagrams for various values of a, b, and c are presented in Refs. [140–142]. By altering these parameters, the system's dynamics can transition from chaotic to periodic behavior within specific ranges of the delay time, followed by a return to chaotic regimes. However, this particular behavior is not observed with the parameters used in this paper.

The vertical lines in the bifurcation diagram, Fig. (4.5), correspond to the values of $\tau = 1.2, 1.4, 1.55$, and 2.5, representing the regimes (a)-(d) illustrated in Fig. (4.6).

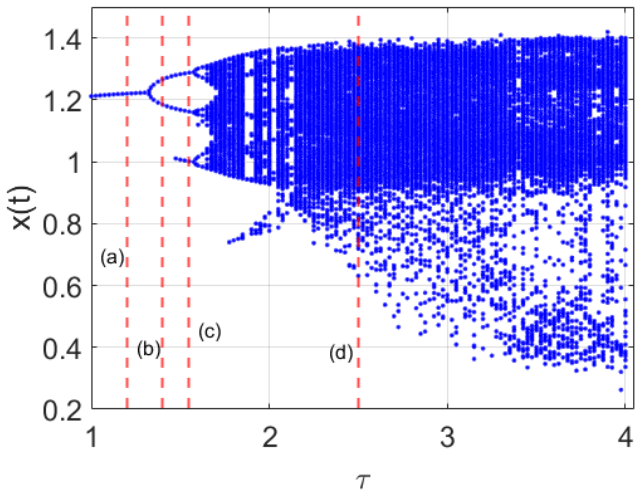

Figure 4.5: The onset of the period-doubling bifurcation cascade. The regimes (a), (b), (c), and (d) correspond to those in Fig. (4.6).

The transient solutions are not included in this analysis. In Fig. (4.6a), the oscillations deviate from the fixed point $x = 1$ and eventually evolve into limit cycle oscillations with a single period. Fig. (4.6b) exhibits oscillations with two periods, and a new periodic trajectory (the third one) emerges from an existing one in Fig. (4.6c). Period-doubling bifurcation is often regarded as a typical pathway to temporal chaos [145, 146], and Fig. (4.6d) illustrates a fully chaotic state.

In Refs. [73, 75], the stable and unstable oscillations at the fixed point $x = 1$ were categorized by altering τ, while keeping the same values for a, b, and c. It was determined that the solutions exhibit chaotic behavior when $\tau > 1.68$. In the subsequent analysis, we consider a fully chaotic state with $\tau = 100$.

4.4 Synchronization of chaos

The unidirectionally coupled Mackey-Glass systems with the constants mentioned in previous section are defined as follows.

$$\frac{dx}{dt} = \frac{2x_\tau}{1 + x_\tau^{10}} - x\,, \tag{4.3a}$$

$$\frac{dy}{dt} = \frac{2y_\tau}{1 + y_\tau^{10}} - y + \varepsilon(x - y)\,. \tag{4.3b}$$

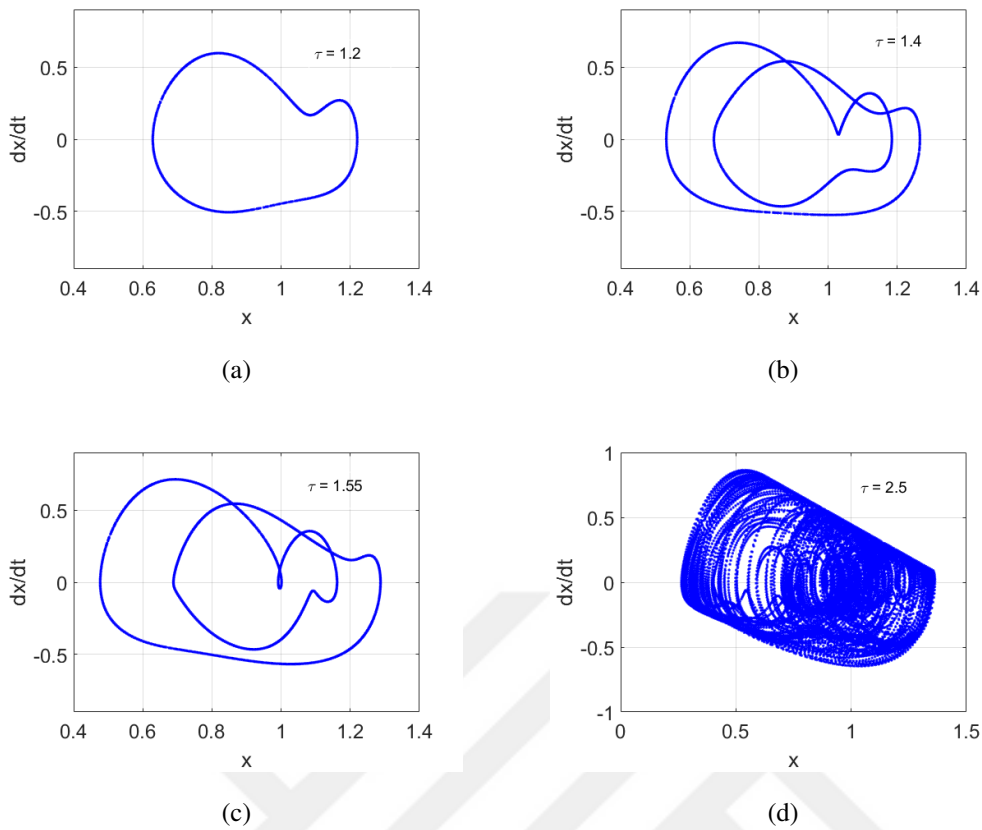

Figure 4.6: Phase space trajectories of the oscillations in the plane of $\frac{\mathrm{d}x}{\mathrm{d}t}$ and x for various delay values τ defined in Fig. (4.5).

Here, $x_\tau \equiv x(t-\tau)$, $y_\tau \equiv y(t-\tau)$, and ε represents the coupling constant. Equations (4.3a) and (4.3b) are referred to as the drive and response systems, respectively. The value of τ is fixed at $\tau = 100$ to ensure chaotic motion [73, 75].

To analyze generalized synchronization, the auxiliary system can be defined as follows.

$$\frac{dz}{dt} = \frac{2z_\tau}{1+z_\tau^{10}} - z + \varepsilon(x-z). \tag{4.4}$$

The only difference between the auxiliary and response systems is their histories, or solutions at $t \leq \tau$. Generalized synchronization is achieved for the drive and response systems if the asymptotic stability condition (2.11) is satisfied for the response and auxiliary systems. It is important to note that transient solutions are ignored in this analysis.

The synchronization threshold for generalized synchronization is provided in the paper [75], with a value of approximately $\varepsilon_c \approx 0.702$. Generalized synchronization occurs when ε surpasses the synchronization threshold, i.e., $\varepsilon > \varepsilon_c$, while it is absent when ε falls below the threshold, i.e., $\varepsilon < \varepsilon_c$. In this study, we consider two specific coupling constants to compare the DSC with generalized synchronization. One coupling constant is slightly above but still in the vicinity of the synchronization threshold, with $\varepsilon = 0.71$. The other has a lower value, significantly below the threshold, at $\varepsilon = 0.6$.

The unpredictability and DSC analyses in both regions are conducted with a simulation time of $t_{sim} = 500000$ and a time step of $\Delta t = 0.2$. The drive and response systems also use the same values of t_{sim} and Δt for consistency.

4.4.1 Synchronization of chaos above the threshold

At $\varepsilon = 0.71$, for the coupled systems (4.3a) and (4.3b), generalized synchronization has been confirmed using the auxiliary system (4.4), indicated in Fig. (4.7). The figure illustrates the motion occurring on the $y = z$ line, signifying the fulfillment of the asymptotic stability condition (2.11). The analysis excludes the transient regime.

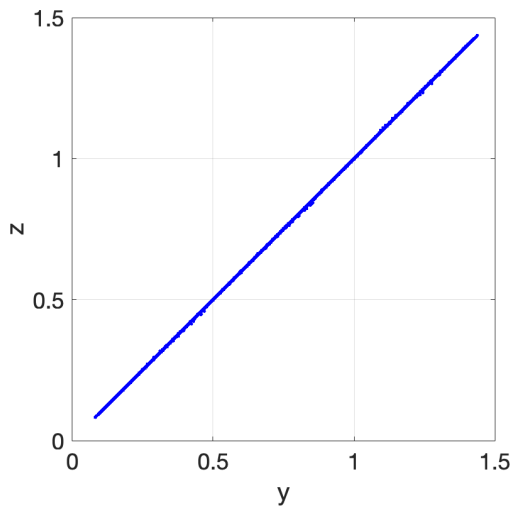

Figure 4.7: Projection of response and auxiliary systems on (y, z) plane for $\epsilon = 0.71$ after transient regime.

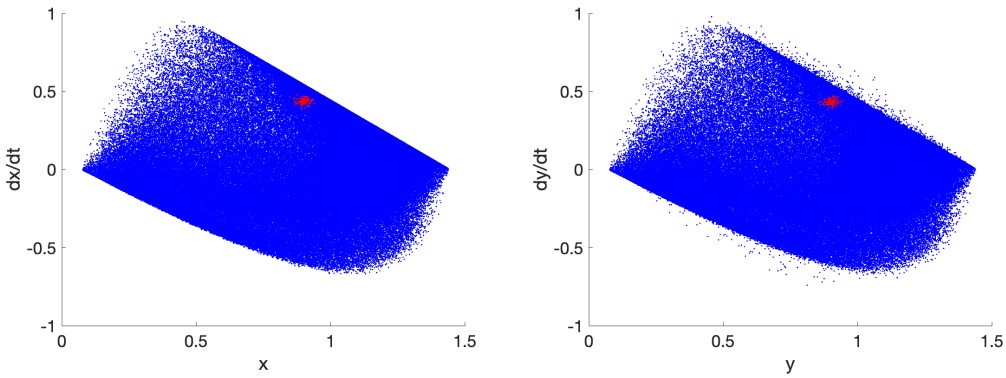

(a) Drive system

(b) Response system

Figure 4.8: Phase portraits of drive and response systems for $\varepsilon = 0.71$. Red marks represent $(x(t_n), \dot{x}(t_n))$ and $(y(t_n), \dot{y}(t_n))$.

In the unpredictability analysis, we have set $\Delta_d = 1.4$ for the drive system and $\Delta_r = 1.19$ for the response system. The values of δ decrease for each member of the convergence and separation sequences, starting with $\delta_1 = 0.0500$, $\delta_2 = 0.0497$, $\delta_3 = 0.0494$, and so on. The phase portraits of the drive and response systems are presented in Fig. (4.8). In Figs.(4.8a) and (4.8b), the red marks indicate $(x(t_n), \dot{x}(t_n))$ and $(y(t_n), \dot{y}(t_n))$, respectively.

The drive system's unpredictable motion is outlined in Table (4.1), which provides details about the sequences of convergence and separation, along with the corresponding δ_n values. The table includes 163 pairs of t_n and s_n, with $\delta_{163} = 0.0014$. The degree of numerical unpredictability, denoted as α, is calculated as $\alpha_{163} = 0.0014/1.4 = 0.001$. This small value is achieved over an extensive simulation time of $t_{sim} = 500000$. Consequently, the drive system exhibits unpredictability in accordance with the conditions outlined in Def. (1).

The unpredictable behavior of the response system is illustrated in Table (4.2). The table lists the sequences of convergence and separation at 165 time instances. Over the extensive simulation time of $t_{sim} = 500000$, the smallest distance between the trajectories and the initial point is $\delta_{165} = 0.0008$. The degree of unpredictability, denoted as α, is calculated as $\alpha_{165} = 0.0008/1.19 \approx 0.0007$, which is a sufficiently small value indicative of the chaotic nature of the motion. Therefore, the response system

Table 4.1: Sequences of convergence t_n and separation s_n with δ_n values for the drive system.

n	t_n	s_n	δ_n
1	1006	1420	0.0500
2	1017	2332	0.0497
3	1114	3401	0.0494
4	1409	3667	0.0491
5	1606	4384	0.0488
	⋮		
	⋮		
159	126954	139195	0.0026
160	182244	139343	0.0023
161	211316	141346	0.0020
162	216785	141724	0.0017
163	307457	141799	0.0014

exhibits unpredictable behavior in line with the conditions specified in Def. (1).

The common sequences of convergence u_n and separation v_n, according to the conditions specified in Def. (3), are presented in Table (4.3). The sequence of convergence u_n consists of 155 time instances, while the sequence of separation v_n comprises 151 time moments. For the largest v_n value, δ_n value observed during the simulation is $\delta_n = 0.005$, which is a small value given the simulation time $t_{sim} = 500000$.

It is essential to note that the separation moments v_n for $n = 152, 153, 154,$ and 155 are not detected within the simulation time. Prolonging the simulation further to detect more v_n moments is not necessary for two reasons. First, the 151 elements in the sequence of separation are sufficiently close in number to the lengths of the sequences in the drive and response systems, which consist of 163 and 165 time instances, respectively. Second, the value of $\delta_{151} = 0.005$ is considered sufficiently small for the synchronization analysis.

Hence, based on the conditions set forth in Def. (3), the complete synchronization

Table 4.2: Sequences of convergence t_n and separation s_n with δ_n values for the response system for $\varepsilon = 0.71$.

n	t_n	s_n	δ_n
1	1006	110	0.0500
2	1017	197	0.0497
3	1114	713	0.0494
4	1409	832	0.0491
5	1606	833	0.0488
	⋮		
	⋮		
161	126235	13408	0.0020
162	126954	13416	0.0017
163	182244	13440	0.0014
164	183663	13502	0.0011
165	486244	13587	0.0008

of unpredictability is verified with the degree of numerical synchronization $\alpha_{151}^{synch} = 0.0036$. This is a stronger form of delta synchronization of chaos implying almost equal amount of elements of the sequences of convergence and separation in unpredictability analysis is synchronized in a sufficiently large simulation time. Furthermore, it will be demonstrated in the next subsection that the degree of numerical synchronization in complete synchronization of unpredictability is smaller compared to delta synchronization of chaos.

The analysis demonstrates the coexistence of generalized synchronization and complete synchronization of unpredictability above the synchronization threshold. The coupling constant $\varepsilon = 0.71$ is intentionally selected near the threshold value of $\varepsilon_c \approx 0.702$. This choice is deliberate as the increase in this value strengthens synchronization and already implies the simultaneous presence of both synchronization types.

Table 4.3: Common sequences of convergence u_n and separation v_n with δ_n between drive and response systems $\varepsilon = 0.71$.

n	u_n	v_n	δ_n
1	1006	3607	0.0500
2	1017	3913	0.0497
3	1738	4369	0.0494
	⋮		
	⋮		
145	216785	181017	0.0068
146	216959	181879	0.0065
147	235239	182025	0.0062
148	254539	182691	0.0059
149	282905	183994	0.0056
150	302035	185132	0.0053
151	307457	187115	0.0050
152	312688	-	0.0047
153	343333	-	0.0044
154	362248	-	0.0041
155	486244	-	0.0038

4.4.2 Synchronization of chaos below the threshold

Synchronization of chaos below the threshold is explored for the coupled systems described in Eqs. (4.3a) and (4.3b) at $\varepsilon = 0.60$. By utilizing the auxiliary system defined in Eq. (4.4), it is apparent that the coupled systems lack generalized synchronization at $\varepsilon = 0.60$, as depicted in Fig. (4.9). This figure illustrates that the motion does not occur along the $y = z$ line, affirming the non-satisfaction of the asymptotic stability condition (2.11) and thus confirming the absence of generalized synchronization.

The unpredictability analysis is conducted on the response system with the new coupling value of $\varepsilon = 0.60$ and $\Delta_r = 1.42$. The distance values between the initial point and $y(t_n)$ are $\delta_1 = 0.0500, \delta_2 = 0.0497, \delta_3 = 0.0494$, and so on. The phase portrait

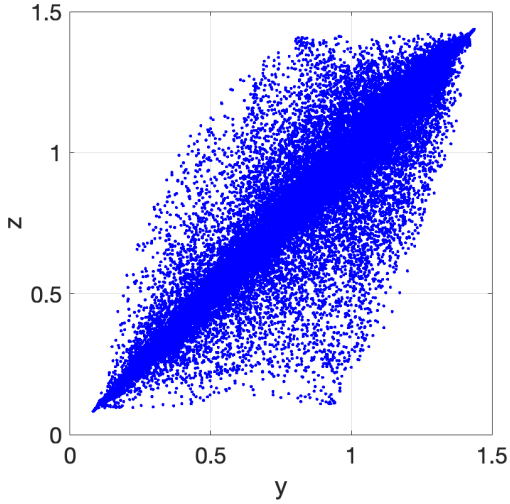

Figure 4.9: Projection of response and auxiliary systems on (y, z) plane for $\epsilon = 0.60$ after transient regime.

of the response system, represented by red marks, is shown in Fig. (4.10). Since the coupling ε remains unchanged in the drive system, it is exactly the same as in section 4.4.1. Therefore, the phase portrait and unpredictability table from the previous subsection, shown in Fig. (4.8a) and table (4.1), are still applicable for this analysis. It's essential to note that the sole difference between the response system in this section and that in section 4.4.1 is the coupling constant.

The response system's sequences of convergence and separation, along with the corresponding δ_n values, are displayed in Table (4.4). This table comprises 165 time points, with a final distance of $\delta_{165} = 0.0008$ between $y(0)$ and $y(t_{165})$. The degree of numerical unpredictability, $\alpha_{165} \approx 0.0006$, is a sufficiently small value achieved within the extensive simulation duration of $t_{sim} = 500000$. Therefore, the unpredictability is confirmed based on the conditions outlined in Def. (1).

The common sequences of finite convergence and divergence, as defined in Def. (3), are detailed in Table (4.5). This table contains 132 u_n values in the sequence of finite convergence, and no common time moment is detected after v_{108} in the sequence of separation. The minimum relevant distance, $\delta_{108} = 0.0179$, is comparatively larger than in the previous unpredictability and complete synchronization of unpredictability analyses. The degree of numerical synchronization, $\alpha_{108}^{synch} = 0.013$, is 3.6 times

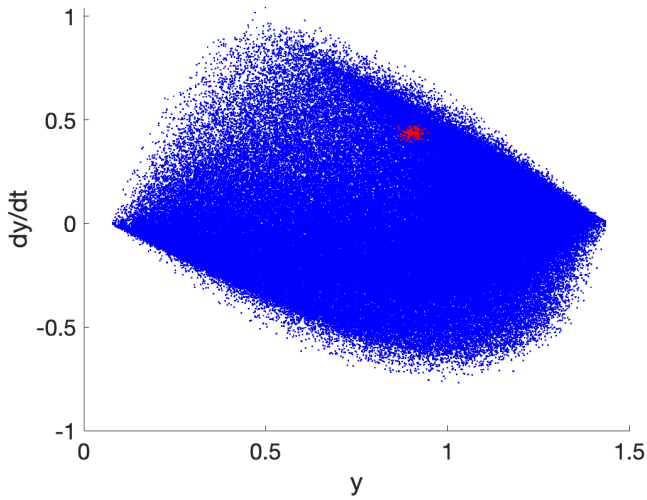

Figure 4.10: Phase portrait of response system for $\varepsilon = 0.6$. Red marks represent $(y(t_n), \dot{y}(t_n))$.

greater than the degree of numerical synchronization for the analysis above the threshold, yet still less than one. Hence, delta synchronization of chaos is confirmed according to Def. (3).

At $\varepsilon = 0.60$, falling below the synchronization threshold of approximately $\varepsilon \approx 0.702$ specified for the generalized synchronization analysis with the provided parameters [75], the delta synchronization of chaos is identified in the absence of generalized synchronization.

Previous analyses in literature, such as [73, 75], have explored chaos synchronization and identified the critical coupling value in the Mackey-Glass system for this phenomenon. In our study, we reproduced the results above the threshold as presented in Ref. [75] and demonstrated the coexistence of generalized synchronization and complete synchronization of unpredictability. Existing literature predominantly addresses synchronization types above the threshold [65, 73–76]. However, our research shows the existence and detection of this phenomenon using the DSC method below the threshold. Hence, our study verifies the synchronization of chaos through unpredictability on both sides of the threshold.

Table 4.4: Sequences of convergence t_n and divergence s_n with δ_n values for the response system with $\varepsilon = 0.60$.

n	t_n	s_n	δ_n
1	1006	2823	0.0500
2	1017	3306	0.0497
3	1111	3340	0.0494
4	1409	3667	0.0491
5	1606	4384	0.0488
	⋮		
	⋮		
161	188812	178538	0.0020
162	219069	179205	0.0017
163	235464	179861	0.0014
164	238264	180461	0.0011
165	301502	180473	0.0008

4.5 Discussion

In this research, we've delved into chaos synchronization within Mackey-Glass time-delay systems. Through investigating the unpredictability of both the drive and response systems, we have substantiated the presence of chaos in both contexts. Our exploration of the synchronization phenomenon has been carried out using the innovative DSC method, rooted in unpredictability analysis. The main novelty of our work lies in uncovering synchronization in an area previously deemed unattainable by traditional methods [75]. Notably, we've detected chaotic systems' synchronization for a coupling constant situated below the typical synchronization threshold.

Through adjusting the coupling constant beyond the synchronization threshold in unidirectionally coupled Mackey-Glass systems, we observed alterations in the synchronization properties of the model. Above the synchronization threshold, we noted the simultaneous presence of generalized synchronization and complete synchronization of unpredictability. Notably, even when the coupling approached the threshold

Table 4.5: Common sequences of convergence u_n and divergence v_n with δ_n between drive and response systems $\varepsilon = 0.60$.

n	u_n	v_n	δ_n
1	1017	2332	0.0500
2	1738	2389	0.0497
3	1938	3710	0.0494
	⋮		
	⋮		
105	159340	310116	0.0188
106	167894	311753	0.0185
107	169829	312105	0.0182
108	172648	314333	0.0179
109	188812	-	0.0176
	⋮		
	⋮		
132	497535	-	0.0107

closely but still exceeded it, the DSC analysis identified the existence of complete synchronization of unpredictability.

Our most significant finding emerges from the analysis below the synchronization threshold, where generalized synchronization is not observed. In this domain, we've demonstrated the presence of delta synchronization of chaos, a unique form of synchronization that examines time sequences within the model. Consequently, the threshold is no longer a prerequisite for chaos synchronization uncovered via unpredictability. These results align with analogous findings in other models as documented in Refs. [11,22], underscoring the potential of the DSC method to reveal synchronization in the absence of generalized synchronization. However, whether there exists a boundary for achieving synchronization through unpredictability remains an open question.

To support our analyses and findings, we have included numerical details regarding unpredictability and DSC, along with tables illustrating time sequences of conver-

gence and separation. Our results show that both the drive and response systems exhibit unpredictable behavior for all coupling constants, as evidenced by the degree of numerical unpredictability. Above the threshold, strong degree of numerical synchronization is observed, supporting the existence of complete synchronization of unpredictability. However, below the threshold, the numerical characteristic shows a substantial increase, signifying weaker synchronization and confirming the presence of delta synchronization of chaos.

CHAPTER 5

MARKOVIAN NOISE-INDUCED DELTA SYNCHRONIZATION APPROACH FOR HINDMARSH-ROSE MODEL

Synchronization's importance spans to neural network studies, particularly in information exchange among neurons within an ensemble [89–91]. It has implications for neurodegenerative diseases like Alzheimer's and Parkinson's, where abnormal synchronization patterns in the brain have been noted [92, 93]. This underscores the necessity to comprehend and measure synchronization, offering potential applications in both scientific inquiry and practical contexts.

Experimental evidence highlights how external currents can induce chaotic behavior in neurons [94, 95]. However, deterministic models often struggle to capture real-world scenarios due to inherent external perturbations, termed noise. Previous studies have shown that this noise can trigger synchronization in neural networks [96–101]. Our research delves into understanding noise-induced synchronization within individual Hindmarsh-Rose neurons, using innovative methods to explore this phenomenon more comprehensively.

The Hindmarsh-Rose model comprises three differential equations that represent distinct aspects of a single neuron's behavior. These equations relate to the neuron's membrane potential, the recovery variable that is responsible for fast ion transport, and the adaptation current [77]. Extensive research has focused on this model, exploring diverse synchronization scenarios [83–88].

In the field of noise-induced synchronization, previous studies have primarily employed Gaussian white noise, as seen in Refs. [99–101]. This study, on the other hand, takes a novel approach by investigating synchronization within the Hindmarsh-

Rose model in the presence of Markovian noise. This extension of our research scope provides a fresh perspective on the phenomenon of synchronization.

Noise terms based on Markov properties find a wide array of applications across diverse research domains [102–104]. In our study, we construct noise using Markov chains, designed to adhere to the fundamental principles of Markov properties [105–107]. The specific methods used to generate these noise terms are detailed in Ref. [108], which introduces the concept of Markov coefficients within Duffing-type equations. This stochastic noise, derived through these methods, possesses a distinct and notable attribute—unpredictability [109]. This inherent unpredictability is characterized by specific numerical features related to convergence and separation sequences, making it particularly suitable for observing novel synchronization phenomena that cannot be detected using Gaussian white noise. However, it's important to note that the unpredictability of Gaussian noise remains an open problem in the field. This inherent unpredictability plays a significant role in our investigation of synchronization phenomena within the Hindmarsh-Rose model.

This study introduces significant advancements in the study of Hindmarsh-Rose neural networks. It breaks from traditional studies that mostly employ Gaussian white noise and explore generalized or identical synchronization [99–101]. Instead, it adopts an innovative approach by incorporating continuous and unpredictable Markovian noise in these systems, revealing synchronization phenomena through novel methods.

Notably, this research demonstrates the existence of delta synchronization of chaos (DSC) in the absence of identical synchronization (IS), similar to other instances where DSC occurs independently of generalized synchronization [11, 22, 23]. Moreover, it unveils complete synchronization of unpredictability past a specific threshold of noise intensity, akin to synchronization observations triggered by certain coupling constants in Mackey-Glass systems [23]. These findings highlight the broad applicability and importance of these synchronization discoveries. The findings and details of this research, which is rigorously covered in the present chapter, have been published in Ref. [24].

5.1 Hindmarsh-Rose Model with Markovian Noise

The Hindmarsh-Rose neuron model characterizes the dynamics of a single neuron, capturing phenomena such as spiking-bursting behavior and chaos. The model can be described as follows [77].

$$\begin{aligned} \dot{x} &= y - ax^3 + bx^2 - z + I \,, \\ \dot{y} &= c - dx^2 - y \,, \\ \dot{z} &= r(s(x - x_0) - z) \,, \end{aligned} \tag{5.1}$$

where x is membrane potential, y is the recovery variable associated with the transport of fast ions, sodium and potassium, and z is the adaptation current. a, b, c, d, r, s, x_0 are real constants. I is the external current. The parameters are taken as $a = 1$, $b = 3$, $c = 1$, $d = 5$, $r = 0.006$, $s = 4$, and $x_0 = -1.6$.

The system displays various bursting patterns as the parameter I is varied. The membrane potential x exhibits spiking-bursting behavior, as depicted in Fig. (5.1). At $I = 1$, the solution is stationary. As I increases beyond 1, spiking-bursting behavior is initiated. Periodic patterns are observed at $I = 1.5$ and $I = 2$, while chaotic dynamics emerge at $I = 3$ and $I = 3.4$. The system transitions back to a periodic regime at $I = 4$.

To depict the shift between periodic and chaotic dynamics, Fig. (5.2) displays the bifurcation cascade of interspike intervals (ISI) concerning the external current I. The ISI measures the time gap between consecutive spikes, excluding the transient regime. Within the range $I = [2.9, 3.4]$, irregular ISIs leading to chaos dominate, while periodic dynamics are evident before and after this interval. This study specifically concentrates on the chaotic behavior observed at $I = 3$.

5.1.1 Markovian noise

Let a Markov chain be given for $n \geq 0$ as follows

$$X_{n+1} = X_n + \Theta_n \,, \tag{5.2}$$

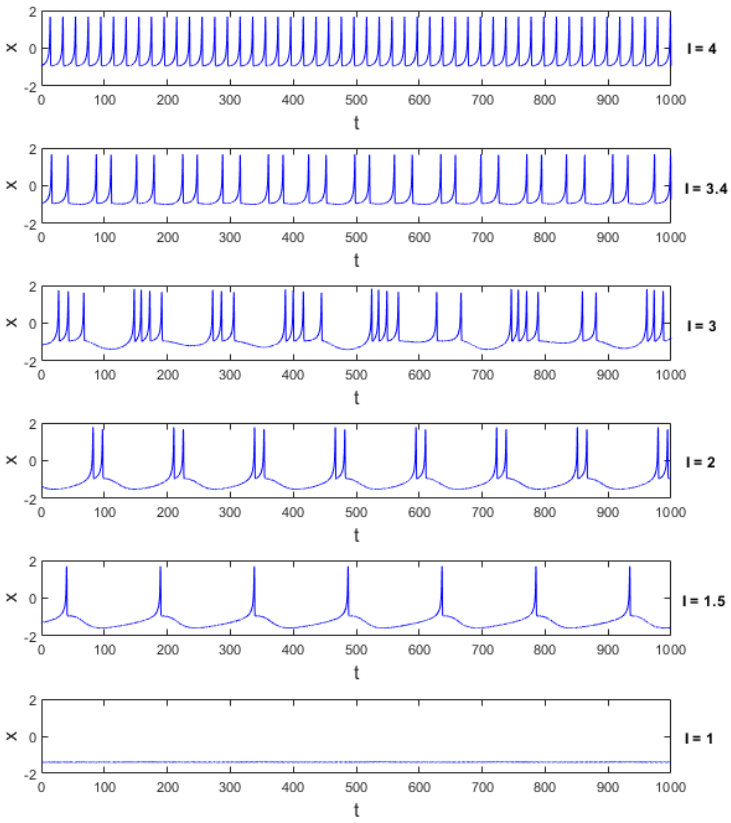

Figure 5.1: Different bursting patterns of membrane potential x for various external currents I.

with $X_0 = 0$, and random numbers Θ_n are defined as

$$\Theta_n = \begin{cases} -0.5\,, & \text{for } X_n = 5 \\ -0.5 \text{ or } 0.5\,, & \text{for } X_n \neq -5 \text{ or } 5 \\ 0.5\,, & \text{for } X_n = -5 \end{cases} \tag{5.3}$$

Hence, the values of X_n are confined within the interval $[-5, 5]$ with a probability distribution given by $P(\Theta_n = 0.5) = P(\Theta_n = -0.5) = \frac{1}{2}$ when $X_n \neq -5, 5$. The probabilities at the boundaries are $P(\Theta_n = -0.5) = 1$ and $P(\Theta_n = 0.5) = 1$ for $X_n = 5$ and $X_n = -5$, respectively. Defining the state space as $S = \{s_0, s_1, \ldots, s_{21}\} = \{-5, -4.5, \ldots, 5\}$, the sequence conforms to a Markov chain with the Markov property $P(X_{n+1} = s_i | X_0 \ldots X_n) = P(X_{n+1} = s_i | X_n)$ for $s_i \in S$ and $n \geq 0$ [105–107].

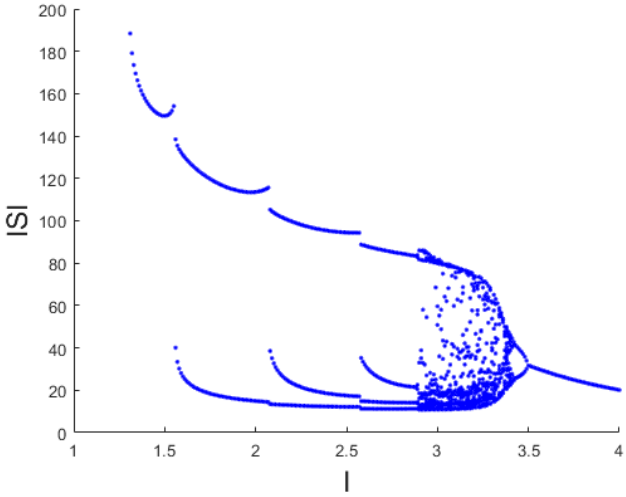

Figure 5.2: Bifurcation diagram of ISIs vs external current I.

It's important to note that the infinite realizations of the dynamics exhibit unpredictability, as demonstrated in Ref. [109].

Let ρ-type piecewise constant unpredictable functions be constructed through the Markov chain X_n such that $\rho(t) = X_n$ for $t \in [hn, h(n+1))$. Fig. (5.3) depicts the time evolution of $\rho(t)$ for $h = 0.001$ and $t = [0, 2]$.

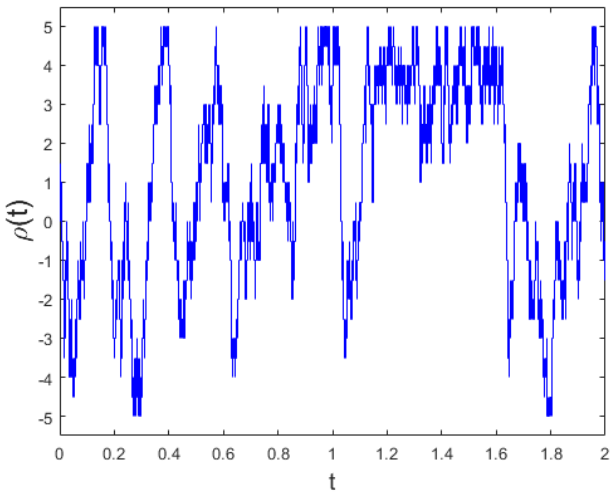

Figure 5.3: Time evolution of $\rho(t)$.

σ-type piecewise functions can be derived from ρ-type functions, specifically using the relationship $\sigma(t) = \rho^2(t) + \rho(t)$. This function, determined by the Markov chain,

is both discontinuous and unpredictable, as demonstrated in Ref. [13]. Fig. (5.4) presents the time evolution of $\sigma(t)$.

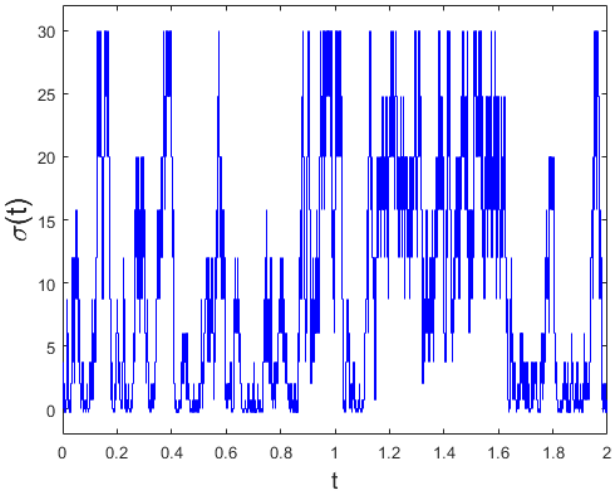

Figure 5.4: Time evolution of $\sigma(t)$.

Consider the stochastic differential equation given by

$$\gamma'(t) = \alpha\gamma(t) + \sigma(t)\,, \tag{5.4}$$

where α is a negative number. It has been demonstrated that Eq.(5.4) possesses a continuous, unpredictable, and exponentially stable unique solution denoted as $\Theta(t)$ [147]. For our analysis, we will utilize the solution $\gamma(t)$ with initial condition $\gamma(0) = 0.6$ and $\alpha = -3$, which exponentially converges to the unpredictable function $\Theta(t)$ [108]. The solution is illustrated in Fig. (5.5) for $t \in [0, 50]$.

Given the specified parameters, the solution of Eq.(5.4) is utilized as noise in this investigation. It's important to note that Figs.(5.3), (5.4), and (5.5) provide snapshots of $\rho(t)$, $\sigma(t)$, and $\gamma(t)$ in small-time intervals, primarily for illustrative purposes.

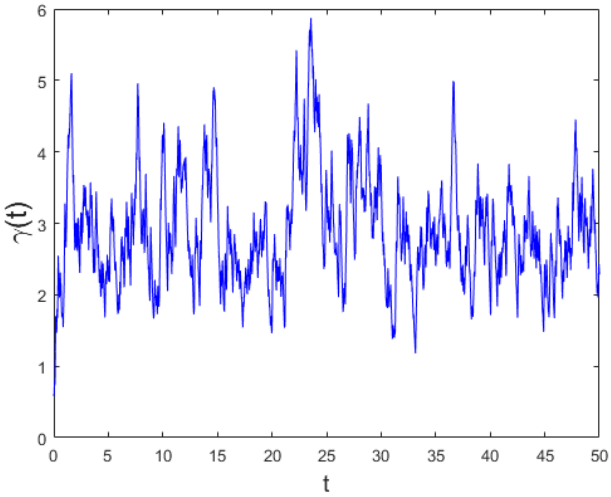

Figure 5.5: Time evolution of the noise.

5.1.2 Uncoupled Hindmarsh-Rose neurons with Markovian noise

The uncoupled Hindmarsh-Rose equations with Markovian noise are expressed as follows.

$$\begin{aligned} \dot{x}_i &= y_i - ax_i^3 + bx_i^2 - z_i + I + D\gamma(t)\,, \\ \dot{y}_i &= c - dx_i^2 - y_i\,, \\ \dot{z}_i &= r(s(x_i - x_0) - z_i)\,, \end{aligned} \tag{5.5}$$

where $i = 1, 2$ denotes systems one and two. The parameters are set as $a = 1$, $b = 3$, $c = 1$, $d = 5$, $r = 0.006$, $s = 4$, $x_0 = -1.6$, and $I = 3.0$. Here, D represents the noise intensity, and $\gamma(t)$ is the Markovian noise generated as described in section 5.1.1. This same $\gamma(t)$ is employed as noise in Eq. (5.5) for $i = 1, 2$. The only distinction between the two neurons lies in their initial conditions.

Synchronization is examined in the uncoupled systems based on the provided parameters. identical synchronization is identified through the analysis of synchronization errors between the two neurons. The average error is calculated as follows.

$$\langle e \rangle = \left\langle \sqrt{(x_1 - x_2)^2 + (y_1 - y_2)^2 + (z_1 - z_2)^2} \right\rangle\,, \tag{5.6}$$

where $\langle \cdot \rangle$ denotes a time average. $\langle e \rangle = 0$ indicates that the neurons exhibit identical synchronization. The phenomenon is further explored through the lens of unpre-

dictability. Def. (3) is applied to the neurons, and the obtained results are compared to identical synchronization.

5.2 Numerical Results

The uncoupled Hindmarsh-Rose neurons, governed by equation (5.5), undergo simulation with Markovian noise over the interval $t \in [0, 10^6]$. In this context, throughout the paper, the terms "neuron-1" and "neuron-2" refer to the instances where $i = 1$ and $i = 2$ in equation (5.5). The synchronization errors corresponding to various noise intensities are depicted in Fig. (5.6). This figure demonstrates that identical synchronization is attained when $D \geq 3$, as indicated by $e = 0$ within this range.

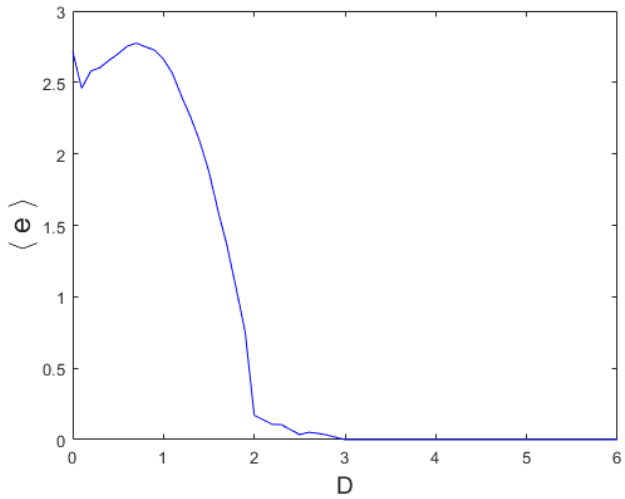

Figure 5.6: Average errors for different noise intensities.

The unpredictability of neuron-1 and neuron-2 is evaluated using Def. (1) and Algorithm (1). This involves employing a sequence of δ values starting from 0.2 and decreasing incrementally $(0.199, 0.198, \ldots)$ with $\Delta = 6$. Fig. (5.7) illustrates the degrees of numerical unpredictability for different noise intensities.

Remarkably, the results depicted in Figs.(5.7a) and (5.7b) closely match each other, indicating that both neurons consistently display sufficiently small degrees of unpredictability across all noise intensities. Furthermore, the numbers of elements n in all sequences t_n and s_n fall within the range of $n = [109, 200]$ for all noise intensities.

This confirms that unpredictability for both neurons is validated according to Def. (1).

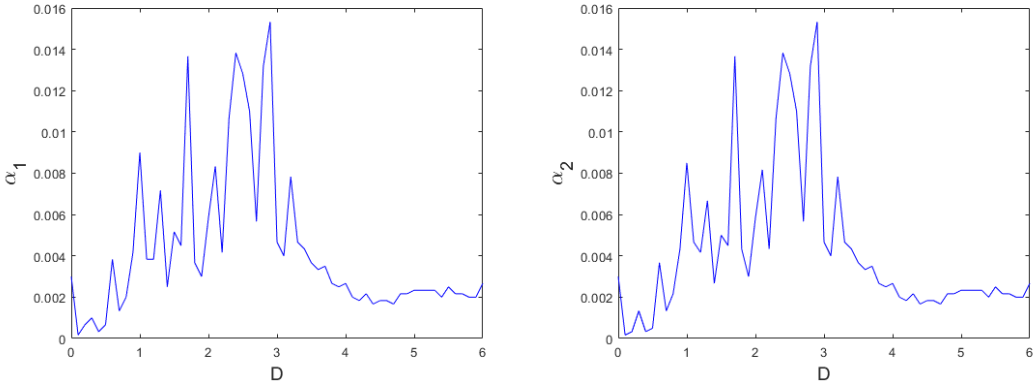

(a) Neuron-1

(b) Neuron-2

Figure 5.7: Degrees of numerical unpredictability for different noise intensities.

To explore synchronization through unpredictability, we employ Def. (3) on both neurons using Algorithm (2), maintaining consistent values for δ and Δ as in the unpredictability test. In Fig. (5.8), the degree of numerical synchronization is depicted for each D value. It is evident that small α_s values confirm synchronization, and the number of elements n in the corresponding sequences ranges from 65 to 101 for stochastic cases with low noise intensities D. In contrast, in the deterministic case where $D = 0$, the number of elements in these sequences is limited to $n = 12$, which is insufficient to confirm synchronization.

Moreover, for $D \geq 3.8$, α_s noticeably decreases, and the number of elements in the sequences significantly increases, reaching values of $n \geq 185$ within this range. Notably, the number of elements in the sequences of unpredictability matches those in the sequences of synchronization for $D \geq 3.8$. Based on Def. (3), it can be inferred that DSC exists for $D < 3.8$, while complete synchronization of unpredictability occurs for $D \geq 3.8$. For a more in-depth analysis, we will concentrate on two specific noise intensities: $D = 1$ and $D = 4.7$.

Let's consider the case with $D = 1$. Unpredictability is indeed affirmed by the numerical characteristics $\alpha_1 = 0.0090$ and $\alpha_2 = 0.0085$ for neuron-1 and neuron-2, respectively. Table (5.1) furnishes details regarding the initial and final elements of the convergence and separation sequences. Tables (5.1a) and (5.1b) document the

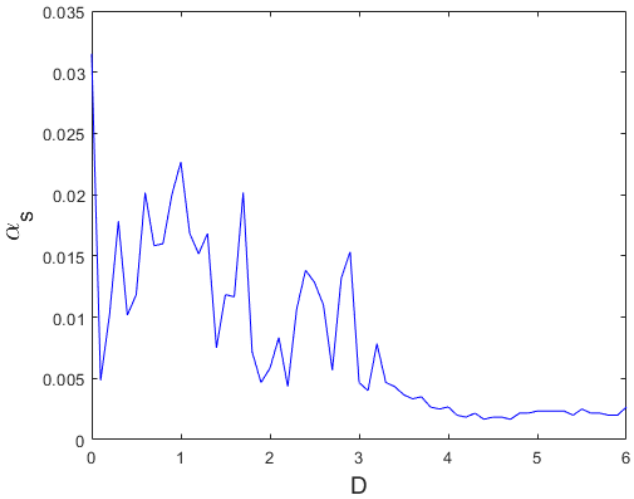

Figure 5.8: Degrees of numerical synchronization for different noise intensities.

instances of convergence and separation throughout the entire simulation time, which spans $t = 10^6$. However, a form of weak synchronization is apparent between the two neurons, as indicated by Table (5.2). This table reveals that the sequences of finite convergence and separation consist of only 65 elements, adequate for demonstrating synchronization but not robust synchronization. The numerical degree of synchronization is $\alpha_s = 0.023$. Hence, it can be inferred that the neurons exhibit delta synchronization of chaos, as outlined in Def. (3).

Unpredictability for $D = 4.7$ is confirmed through the numerical degrees of unpredictability, yielding $\alpha_1 = \alpha_2 = 0.0017$ for neuron-1 and neuron-2. Table (5.3) provides details regarding the initial and final elements of the convergence and separation sequences. There are 191 elements in the sequences, which are listed in Tables (5.3a) and (5.3b) for both neurons. These sequences span the entire simulation duration, suggesting that extending the simulation further would result in even larger sequences. With these observations and the substantial simulation time, it is established that Def. (1) holds true for both neurons.

Table (5.4) provides the moments of convergence and separation for the synchronization analysis of both neurons. A comparison between Tables (5.3) and (5.4) reveals that all elements within them are identical. Considering this, along with the fact that $\alpha_s = 0.0017$, it can be concluded that a stronger form of synchronization exists,

Table 5.1: Sequences of convergence and separation at $D = 1$ for unpredictability analysis.

n	t_n	s_n	δ_n
1	10115	10	0.200
2	11695	20	0.199
3	14673	32	0.198
4	17222	42	0.197
5	19254	53	0.196
	⋮		
	⋮		
143	857496	1506	0.058
144	884036	1518	0.057
145	896628	1529	0.056
146	953966	1540	0.055
147	962762	1550	0.054

(a) Neuron-1

n	t_n	s_n	δ_n
1	10114	10	0.200
2	11695	20	0.199
3	14502	31	0.198
4	17722	42	0.197
5	19537	53	0.196
	⋮		
	⋮		
146	889607	1550	0.055
147	910979	1561	0.054
148	914535	1571	0.053
149	938866	1582	0.052
150	982731	1592	0.051

(b) Neuron-2

specifically, complete synchronization of unpredictability.

The occurrence of synchronization induced by noise has been thoroughly investigated in the realm of Hindmarsh-Rose neurons, with a predominant focus on Gaussian white noise, as evidenced in references [83, 99–101]. These inquiries have unveiled that Gaussian noise prompts identical synchronization among Hindmarsh-Rose neurons. Nevertheless, there has been a conspicuous lack of research thus far employing Markovian noise to explore synchronization within Hindmarsh-Rose neural systems.

Nevertheless, our numerical findings indicate that synchronization can indeed be induced by Markovian noise, resulting in both identical synchronization and DSC. In the case of identical synchronization, the phenomenon between both neurons becomes evident beyond a certain threshold of noise intensity. This suggests that synchronization is not immediately apparent when examining the synchronization error right after the introduction of noise into the system. However, in alignment with pre-

Table 5.2: Sequences of finite convergence and separation at $D = 1$ in synchronization analysis.

n	u_n	v_n	δ_n
1	10302	10	0.200
2	17722	22	0.199
3	39972	32	0.198
4	43708	45	0.197
5	55483	57	0.196
	$\vdots$		
	$\vdots$		
61	864683	713	0.140
62	870097	725	0.139
63	907934	736	0.138
64	914535	750	0.137
65	972672	761	0.136

vious studies that have compared DSC to generalized synchronization [11, 22, 23], our results demonstrate that synchronization can be identified through unpredictability analysis.

Specifically, DSC starts to manifest itself following the application of Markovian noise. This intriguing discovery implies that the synchronization phenomenon occurs in a domain where identical synchronization is not present. Furthermore, our results unveil another notable insight: complete synchronization of unpredictability, representing a more robust form of synchronization, emerges in the vicinity where identical synchronization begins to occur.

Essentially, our study introduces two innovations. First, it pioneers the use of Markovian noise as a novel tool for exploring synchronization in Hindmarsh-Rose neural systems. Second, it reveals the presence of synchronization in domains where conventional methods fail to detect it, thus enhancing our understanding of synchronization phenomena within these neural systems.

Table 5.3: Sequences of convergence and separation for $D = 4.7$

n	t_n	s_n	δ_n
1	10372	10	0.200
2	12052	20	0.199
3	13734	30	0.198
4	15296	40	0.197
5	16845	50	0.196
	⋮		
	⋮		
187	884876	1880	0.014
188	930712	1890	0.013
189	944907	1900	0.012
190	957918	1910	0.011
191	979328	1920	0.010

(a) Neuron-1

n	t_n	s_n	δ_n
1	10372	10	0.200
2	12052	20	0.199
3	13734	30	0.198
4	15296	40	0.197
5	16845	50	0.196
	⋮		
	⋮		
187	884876	1880	0.014
188	930712	1890	0.013
189	944907	1900	0.012
190	957918	1910	0.011
191	979328	1920	0.010

(b) Neuron-2

5.3 Discussion

This research delves into the complex domain of synchronization phenomena within uncoupled Hindmarsh-Rose systems. It introduces a novel approach by employing continuous and unpredictable Markovian noise on both neurons, resulting in several noteworthy findings and contributions.

In the absence of noise, the deterministic system lacks any synchronization. However, the introduction of Markovian noise induces synchronization, and its strength escalates with increasing noise intensities. Expanding on previous studies that have investigated identical synchronization induced by Gaussian white noise [83, 99–101], this research reaffirms similar synchronization patterns when Markovian noise is applied to the neurons.

What distinguishes this research is the discovery that synchronization can manifest in regions where traditional methods, such as generalized and identical synchronization,

Table 5.4: Common sequences of convergence and separation for $D = 4.7$

n	u_n	v_n	δ_n
1	10372	10	0.200
2	12052	20	0.199
3	13734	30	0.198
4	15296	40	0.197
5	16845	50	0.196
	$\vdots$		
	$\vdots$		
187	884876	1880	0.014
188	930712	1890	0.013
189	944907	1900	0.012
190	957918	1910	0.011
191	979328	1920	0.010

are unable to detect it. This intriguing phenomenon, in line with our previous findings in other dynamical systems [11,22,23], is also observed in Hindmarsh-Rose neurons. Within these regions, the neurons demonstrate delta synchronization of chaos.

Numerical analyses illuminate the existence of unpredictability in the neurons across all noise intensities. Crucially, synchronization arises as a consequence of noise. Different levels of noise intensity lead to various synchronization types of unpredictability. Lower intensities give rise to delta synchronization, while higher intensities result in complete synchronization of unpredictability—a more robust form of synchronization.

To gain a more profound understanding, the study analyzes two specific noise intensities: $D = 1$ and $D = 4.7$. In the case of $D = 1$, a portion of the sequences in the unpredictability analysis displays synchronization, indicating a weak form of synchronization known as delta synchronization of chaos. Conversely, for $D = 4.7$, all elements of the sequences of convergence and separation synchronize throughout the simulation. Thus, complete synchronization of unpredictability is confirmed, representing a more robust form of synchronization. These findings are supported

by numerical degrees of synchronization, providing the evidence of synchronization between stochastic neurons.

In summary, this study not only introduces a pioneering approach using Markovian noise to examine synchronization in Hindmarsh-Rose neural systems but also reveals synchronization phenomena in regions that traditional methods fail to capture. It advances our comprehension of synchronization by showing various synchronization types induced by different noise intensities in the presence of Markovian noise.

CHAPTER 6

CONCLUSION

Unpredictability is the core of the analyses covered in this thesis. It characterizes a chaotic behavior with sequences of convergence and separation. While the former explains the recurrence in the dynamics by indicating the Poisson stability, the latter describes the Lorenz sensitivity. The theory was constructed in Ref. [12], and has been applied to various models. The method requires a single trajectory to explain sensitivity and confirm chaotic motion. Hence, chaos stems from a single function, expanding the range of possibilities beyond equilibrium, periodic, quasi-periodic, almost periodic, recurrent functions, and Poisson stable motion to include unpredictable motion as a novel element. Particularly, this type of chaotic motion is called Poincaré chaos.

Numerical investigation of unpredictability is conducted by exploring the convergence and separation sequences in a sufficiently long simulation after the transient regime of the dynamics. The sequence of convergence includes the moments when the trajectory passes close to its initial point with a distance δ. This distance gets smaller at each iteration, indicating that the motion is Poisson stable. The time values in the sequence, covering the entire simulation, imply that prolonging the simulation assures convergence. In the sequence of separation, two trajectories starting from the convergence time and initial state are analyzed. The moments when both trajectories separate from each other with a distance Δ are recorded in the sequence of separation. The sensitivity in the dynamics is revealed by the existence of these sequences.

The theoretical background of unpredictability, as detailed in Ref. [12], is thoroughly explained. Additionally, the numerical implementation, utilizing an algorithm for finding the sequences of convergence and separation, is discussed. The algorithm pre-

sented in this thesis is general and can be applied to most dynamical systems. In this study, it is tested on partial, delay and ordinary differential equations. To determine the existence and strength of unpredictability, a numerical degree of unpredictability is introduced and applied in all analyses of this study.

The synchronized behavior of chaotic systems can be identified by analyzing the common sequences of convergence and separation, a phenomenon we term delta synchronization of chaos. In contrast to other synchronization methods which focuses on fully synchronized motions, such as generalized synchronization, delta synchronization reveals unison patterns in the dynamics. This is achieved by examining the characteristic time values of unpredictability.

The finite sequence of convergence records time values when trajectories simultaneously pass near their initial state, with the distance between them decreasing at each iteration. Conversely, the common sequence of separation includes time values when trajectories, starting at convergence time, simultaneously diverge from their initial state. These common characteristic time values of unpredictability effectively demonstrate the synchronized patterns of the systems.

Complete synchronization of unpredictability is achieved when the distance to the initial state converges zero in a sufficiently long simulation. In this scenario, the sequences have more elements, with the number of elements approaching that of the sequences in unpredictability analysis. To infer the existence and strength of synchronization, a numerical degree of synchronization is introduced and applied across all models in this thesis.

The delta synchronization method is defined, and the algorithm for its application is presented. Tables containing the sequences of delta synchronization are provided in the models presented in this thesis, along with necessary comparisons to other methods in the literature. Particularly, generalized synchronization with auxiliary systems approach and identical synchronization is utilized for comparison.

Identical synchronization examines chaotic systems that are identical (or nearly identical) but initiated with different initial conditions. Synchronization is achieved if the difference between the drive and response systems' solutions is zero after the transient

time. On the other hand, generalized synchronization examines the synchronization of nonidentical chaotic systems. It is achieved if the asymptotic stability condition is satisfied after the transient regime. The auxiliary systems approach is utilized in the analyses presented in this thesis. With this approach, the synchronization between the response system and the auxiliary system ensures the synchronization of the drive and response systems. The auxiliary system is identical to the response system, differing only in initial conditions.

In the first model [11], we analyzed a gas discharge semiconductor system that combines gas discharge with a high-ohmic semiconductor barrier for the synchronization of chaos. A one-dimensional fluid model is constructed using the drift-diffusion approximation. This model considers only electrons and ions as plasma species, referred to as a simple fluid model, and focuses on ionization processes occurring in regions with weak electric fields within the discharge gap. The fluid equations and modeling are comprehensively described.

The transition of the gas discharge semiconductor model from regular periodic behavior to fully chaotic states in subnormal oscillations is demonstrated. The chaotic region is considered for synchronization analysis within a defined parameter regime. Drive and response systems are constructed such that the discharge potential of the drive system is supplied to the response system as a perturbation with a constant multiplier. In the literature, it is concluded that there is no generalized synchronization for the same coupled systems [53]. Similarly, the absence of generalized synchronization is demonstrated using the auxiliary systems approach.

Unpredictability is confirmed in both drive and response systems by applying Algorithm (1). The numerical degrees of unpredictability are small numbers for both systems, approximately $\alpha \approx 0.0011$ for the drive system and $\alpha \approx 0.003$ for the response system. The delta synchronization analysis demonstrates that approximately $1/3$ of the unpredictability sequence is synchronized, with a degree of numerical synchronization $\alpha^{sync} \approx 0.046$. The outcomes are supported by figures, tables and numerical characteristics of unpredictability and delta synchronization.

The results reveal a synchronized pattern in gas discharge semiconductor systems, detectable by delta synchronization methods. However, conventional methods such

as generalized synchronization, which focus on fully synchronized dynamics, fail to detect this pattern. It is important to note that similar results are observed in the same system modeled with local mean energy [22], considering a more realistic modeling approach that better aligns with experiments.

The second model studied in this thesis is the Mackey-Glass system [23]. It consists of a delay differential equation in which the delay time defines the transition from periodic regimes to chaos. This transition is comprehensively investigated in this study. For a given parameter regime, the delay time is used as a control parameter, and the emergence of new periods is demonstrated by adjusting this parameter. It is demonstrated that the formation of an inflection point corresponds to a new period. The transition is also depicted via a period-doubling bifurcation diagram.

By using the solution of the drive system as a perturbation in the response, synchronization of chaos is examined for unidirectionally coupled Mackey-Glass systems. The auxiliary system is constructed as a copy of the response system with different initial conditions. Both the drive and response systems exhibit unpredictability for different values of the coupling constant.

Varying the coupling constant change the synchronized behavior of the systems. Thus, a threshold for the coupling constant is defined in the literature [65, 73–76]. In a similar manner to the literature, it is demonstrated that generalized synchronization exists above the threshold and it is absent below it via the auxiliary system approach.

Applying the delta synchronization method to the model shows that complete synchronization of unpredictability coexists with generalized synchronization. The coupling constant is taken near the threshold, as larger values imply coexistence with increased strength of synchronization. The number of elements in the sequences of unpredictability and synchronization is close to each other. The numerical degree of synchronization is $\alpha^{sync} = 0.0036$.

The main novelty of the study lies in the analysis of synchronization below the threshold, where generalized synchronization does not exist. The coupling constant is taken relatively far away from the threshold since close values already imply synchronization. The existence of delta synchronization is confirmed with the degree of numerical

synchronization $\alpha^{sync} = 0.013$, which is 3.6 times larger than the value in the above-threshold analysis; thus, it shows weaker synchronization. Hence, the synchronized patterns are detected via the delta synchronization method when other methods fail.

The final model discussed in this thesis is the Hindmarsh-Rose neural network [24]. This model elucidates the dynamics of a single neuron characterized by spiking-bursting behavior, with synchronization being attributed to the communication between neurons. By manipulating the external current as a control parameter, the model exhibits both periodic and chaotic membrane potential patterns. The transition between chaotic and periodic dynamics, and vice versa, is illustrated through the bifurcation diagram of interspike intervals.

The study explores noise-induced synchronization in the uncoupled Hindmarsh-Rose model. While Gaussian white noise is typically employed in the literature for such analyses, we construct Markovian noise based on Markov chains, utilizing unpredictable functions. This choice stems from the unpredictability inherent in the final function used as noise. The stochastic construction of the model with Markovian noise is elaborated upon in detail.

By holding all parameters constant, except for the noise intensity, we observe diverse synchronization patterns and dynamics as the noise intensity serves as a control parameter. At higher levels of noise intensity, neurons exhibit identical synchronization, a phenomenon detected through the time average of an error function. The presence of unpredictability across all domains of noise intensity is demonstrated for both neurons through the numerical degree of unpredictability.

The application of the delta synchronization method to the model reveals that synchronization initiates immediately after the introduction of noise, and neurons become synchronized irrespective of noise intensity. This is evidenced by the numerical degree of synchronization consistently observed across all noise intensities. In the deterministic case, or when noise intensity is absent, the sequences exhibit an insufficient number of elements, failing to span the entire simulation.

By analyzing both the number of elements in the sequences and the numerical degree of synchronization, we deduce the existence of delta synchronization for lower

noise intensities, while complete synchronization of unpredictability is observed for higher noise intensities. To provide further insight into the results, we concentrate on two specific noise intensities: one below and one above the threshold for identical synchronization.

Below the threshold, we illustrate that unpredictability sequences are partially synchronized, covering the entire simulation. The numerical degree of synchronization is small enough to signify delta synchronization. In contrast, above the threshold, all members of unpredictability sequences are synchronized, and the numerical degree of synchronization is significantly smaller, indicating the presence of complete synchronization of unpredictability.

In conclusion, this thesis introduces a method of delta synchronization grounded in unpredictability and applies it to various dynamical systems [11, 22–24]. The results demonstrate that delta synchronization successfully detects synchronized patterns in domains where conventional methods fail to do so. Additionally, it is observed that complete synchronization of unpredictability coexists with conventional methods in approximately the same domains.

REFERENCES

[1] L. M. Pecora and T. L. Carroll, "Synchronization in chaotic systems," *Physical review letters*, vol. 64, no. 8, p. 821, 1990.

[2] M. J. Ogorzalek, "Taming chaos-part i: Synchronization," *IEEE Transactions on Circuits and Systems I: Fundamental Theory and Applications*, vol. 40, no. 10, pp. 693–699, 1993.

[3] N. F. Rulkov, M. M. Sushchik, L. S. Tsimring, and H. D. Abarbanel, "Generalized synchronization of chaos in directionally coupled chaotic systems," *Physical Review E*, vol. 51, no. 2, p. 980, 1995.

[4] L. Kocarev and U. Parlitz, "Generalized synchronization, predictability, and equivalence of unidirectionally coupled dynamical systems," *Physical review letters*, vol. 76, no. 11, p. 1816, 1996.

[5] H. D. Abarbanel, N. F. Rulkov, and M. M. Sushchik, "Generalized synchronization of chaos: The auxiliary system approach," *Physical review E*, vol. 53, no. 5, p. 4528, 1996.

[6] K. Pyragas, "Weak and strong synchronization of chaos," *Physical Review E*, vol. 54, no. 5, p. R4508, 1996.

[7] J. M. González-Miranda, *Synchronization and Control of Chaos*. London, UK: Imperial College Press, 2004.

[8] F. Min and A. C. Luo, "Complex dynamics of projective synchronization of chua circuits with different scrolls," *International Journal of Bifurcation and Chaos*, vol. 25, no. 05, p. 1530016, 2015.

[9] F. Min and H. Ma, "The mechanism of switching combination synchronization for three distinct nonautonomous systems under sinusoidal constraints," *Nonlinear Dynamics*, vol. 100, no. 1, pp. 475–492, 2020.

[10] A. Pikovsky, M. Rosenblum, and J. Kurths, *Synchronization, a Universal Concept in Nonlinear Sciences*. Cambridge, UK: Cambridge University Press, 2001.

[11] M. Akhmet, K. Başkan, and C. Yeşil, "Delta synchronization of poincaré chaos in gas discharge-semiconductor systems," *Chaos: An Interdisciplinary Journal of Nonlinear Science*, vol. 32, no. 8, p. 083137, 2022.

[12] M. Akhmet and M. O. Fen, "Unpredictable points and chaos," *Communications in Nonlinear Science and Numerical Simulation*, vol. 40, pp. 1–5, 2016.

[13] M. Akhmet, *Domain Structured Dynamics: Unpredictability, Chaos, Randomness, Fractals, Differential Equations and Neural Networks*. Bristol, UK: IOP publishing, 2021.

[14] M. Akhmet, M. O. Fen, and E. M. Alejaily, *Dynamics with Chaos and Fractals*. Cham, Switzerland: Springer, 2020.

[15] M. Akhmet and M. O. Fen, "Poincaré chaos and unpredictable functions," *Communications in Nonlinear Science and Numerical Simulation*, vol. 48, pp. 85–94, 2017.

[16] M. Akhmet, "Shadowing and dynamical synthesis," *International Journal of Bifurcation and Chaos*, vol. 19, no. 10, pp. 3339–3346, 2009.

[17] M. Akhmet, "Dynamical synthesis of quasi-minimal sets," *International Journal of Bifurcation and Chaos*, vol. 19, no. 07, pp. 2423–2427, 2009.

[18] M. Akhmet and M. O. Fen, "Entrainment by chaos," *Journal of Nonlinear Science*, vol. 24, pp. 411–439, 2014.

[19] M. Akhmet and M. O. Fen, *Replication of chaos in neural networks, economics and physics*. Beijing/Heidelberg: Springer, 2015.

[20] F. T. Fen, M. O. Fen, and M. Akhmet, "A novel criterion for unpredictable motions," *Filomat*, vol. 37, no. 18, p. 6149–6158, 2023.

[21] M. Akhmet, M. Tleubergenova, and A. Zhamanshin, "Compartmental unpredictable functions," *Mathematics*, vol. 11, no. 5, p. 1069, 2023.

[22] M. Akhmet, C. Yeşil, and K. Başkan, "Synchronization of chaos in semiconductor gas discharge model with local mean energy approximation," *Chaos, Solitons & Fractals*, vol. 167, p. 113035, 2023.

[23] M. Akhmet, K. Başkan, and C. Yeşil, "Revealing chaos synchronization below the threshold in coupled mackey-glass systems," *Mathematics*, vol. 11, no. 14, 2023.

[24] M. Akhmet, K. Başkan, and C. Yeşil, "Markovian noise-induced delta synchronization approach for hindmarsh-rose model," *Manuscript submitted for publication*.

[25] J. W. S. B. Rayleigh, *The theory of sound*, vol. 2. Macmillan, 1896.

[26] W. H. Eccles, J. H. Vincent, and W. H. Bragg, "On the variations of wavelength of the oscillations generated by three-electrode thermionic tubes due to changes in filament current, plate voltage, grid voltage, or coupling," *Proceedings of the Royal Society of London. Series A, Containing Papers of a Mathematical and Physical Character*, vol. 96, no. 680, pp. 455–465, 1920.

[27] E. V. Appleton and B. van der Pol, "Xvi. on a type of oscillation-hysteresis in a simple triode generator," *The London, Edinburgh, and Dublin Philosophical Magazine and Journal of Science*, vol. 43, no. 253, pp. 177–193, 1922.

[28] B. Van Der Pol, "Vii. forced oscillations in a circuit with non-linear resistance.(reception with reactive triode)," *The London, Edinburgh, and Dublin Philosophical Magazine and Journal of Science*, vol. 3, no. 13, pp. 65–80, 1927.

[29] M. G. Rosenblum, A. S. Pikovsky, and J. Kurths, "Phase synchronization of chaotic oscillators," *Physical review letters*, vol. 76, no. 11, p. 1804, 1996.

[30] H. U. Voss, "Anticipating chaotic synchronization," *Physical review E*, vol. 61, no. 5, p. 5115, 2000.

[31] J. M. González-Miranda, "Amplitude envelope synchronization in coupled chaotic oscillators," *Physical Review E*, vol. 65, no. 3, p. 036232, 2002.

[32] M. G. Rosenblum, A. S. Pikovsky, and J. Kurths, "From phase to lag synchronization in coupled chaotic oscillators," *Physical Review Letters*, vol. 78, no. 22, p. 4193, 1997.

[33] L. Shilnikov, "Homoclinic chaos by leonid shilnikov," in *Nonlinear Dynamics, Chaotic and Complex Systems: Proceedings of an International Conference Held in Zakopane, Poland, November 7-12 1995, Plenary Invited Lectures*, (Cambridge, U.K), p. 39, Cambridge University Press, 1997.

[34] H. Poincaré, *Les Méthods Nouvelles de la Méchanique Céleste*. Paris, France: Gauther-Villars et Fils, Imprimeurs-Libraires, 1892.

[35] R. L. Devaney, *An Introduction to Chaotic Dynamical Systems*. U.S.A: Addison-Wesley, 1989.

[36] E. N. Lorenz, "Deterministic nonperiodic flow," *Journal of Atmospheric Sciences*, vol. 20, no. 2, pp. 130 – 141, 1963.

[37] T.-Y. Li and J. A. Yorke, "Period three implies chaos," *American Mathematical Monthly*, vol. 82, no. 10, pp. 985–992, 1975.

[38] H. Poincaré, "Sur le problème des trois corps et les équations de la dynamique," *Acta mathematica*, vol. 13, no. 1, pp. A3–A270, 1890.

[39] C. Carathéodory, *Über den Wiederkehrsatz von Poincaré*. Berl. Sitzungsber., 1919.

[40] F. F. Chen *et al.*, *Introduction to plasma physics and controlled fusion*, vol. 1. LosAngeles, C.A, U.S.A: Springer, 1984.

[41] D. B. Graves, "Low temperature plasma biomedicine: A tutorial review," *Physics of Plasmas*, vol. 21, no. 8, 2014.

[42] G. Fridman, G. Friedman, A. Gutsol, A. B. Shekhter, V. N. Vasilets, and A. Fridman, "Applied plasma medicine," *Plasma processes and polymers*, vol. 5, no. 6, pp. 503–533, 2008.

[43] E. C. Neyts, K. Ostrikov, M. K. Sunkara, and A. Bogaerts, "Plasma catalysis: synergistic effects at the nanoscale," *Chemical reviews*, vol. 115, no. 24, pp. 13408–13446, 2015.

[44] I. Rafatov and A. Kudryavtsev, *Introduction to Simulation Methods for Gas Discharge Plasmas*. 2053-2563, IOP Publishing, 2020.

[45] C. Yeşil, *Comprehensive investigation of plasma behavior in diverse gas discharge phenomena: fluid modeling, chaotic dynamics, and synchronization*. PhD thesis, Middle East Technical University, 2023.

[46] H. Willebrand, T. Hünteler, F.-J. Niedernostheide, R. Dohmen, and H.-G. Purwins, "Periodic and turbulent behavior of solitary structures in distributed active media," *Physical Review A*, vol. 45, no. 12, p. 8766, 1992.

[47] C. Strümpel, Y. A. Astrov, and H.-G. Purwins, "Multioscillatory patterns in a hybrid semiconductor gas-discharge system," *Physical Review E*, vol. 65, no. 6, p. 066210, 2002.

[48] C. Strümpel, Y. A. Astrov, and H.-G. Purwins, "Nonlinear interaction of homogeneously oscillating domains in a planar gas discharge system," *Physical Review E*, vol. 62, no. 4, p. 4889, 2000.

[49] E. Gurevich, Y. A. Astrov, and H. Purwins, "Pattern formation in planar dc-driven semiconductor–gas discharge devices: two mechanisms," *Journal of Physics D: Applied Physics*, vol. 38, no. 3, p. 468, 2005.

[50] C. Radehaus, R. Dohmen, H. Willebrand, and F.-J. Niedernostheide, "Model for current patterns in physical systems with two charge carriers," *Physical Review A*, vol. 42, no. 12, p. 7426, 1990.

[51] R. R. Arslanbekov and V. I. Kolobov, "Two-dimensional simulations of the transition from townsend to glow discharge and subnormal oscillations," *Journal of Physics D: Applied Physics*, vol. 36, no. 23, p. 2986, 2003.

[52] M. Benilov, "Multiple solutions in the theory of dc glow discharges and cathodic part of arc discharges. application of these solutions to the modeling of cathode spots and patterns: a review," *Plasma Sources Science and Technology*, vol. 23, no. 5, p. 054019, 2014.

[53] M. Akhmet, I. Rafatov, and M. O. Fen, "Extension of spatiotemporal chaos in glow discharge-semiconductor systems," *Chaos: An Interdisciplinary Journal of Nonlinear Science*, vol. 24, no. 4, p. 043127, 2014.

[54] C. Yuan, C. Yesil, J. Yao, Z. Zhou, and I. Rafatov, "Transition from periodic to chaotic oscillations in a planar gas discharge-semiconductor system," *Plasma Sources Science and Technology*, vol. 29, no. 6, p. 065009, 2020.

[55] Y. P. Raizer and M. Mokrov, "Physical mechanisms of self-organization and formation of current patterns in gas discharges of the townsend and glow types," *Physics of Plasmas*, vol. 20, no. 10, p. 101604, 2013.

[56] D. D. Šijačić, U. Ebert, and I. Rafatov, "Period doubling cascade in glow discharges: Local versus global differential conductivity," *Physical Review E*, vol. 70, no. 5, p. 056220, 2004.

[57] I. Rafatov, "Three-dimensional numerical modelling of temporal and spatial pattern formation in a dc-driven gas discharge-semiconductor system," *Plasma Sources Science and Technology*, vol. 25, no. 6, p. 065014, 2016.

[58] G. Grubert, M. Becker, and D. Loffhagen, "Why the local-mean-energy approximation should be used in hydrodynamic plasma descriptions instead of the local-field approximation," *Physical Review E*, vol. 80, no. 3, p. 036405, 2009.

[59] M. C. Mackey and L. Glass, "Oscillation and chaos in physiological control systems," *Science*, vol. 197, no. 4300, pp. 287–289, 1977.

[60] H. T. Milhorn JR and A. Guyton, "An analog computer analysis of cheyne-stokes breathing," *Journal of applied physiology*, vol. 20, no. 2, pp. 328–333, 1965.

[61] S. Rubinow and J. Lebowitz, "A mathematical model of neutrophil production and control in normal man," *Journal of Mathematical Biology*, vol. 1, no. 3, pp. 187–225, 1975.

[62] R. M. May, "Simple mathematical models with very complicated dynamics," *Nature*, no. 10, pp. 459–467, 1976.

[63] R. M. May and G. F. Oster, "Bifurcations and dynamic complexity in simple ecological models," *The American Naturalist*, vol. 110, no. 974, pp. 573–599, 1976.

[64] A. Namajūnas, K. Pyragas, and A. Tamaševičius, "An electronic analog of the mackey-glass system," *Physics Letters A*, vol. 201, no. 1, pp. 42–46, 1995.

[65] A. Kittel, J. Parisi, and K. Pyragas, "Generalized synchronization of chaos in electronic circuit experiments," *Physica D: Nonlinear Phenomena*, vol. 112, no. 3-4, pp. 459–471, 1998.

[66] S. Sano, A. Uchida, S. Yoshimori, and R. Roy, "Dual synchronization of chaos in mackey-glass electronic circuits with time-delayed feedback," *Physical Review E*, vol. 75, no. 1, p. 016207, 2007.

[67] W. Kinzel, A. Englert, and I. Kanter, "On chaos synchronization and secure communication," *Philosophical Transactions of the Royal Society A: Mathematical, Physical and Engineering Sciences*, vol. 368, no. 1911, pp. 379–389, 2010.

[68] D. Li, Z. Wang, J. Zhou, J. Ni, *et al.*, "A note on chaotic synchronization of time-delay secure communication systems," *Chaos, Solitons & Fractals*, vol. 38, no. 4, pp. 1217–1224, 2008.

[69] O. Kwon, J. H. Park, and S. Lee, "Secure communication based on chaotic synchronization via interval time-varying delay feedback control," *Nonlinear Dynamics*, vol. 63, pp. 239–252, 2011.

[70] C. Li, X. Liao, and K.-w. Wong, "Chaotic lag synchronization of coupled time-delayed systems and its applications in secure communication," *Physica D: Nonlinear Phenomena*, vol. 194, no. 3-4, pp. 187–202, 2004.

[71] T. M. Hoang, N. V. Son, and M. Nakagawa, "A secure communication system using projective-lag synchronization of multidelay mackey-glass systems," in *2006 First International Conference on Communications and Electronics*, pp. 325–330, IEEE, 2006.

[72] J. D. Farmer, "Chaotic attractors of an infinite-dimensional dynamical system," *Physica D: Nonlinear Phenomena*, vol. 4, no. 3, pp. 366–393, 1982.

[73] L. Dong and Z. Zhi-Gang, "Multiple attractors and generalized synchronization in delayed mackey–glass systems," *Chinese Physics B*, vol. 17, no. 11, p. 4009, 2008.

[74] K. Pyragas, “Synchronization of coupled time-delay systems: Analytical estimations,” *Physical Review E*, vol. 58, no. 3, p. 3067, 1998.

[75] M. Zhan, X. Wang, X. Gong, G. Wei, and C.-H. Lai, “Complete synchronization and generalized synchronization of one-way coupled time-delay systems,” *Physical Review E*, vol. 68, no. 3, p. 036208, 2003.

[76] E. Shahverdiev, R. Nuriev, R. Hashimov, and K. Shore, “Chaos synchronization between the mackey–glass systems with multiple time delays,” *Chaos, Solitons & Fractals*, vol. 29, no. 4, pp. 854–861, 2006.

[77] J. L. Hindmarsh and R. Rose, “A model of neuronal bursting using three coupled first order differential equations,” *Proceedings of the Royal society of London. Series B. Biological sciences*, vol. 221, no. 1222, pp. 87–102, 1984.

[78] S. H. Thompson and S. J. Smith, “Depolarizing afterpotentials and burst production in molluscan pacemaker neurons,” *Journal of Neurophysiology*, vol. 39, no. 1, pp. 153–161, 1976.

[79] D. F. Russell and D. K. Hartline, “Slow active potentials and bursting motor patterns in pyloric network of the lobster, panulirus interruptus,” *Journal of Neurophysiology*, vol. 48, no. 4, pp. 914–937, 1982.

[80] P. Schwindt and W. Crill, “Role of a persistent inward current in motoneuron bursting during spinal seizures.,” *Journal of Neurophysiology*, vol. 43, no. 5, pp. 1296–1318, 1980.

[81] R. Plant and M. Kim, “Mathematical description of a bursting pacemaker neuron by a modification of the hodgkin-huxley equations,” *Biophysical journal*, vol. 16, no. 3, pp. 227–244, 1976.

[82] A. L. Hodgkin and A. F. Huxley, “A quantitative description of membrane current and its application to conduction and excitation in nerve,” *The Journal of physiology*, vol. 117, no. 4, p. 500, 1952.

[83] Q. Lu, H. Gu, Z. Yang, X. Shi, L. Duan, and Y. Zheng, “Dynamics of firing patterns, synchronization and resonances in neuronal electrical activities: experiments and analysis,” *Acta Mechanica Sinica*, vol. 24, no. 6, pp. 593–628, 2008.

[84] D. Hrg, "Synchronization of two hindmarsh–rose neurons with unidirectional coupling," *Neural Networks*, vol. 40, pp. 73–79, 2013.

[85] A. Bandyopadhyay and S. Kar, "Impact of network structure on synchronization of hindmarsh–rose neurons coupled in structured network," *Applied Mathematics and Computation*, vol. 333, pp. 194–212, 2018.

[86] Z.-L. Wang and X.-R. Shi, "Chaotic bursting lag synchronization of hindmarsh–rose system via a single controller," *Applied Mathematics and Computation*, vol. 215, no. 3, pp. 1091–1097, 2009.

[87] M. Ge, Y. Jia, Y. Xu, L. Lu, H. Wang, and Y. Zhao, "Wave propagation and synchronization induced by chemical autapse in chain hindmarsh–rose neural network," *Applied Mathematics and Computation*, vol. 352, pp. 136–145, 2019.

[88] S. Xia and L. Qi-Shao, "Firing patterns and complete synchronization of coupled hindmarsh–rose neurons," *Chinese Physics*, vol. 14, no. 1, p. 77, 2005.

[89] H. Yu and J. Peng, "Chaotic synchronization and control in nonlinear-coupled hindmarsh–rose neural systems," *Chaos, Solitons & Fractals*, vol. 29, no. 2, pp. 342–348, 2006.

[90] I. Belykh, E. De Lange, and M. Hasler, "Synchronization of bursting neurons: What matters in the network topology," *Physical review letters*, vol. 94, no. 18, p. 188101, 2005.

[91] M. Dhamala, V. K. Jirsa, and M. Ding, "Enhancement of neural synchrony by time delay," *Physical review letters*, vol. 92, no. 7, p. 074104, 2004.

[92] M. G. Knyazeva, M. Jalili, A. Brioschi, I. Bourquin, E. Fornari, M. Hasler, R. Meuli, P. Maeder, and J. Ghika, "Topography of eeg multivariate phase synchronization in early alzheimer's disease," *Neurobiology of Aging*, vol. 31, no. 7, pp. 1132–1144, 2010.

[93] P. J. Uhlhaas and W. Singer, "Neural synchrony in brain disorders: Relevance for cognitive dysfunctions and pathophysiology," *Neuron*, vol. 52, no. 1, pp. 155–168, 2006.

[94] J.-W. Shuai and D. M. Durand, "Phase synchronization in two coupled chaotic neurons," *Physics Letters A*, vol. 264, no. 4, pp. 289–297, 1999.

[95] M. V. Ivanchenko, G. V. Osipov, V. D. Shalfeev, and J. Kurths, "Phase synchronization in ensembles of bursting oscillators," *Phys. Rev. Lett.*, vol. 93, p. 134101, Sep 2004.

[96] C. Kurrer and K. Schulten, "Noise-induced synchronous neuronal oscillations," *Phys. Rev. E*, vol. 51, pp. 6213–6218, Jun 1995.

[97] J. D. Touboul, C. Piette, L. Venance, and G. B. Ermentrout, "Noise-induced synchronization and antiresonance in interacting excitable systems: Applications to deep brain stimulation in parkinson's disease," *Phys. Rev. X*, vol. 10, p. 011073, Mar 2020.

[98] J. W. Shuai and K. W. Wong, "Noise and neural networks," *Phys. Rev. E*, vol. 57, pp. 7002–7007, Jun 1998.

[99] Y. Wu, J. Xu, D. He, and D. J. Earn, "Generalized synchronization induced by noise and parameter mismatching in hindmarsh–rose neurons," *Chaos, Solitons & Fractals*, vol. 23, no. 5, pp. 1605–1611, 2005.

[100] S. Xia and L. Qi-Shao, "Coherence resonance and synchronization of hindmarsh–rose neurons with noise," *Chinese physics*, vol. 14, no. 6, p. 1088, 2005.

[101] D. He, P. Shi, and L. Stone, "Noise-induced synchronization in realistic models," *Physical Review E*, vol. 67, no. 2, p. 027201, 2003.

[102] D. Jones and M. Lorenz, "An application of a markov chain noise model to wind generator simulation," *Mathematics and Computers in Simulation*, vol. 28, no. 5, pp. 391–402, 1986.

[103] A. Mahmood and M. Chitre, "Modeling colored impulsive noise by markov chains and alpha-stable processes," in *OCEANS 2015 - Genova*, pp. 1–7, 2015.

[104] M. Kaledin, E. Moulines, A. Naumov, V. Tadic, and H.-T. Wai, "Finite time analysis of linear two-timescale stochastic approximation with markovian noise," in *Proceedings of Thirty Third Conference on Learning Theory*

(J. Abernethy and S. Agarwal, eds.), vol. 125 of *Proceedings of Machine Learning Research*, pp. 2144–2203, PMLR, 09–12 Jul 2020.

[105] J. A. Gubner, *Probability and random processes for electrical and computer engineers*. New York, U.S.A: Cambridge University Press, 2006.

[106] S. Karlin and H. M. Taylor, *A First Course in Stochastic Processes*. New York, U.S.A: Academic Press, second edition ed., 1975.

[107] S. P. Meyn and R. L. Tweedie, *Markov chains and stochastic stability*. London, U.K.: Springer London, 1993.

[108] M. Akhmet, M. Tleubergenova, and A. Zhamanshin, "Unpredictable solutions of duffing type equations with markov coefficients," *Carpathian Journal of Mathematics*, vol. 39, no. 3, pp. 568–582, 2023.

[109] M. Akhmet, "Unpredictability in markov chains," *Carpathian Journal of Mathematics*, vol. 38, no. 1, pp. 13–19, 2022.

[110] L. Barreira, "Poincaré recurrence: old and new," in *XIVth International Congress on Mathematical Physics*, pp. 415–422, World Scientific, 2006.

[111] G. D. Birkhoff, *Dynamical systems*, vol. 9. Providence, U.S.A: American Mathematical Soc., 1927.

[112] M. Henon, "A two-dimensional mapping with a strange attractor," *Communications in Mathematical Physics*, vol. 50, pp. 69–77, 1976.

[113] S. Smale, *Diffeomorphisms with Many Periodic Points*, ch. Differential and Combinatorial Topology, pp. 63–80. Princeton, U.S.A: Princeton University Press, 1965.

[114] H. Hilmy, "Sur les ensembles quasi-minimaux dans les systemes dynamiques," *Annals of Mathematics*, no. 4, pp. 899–907, 1936.

[115] V. V. Nemytskii and V. V. Vladimirovich, *Qualitative theory of differential equations*. Princeton, U.S.A: Princeton University Press, 1960.

[116] G. R. Sell, *Topological dynamics and ordinary differential equations*. London, U.K: Van Nostrand–Reinbold Company, 1971.

[117] R. He and P. Vaidya, "Analysis and synthesis of synchronous periodic and chaotic systems," *Physical Review A*, vol. 46, no. 12, p. 7387, 1992.

[118] G. Grubert, M. Becker, and D. Loffhagen, "Why the local-mean-energy approximation should be used in hydrodynamic plasma descriptions instead of the local-field approximation," *Physical Review E*, vol. 80, no. 3, p. 036405, 2009.

[119] Y. P. Raizer and J. E. Allen, *Gas discharge physics*, vol. 2. Springer Berlin, 1997.

[120] I. Rafatov and C. Yesil, "Transition from homogeneous stationary to oscillating state in planar gas discharge–semiconductor system in nitrogen: Effect of fluid modelling approach," *Physics of Plasmas*, vol. 25, no. 8, p. 082107, 2018.

[121] U. S. Inan and M. Gołkowski, *Principles of plasma physics for engineers and scientists*. Cambridge, UK: Cambridge University Press, 2010.

[122] C. Strümpel, H.-G. Purwins, and Y. A. Astrov, "Spatiotemporal filamentary patterns in a dc-driven planar gas discharge system," *Physical review E*, vol. 63, no. 2, p. 026409, 2001.

[123] E. Ammelt, Y. A. Astrov, and H.-G. Purwins, "Stripe turing structures in a two-dimensional gas discharge system," *Physical Review E*, vol. 55, no. 6, p. 6731, 1997.

[124] Y. A. Astrov, E. Ammelt, and H.-G. Purwins, "Experimental evidence for zigzag instability of solitary stripes in a gas discharge system," *Physical review letters*, vol. 78, no. 16, p. 3129, 1997.

[125] Y. A. Astrov and Y. A. Logvin, "Formation of clusters of localized states in a gas discharge system via a self-completion scenario," *Physical Review Letters*, vol. 79, no. 16, p. 2983, 1997.

[126] E. Gurevich, A. Moskalenko, A. Zanin, Y. A. Astrov, and H.-G. Purwins, "Rotating waves in a planar dc-driven gas-discharge system with semi-insulating gaas cathode," *Physics Letters A*, vol. 307, no. 5-6, pp. 299–303, 2003.

[127] M. Mokrov and Y. P. Raizer, "Simulation of current filamentation in a dc-driven planar gas discharge–semiconductor system," *Journal of Physics D: Applied Physics*, vol. 44, no. 42, p. 425202, 2011.

[128] I. R. Rafatov, D. D. Šijačić, and U. Ebert, "Spatiotemporal patterns in a dc semiconductor-gas-discharge system: Stability analysis and full numerical solutions," *Physical Review E*, vol. 76, no. 3, p. 036206, 2007.

[129] Y. P. Raizer, U. Ebert, and D. Šijačić, "Dependence of the transition from townsend to glow discharge on secondary emission," *Physical Review E*, vol. 70, no. 1, p. 017401, 2004.

[130] Y. P. Raizer, E. Gurevich, and M. Mokrov, "Self-sustained oscillations in a low-current discharge with a semiconductor serving as a cathode and ballast resistor: Ii. theory," *Technical physics*, vol. 51, no. 2, pp. 185–197, 2006.

[131] Y. P. Raizer and M. Mokrov, "A simple physical model of hexagonal patterns in a townsend discharge with a semiconductor cathode," *Journal of Physics D: Applied Physics*, vol. 43, no. 25, p. 255204, 2010.

[132] D. D. Šijačić and U. Ebert, "Transition from townsend to glow discharge: Subcritical, mixed, or supercritical characteristics," *Physical Review E*, vol. 66, no. 6, p. 066410, 2002.

[133] D. D. Šijačić, U. Ebert, and I. Rafatov, "Oscillations in dc driven barrier discharges: Numerical solutions, stability analysis, and phase diagram," *Physical Review E*, vol. 71, no. 6, p. 066402, 2005.

[134] I. Rafatov, "Multiple stationary filamentary states in a planar dc-driven gas discharge-semiconductor system," *Physics of Plasmas*, vol. 23, no. 12, p. 123506, 2016.

[135] Y. P. Raizer and J. E. Allen, *Gas discharge physics*, vol. 1. Berlin: Springer, 1991.

[136] R. Wilson IV and N. Podder, "Observation of period multiplication and instability in a dc glow discharge," *Physical Review E*, vol. 76, no. 4, p. 046405, 2007.

[137] E. Ott, *Chaos in Dynamical Systems*. Cambridge, UK: Cambridge University Press, 2002.

[138] E. A. Jackson, *Perspectives of Nonlinear Dynamics*, vol. 1. Cambridge, UK: Cambridge University Press, 1989.

[139] L. Junges and J. A. Gallas, "Intricate routes to chaos in the mackey–glass delayed feedback system," *Physics letters A*, vol. 376, no. 30-31, pp. 2109–2116, 2012.

[140] J. P. Tarigo, C. Stari, C. Cabeza, and A. C. Marti, "Characterizing multistability regions in the parameter space of the mackey–glass delayed system," *The European Physical Journal Special Topics*, vol. 231, no. 3, pp. 273–281, 2022.

[141] L. Li, "Bifurcation and chaos in a discrete physiological control system," *Applied Mathematics and Computation*, vol. 252, pp. 397–404, 2015.

[142] A. El-Sayed, S. Salman, and N. Elabd, "On the dynamics of the singularly perturbed mackey–glass equation," *Journal of Computational and Applied Mathematics*, vol. 344, pp. 154–160, 2018.

[143] J. Wei, "Bifurcation analysis in a scalar delay differential equation," *Nonlinearity*, vol. 20, no. 11, p. 2483, 2007.

[144] A. Wan and J. Wei, "Bifurcation analysis of mackey–glass electronic circuits model with delayed feedback," *Nonlinear Dynamics*, vol. 57, no. 1-2, pp. 85–96, 2009.

[145] E. A. Jackson, *Perspectives of Nonlinear Dynamics: Volume 1*, vol. 1. CUP Archive, 1989.

[146] E. Ott, *Chaos in dynamical systems*. Cambridge university press, 2002.

[147] M. Akhmet and M. O. Fen, "Non-autonomous equations with unpredictable solutions," *Communications in Nonlinear Science and Numerical Simulation*, vol. 59, pp. 657–670, 2018.

CURRICULUM VITAE

PERSONAL INFORMATION

Surname, Name : Kağan Başkan
Nationality : Turkish (TC)

EDUCATION

Degree	Institution	Year of Graduation
Ph.D.	METU Physics	2024
M.S.	METU Physics	2019
B.S.	METU Physics	2016

SCIENTIFIC PROJECTS

• Researcher (2021-2024), in the project supported by The Scientific and Technological Research Council of Turkey, Project Name: *Unpredictable Oscillations Theory and its Applications to Neural Network Dynamics*, Middle East Technical University.

• Researcher (2018-2021), in the project supported by The Scientific and Technological Research Council of Turkey, Project Name: *Matrix Gauge Models, Fuzzy Spaces and Chaotic Dynamics*, Middle East Technical University.

FOREIGN LANGUAGES

Fluent English, intermediate French.

COMPUTER SKILLS

MATLAB, Python, Mathematica, C#, C++, Lua.

PUBLICATIONS

1. Akhmet, M., Başkan, K., & Yeşil, C. (2023). Revealing chaos synchronization below the threshold in coupled mackey–glass systems. Mathematics, 11(14), 3197.

2. Başkan, K., Kürkçüoğlu, S., & Taşcı, C. (2023). Chaotic dynamics of the mass deformed ABJM model. Physical Review D, 107(6), 066006.

3. Akhmet, M., Yeşil, C., & Başkan, K. (2023). Synchronization of chaos in semiconductor gas discharge model with local mean energy approximation. Chaos, Solitons & Fractals, 167, 113035.

4. Akhmet, M., Başkan, K., & Yeşil, C. (2022). Delta synchronization of Poincaré chaos in gas discharge-semiconductor systems. Chaos: An Interdisciplinary Journal of Nonlinear Science, 32(8).

5. Baskan, K. and Kurkcuoglu, Seckin and Oktay, O. and Tasci, C. (2022). Chaos in Matrix Gauge Theories with Massive Deformations. PoS, CORFU2021, 294.

6. Başkan, K., & Kürkçüoğlu, S. (2021). Chaos in the SU(2) Yang-Mills Chern-Simons matrix model. Physical Review D, 104(6), 066006.

7. Başkan, K., Kürkcüoğlu, S., Oktay, O., & Taşcı, C. (2020). Chaos from massive deformations of Yang-Mills matrix models. Journal of High Energy Physics, 2020(10), 1-34.

CONFERENCES

1. M. Akhmet and K. Başkan, (2022). The delta unpredictability in celestial mechanics. 4th International Conference on Artificial Intelligence and Applied Mathematics in Engineering (ICAIAME 2022).